11-8-2019

The Role of inositol Polyphosphate-4-Phosphatase Type II b (INPP4B) in Obese Models and Endocrine Cancers

Manqi Zhang
mzhan016@fiu.edu

FLORIDA INTERNATIONAL UNIVERSITY

Miami, Florida

THE ROLE OF INOSITOL POLYPHOSPHATE-4-PHOSPHATASE TYPE II B (INPP4B) IN OBESE MODELS AND ENDOCRINE CANCERS

A dissertation submitted in partial fulfillment of

the requirements for the degree of

DOCTOR OF PHILOSOPHY

in

BIOCHEMISTRY

by

Manqi Zhang

2019

To: Dean Michael R. Heithaus
College of Arts, Sciences and Education

This dissertation, written by Manqi Zhang, and entitled The Role of Inositol Polyphosphate-4-Phosphatase Type II B (INPP4B) in Obese Models and Endocrine Cancers, having been approved in respect to style and intellectual content, is referred to you for judgment.

We have read this dissertation and recommend that it be approved.

_____
Jeffrey Boyd

_____
Yuan Liu

_____
Yukching Tse Dinh

_____
Irina Agoulnik, Major Professor

Date of Defense: November 8, 2019

The dissertation of Manqi Zhang is approved.

_____
Dean Michael R. Heithaus
College of Arts, Sciences and Education

_____
Andrés G. Gil
Vice President for Research and Economic Development
and Dean of the University Graduate School

Florida International University, 2019

DEDICATION

I dedicate this dissertation to my parents YajuanXu and Xiaonan Zhang who support me all the time and encourage me to pursue my dreams.

ACKNOWLEDGMENTS

I would like to express my gratitude to the many people who have helped and supported me in completion of this work, stood by me and made my time special in the graduate school. More specifically, I would like to extend my sincere thanks to the people below.

First and foremost, I would like to express my deepest appreciation to my major professor, Dr. Irina Agoulnik, without whom this thesis would not have been possible. I was intrigued by Dr. Agoulnik's ideas that made this work attractive and valuable. Dr. Agoulnik has provided me with numerous opportunities to gain knowledge and skills and encouraged me to overcome the obstacles. With her excellent mentorship, I have gained invaluable experience in writing, scientific research, social communication, and presentation. Therefore, I am extremely grateful to Dr. Agoulnik for her great support and care throughout my Ph.D. years. She helped me become a better student in school and a better person in life.

I would like to extend my sincere thanks to my committee members, Dr. Yuan Liu, Dr. Yuk-Ching Tse-Dinh, and Dr. Jefferey Boyd for their support and constructive advice. I would like to especially thank Dr. Tse-Dinh for her help and guidance during my Dissertation Year Fellowship (DYF) application. I would like to give special thanks to Dr. Liu, the biochemistry graduate program director, for keeping track of my progress during the years.

I would like to acknowledge the National Cancer Institute which funded my stipend and research between 2015 to 2018. I also would like to acknowledge the Department of Chemistry and Biochemistry and University Graduate School at FIU for the financial support.

I had the pleasure of working with great peers and laboratory members. Many thanks to Egla Suarez who has offered me patient instructions and unwavering supports when I first joined the lab and to Judy Vasquez who provided unselfish assistance and guidance for my lab work and my writing. I thank Yasemin Ceyhan and Carlos Sandoval for interesting research discussion and their research fellowship. Special thanks to Dr. Alexander Agoulnik's lab, especially to Courtney Myhr, Maria Lopez, Dr. Elena Kaftanovskaya, and Dr. Alexander Agoulnik for their endless help and support in the course of our experiments. Especially I am very grateful to Dr. Elena who has introduced me to the world of histology.

I would like to extend my gratitude to our collaborators for their generous help and invaluable contribution to our research. Dr. Jean Vacher has provided the mouse model; Dr. Lubov Nathanson has helped us analyze the gene expression profiles and taught us a number of bioinformatics' approaches to data analysis; Dr. Michael Ittmmann has contributed to the histopathological analysis of mouse prostate sections; Dr. Nancy Weigel has provided unique cell lines and insightful suggestions for our work, especially the studies related to the prostate cancer.

I would like to acknowledge the Biochemistry Program and a great team of stuff that worked in the Chemistry and Biochemistry Program, especially Magali Autie, Jackelyn Marcos, and Dr. Watson Lees for their time and help to make our life much easier.

I am also grateful to Dr. Xiaotang Wang who has given me the opportunities to join the FIU Biochemistry and introduced me to Dr. Irina Agoulnik's lab, the beginning of this great adventure. I very much appreciate my friend Wei Zhang and Wenjie Wang, who have been there for me during these five years with their support and encouragement.

Last but not least, I’m deeply indebted to my parents Yajuan Xu and Xiaonan Zhang for their unwavering support. I would like to thank them for encouraging me to pursue my dreams. Their belief in me keeps me moving towards accomplishing my dreams.

ABSTRACT OF THE DISSERTATION

THE ROLE OF INOSITOL POLYPHOSPHATE-4-PHOSPHATASE TYPE II B (INPP4B) IN OBESE MODELS AND ENDOCRINE CANCERS

by

Manqi Zhang

Florida International University, 2019

Miami, Florida

Professor Irina Agoulnik, Major Professor

INPP4B is a dual-specificity phosphatase and a tumor suppressor in prostate and breast cancers. Progression of the prostate and breast cancers depends on the androgen receptor (AR) or estrogen receptor alpha (ERα) signaling, respectively. In this work we demonstrated that INPP4B reprograms ERα transcriptional activity in breast cancer. INPP4B maintains expression and protein levels of progesterone receptor (PR), an ERα direct target gene required for mammary gland development. Consistently we demonstrated that *Inpp4b* knockout severely impairs lateral branching in the mammary gland of maturing virgin females. In advanced prostate cancer, activation and transcriptional reprogramming of AR frequently coincides with the loss INPP4B. We showed that INPP4B regulates AR transcriptional activity in part through inhibiting the oncogenic signaling pathways Akt and PKC. The high-fat diet (HFD) and obesity have been linked to the development of metabolic dysfunction and the promotion of multiple cancers. In obese individuals, the insulin and fatty acid mediated signaling activates AKT and PKC pathways which are involved in metabolic disorders. Therefore, we investigated the roles of INPP4B in obese models. Males were susceptible to diet-induced obesity,

exhibited significant inflammation of the adipose tissue, hepatosteatosis, and type 2 diabetes. Obese HFD *Inpp4b*$^{-/-}$ males developed high grade prostatic intraepithelial neoplasia. Similar to humans, female knockout mice were protected from the insulin resistance despite extreme obesity and fibrotic hepatosteatosis. Development of steatosis in *Inpp4b*$^{-/-}$ mice was caused by increased constitutive proteolytic activation of lipogenic transcription factor SREBP1 in liver. Activated SREBP1 along with the HFD caused increased expression of PPARγ and other genes that are involved in *de novo* lipogenesis leading to the development of non-alcoholic fatty liver disease (NAFLD). Metabolic and steroid signaling changes caused mammary gland hyperplasia in obese knockout females. In conclusion, INPP4B is a tumor suppressor that regulates steroid receptor signaling and protects mice from high-fat diet induced metabolic disorders and neoplastic changes.

TABLE OF CONTENTS

CHAPTER PAGE

CHAPTER 1: INTRODUCTION 1
1.1. Phosphoinositide and phosphatidylinositol signaling 1
1.2. Inositol polyphosphate 3-phosphatase: PTEN 4
1.3. Inositol polyphosphate 4-phosphatase: INPP4B 6
1.3.1. Gene locus, splice variants and patterns of protein expression of INPP4B 6
1.3.2. Biochemistry and structure of INPP4B 6
1.3.3. PI signaling network (Figure 1-6) 9
1.4. Prostate cancer and INPP4B role in prostate cancer 10
1.4.1. Prostate cancer requires androgen receptor (AR) for initiation and progression 10
1.4.2. AR structure and AR splice variants 13
1.4.3. The tumor-suppressive function of INPP4B in prostate cancer 14
1.5. Breast cancer and INPP4B role in breast cancer 16
1.5.1. Four major subtypes of breast cancer 16
1.5.2. ER and PR 16
1.5.3. HER2 enriched breast cancer 18
1.5.4. Triple-negative breast cancer (TNBC) 18
1.5.5. Paradoxical role of INPP4B in breast cancer 19
1.6. Crosstalk between INPP4B regulated signaling and metabolic disorders 19
1.6.1. Metabolic disorders 20
1.6.2. AKT signaling under normal or high fat feeding conditions 21
1.6.3. Activation of PKC pathways under obese conditions 21
1.7. INPP4B knockout (*Inpp4b*$^{-/-}$) mouse model 22
1.8. OVERVIEW 23

CHAPTER 2: THE ROLE OF INOSITOL POLYPHOSPHATE 4-PHOSPHATASE TYPE II IN PROSTATE CANCER CELLS AND NORMAL MOUSE PROSTATE 27
2.1. ABSTRACT 27
2.2. INTRODUCTION 27
2.3. RESULTS 31
2.3.1. Loss of INPP4B changes AR transcriptional output. 31
2.3.2. Reciprocal regulation of AR-V7 and INPP4B. 35
2.3.3. INPP4B regulates AR transcriptome via inhibition of PI3K/AKT and PKC signaling pathways. 37
2.3.4. INPP4B signaling in the normal mouse prostate. 39
2.3.5. INPP4B regulates AR transcriptional activity in normal mouse prostate. 42
2.4. Discussion: 44
2.5. Materials and Methods 48

CHAPTER 3: INPP4B PROTECTS FROM METABOLIC DISEASE AND ASSOCIATED DISORDERS. 56
3.1. Abstract 56
3.2. Introduction 56
3.3. Results 60
3.3.1. Accelerated weight gain in Inpp4b deficient male mice fed high fat diet. 60
3.3.2. High levels of inflammatory cytokines and expression of macrophage markers in visceral fat of *Inpp4b* deficient male mice. 62
3.3.3. *Inpp4b* deficient mice develop hyperglycemia on normal low fat diet and type 2 diabetes on high fat diet. 65
3.3.4. Loss of INPP4B leads to NAFLD. 67
3.3.5. NAFLD in *Inpp4b*$^{-/-}$ males is caused by increased lipogenesis, WAT inflammation, and activation of AKT and PKC signaling. 71
3.3.6. HFD causes neoplastic changes in prostates of *Inpp4b*$^{-/-}$ mice. 73
3.3.7. HFD leads to prostate inflammation in *Inpp4b*$^{-/-}$ males. 79
3.4. Discussion 82
3.5. Materials and Methods 85

CHAPTER 4: INPP4B IS ESSENTIAL FOR MAMMARY GLAND BRANCHING AND PROTECTS FROM NAFLD 92
4.1. Introduction 92
4.2. Results 94
4.2.1. INPP4B is positively correlated with ESR1 in human breast cancer. 94
4.2.2. INPP4B and PTEN depletion both modulate ERα transcriptional activity. 96
4.2.3. Differential expression of INPP4B and PTEN regulated genes in breast cancer cells 99
4.2.4. INPP4B is required for optimal expression of progesterone receptor (PR) 101
4.2.5. INPP4B is essential for ductal branching in the mouse mammary gland 101
4.2.6. INPP4B loss caused weight gain and hyperglycemia in mice fed with an HFD 103
4.2.7. Inpp4b loss leads to NAFLD in female mice fed HFD 106
4.2.8. Inpp4b loss caused hyperplasia in mammary gland and expansion in the extracellular matrix (ECM). 108
4.3. Discussion 110
4.4. Materials and methods 115

CHAPTER 5: Summary and future directions 121

REFERENCES 126

APPENDIX 154

VITA 166

LIST OF TABLES

TABLE PAGE

Table 1. Introduction of INPP4B mutation and corresponded activity 8

Table 2. Molecular subtypes of breast cancer..... 16

Table 3. siRNA sequences. 49

Table 4. Antibodies used in CHAPTER 2. 51

Table 5. Primers and corresponding probes used in CHAPTER 2. 52

Table 6. Primers used in ChIP assay. 53

Table 7. Primers and corresponding probes used in CHAPTER 3. 86

Table 8. Antibodies used in CHAPTER 3. 91

Table 9. Primers and corresponding probes used in CHAPTER 4. 117

Table 10. Antibodies used in CHAPTER 4. 118

TABLE OF FIGURES

FIGURE PAGE

CHAPTER 1

Figure 1-1. The structure of phosphatidylinositol..... 1

Figure 1-2. Major phosphoinositide interconversion diagram shows the structure of phosphatidylinositol and its various phosphorylated forms..... 3

Figure 1-3. Introduction of PTEN functional domains..... 5

Figure 1-4. Introduction of INPP4B DNA locus, transcript, and protein domains. 5

Figure 1-5. INPP4B expression in human and mouse tissues 8

Figure 1-6. INPP4B signaling network..... 12

Figure 1-7. Organization of the AR gene and domain of the full length and splice variants' of AR protein. 15

Figure 1-8. Structures of ERs..... 15

Figure 1-9. The diagram shows the generation of *Inpp4b*$^{-/-}$ mouse model. 23

Figure 1-10. Role of INPP4B in human cancers. Each box shows when INPP4B is lost, the phenotype displayed by each type of cancer. 25

CHAPTER 2

Figure 2-1. Loss of INPP4B changes AR transcriptional activity 30

Figure 2-2**.** Correlations between INPP4B expression and AR expression and transcriptional output 32

Figure 2-3**.** INPP4B is required for optimal induction and repression of a subset of the AR target genes 34

Figure 2-4**.** Reciprocal regulation of AR-V7 and INPP4B 36

Figure 2-5**.** Suppression of AKT and PKC signaling contributes to INPP4B regulation of AR transcriptional activity 38

Figure 2-6**.** Body and urogenital organ weight comparison of 2 month old WT and *Inpp4b*$^{-/-}$ male littermates 40

Figure 2-7. Loss of INPP4B in mouse prostate activates PKC and AKT signaling without changing AR levels 41

Figure 2-8. INPP4B is required for optimal expression of a subset of AR target genes in mouse prostate 43

CHAPTER 3

Figure 3-1. *Inpp4b* knockout accelerates adipose tissue expansion in mice on a high-fat diet. 59

Figure 3-2. Morphometric and metabolic response to HFD and INPP4B loss 62

Figure 3-4. INPP4B protects mice from hyperglycemia and diabetes 64

Figure 3-5. Development of hyperglycemia in LFD *Inpp4b*$^{-/-}$ males 66

Figure 3-6. INPP4B protects mice from liver steatosis 68

Figure 3-7. Aberrant lipid storage in livers of *Inpp4b*$^{-/-}$ males 69

Figure 3-8. INPP4B regulates metabolic and PPAR pathways in mouse liver 70

Figure 3-9. INPP4B regulates lipogenesis and AKT and PKC signaling pathways in mouse liver 72

Figure 3-10. Loss of *Inpp4b* leads to the development of PIN and inflammation in obese males. 79

Figure 3-11. Prostate-specific levels of AR, PTEN and inflammation in WT and *Inpp4b*$^{-/-}$ males. 80

Figure 3-12. Loss of INPP4B promotes proliferation in prostatic epithelial cells in obsess male mice 83

CHAPTER 4

Figure 4-1. A positive correlation between INPP4B and ERα in human breast tissue samples 95

Figure 4-2. Both INPP4B and PTEN affect ERα transcriptional activity 97

Figure 4-3. Comparison between INPP4B and PTEN affected genes 98

Figure 4-4. Differential gene expression patterns for INPP4B and PTEN 100

Figure 4-5. INPP4B is required for optimal induction of PR. 102

Figure 4-6. INPP4B is required for mouse mammary gland side branching..... 104

Figure 4-7. Loss of INPP4B activates AKT and PKC pathways..... 105

Figure 4-8. Loss of INPP4B caused weight gain and hyperglycemia in mice fed an HFD..... 107

Figure 4-9. *Inpp4b* depletion leads to NAFLD with fibrosis..... 109

Figure 4-10. INPP4B loss induced hyperplasia in end buds and duct of mouse mammary gland 110

Figure 4-11. Loss of INPP4B causes hyperplasia in the mammary gland and expansion of ECM. 112

LIST OF ABBREVIATIONS

A	Alanine
Adipoq	adiponectin
ADT	Androgen-ablation therapy
Agre	Ampheiregulin
Akt	Protein kinase B
ANOVA	Analysis of variance
AP	Anterior prostate
Apof	Apolipoprotein F
AR	Androgen receptor
ARE	Androgen response element
AR-V7	AR splice variance V7
AZD5363	AKT inhibitor
BIM-I	Bisindolymaleimide I
BRCA	Breast Cancer 3
BSA	Bovine serum albumin
C	Cysteine
Cas	Casodex, bicalutamide
CCK	cholecystokinin
CD36	CD36 Molecule
CD68	CD68 Molecule

CDC	Centers for Disease Control and Prevention
cDNA	complementary DNA
CHD5	Chromodomain Helicase DNA Binding Protein 5
ChIP	Chromatin immunoprecipitation
Clu	Clusterin
CRPC	Castration resistant prostate cancer
CSS	Charcoal stripped serum
CYP24A1	Cytochrome P450 Family 24 Subfamily A Member 1
Cyp2b13	Cytochrome P450 Family 2 Subfamily B Member 13
Cyp2b9	Cytochrome P450 Family 2 Subfamily B Member 9
D	Aspartic acid
DAG	Diacylglycerol
DBD	DNA binding domain
DEG	Differentially expressed genes
DHT	Dihydrotestosterone
DLP	Dorsal lateral prostate
DNL	De novo lipogenesis
DOI	Diet-induced obesity
Dox	Doxycycline
E	Glutamic acid

E2	Estrodiol
ECM	Extracellular matrix
EDN2	Endothelin 2
EDTA	Ethylenediaminetetraacetic acid
EGF	Epidermal Growth Factor
EGR3	Early Growth Response 3
ELISA	The enzyme-linked immunosorbent assay
ER	Estrogen receptor
ERBB3	Erb-B2 Receptor Tyrosine Kinase 3
ERE	Estrogen-responsive element
ERG	ETS Transcription Factor ERG
ERα	Estrogen receptor α
ETV1	ETS Variant 1
eWAT	Epididymal white adipose tissue
F4/80	EGF-like module-containing mucin-like hormone receptor-like 1
FAS	fatty acid synthase
Fasn	fatty acid synthase
FBS	Fetal bovine serum
FKBP5	FKBP prolyl isomerase 5
FOXA1	Forkhead box A1

Furin	Furin, Paired Basic Amino Acid Cleaving Enzyme
GEO	Gene Expression Omnibus
GO	Gene Ontology
GR	Glucocorticoid receptor
GSEA	Gene set enrichment analysis
Hao2	Hydroxyacid Oxidase 2
HER2/ERBB2	Human epidermal growth factor receptor 2
HERC5	HECT And RLD Domain Containing E3 Ubiquitin Protein Ligase 5
HFD	High fat diet
HK2	Hexokinase 2
IGF1	Insulin Like Growth Factor 1
IGFBP1	Insulin Like Growth Factor Binding Protein 1
IGFBP2	Insulin Like Growth Factor Binding Protein 2
IHC	Immunohistochemistry
Il1b	Interleukin 1 Beta
Il6	Interleukin 6
INPP4A	Inositol Polyphosphate-4-Phosphatase Type I A
INPP4B	Inositol polyphosphate-4-phosphatase type II B
INPP5B	Inositol Polyphosphate-5-Phosphatase B
INPP5E	Inositol Polyphosphate-5-Phosphatase E

Ins(1,3,4)P3	Inositol 1,3,4-trisphosphate
INSR	Insulin receptor
IRS	insulin receptor substrate
K	Lysine
KD	Knock down
KEGG	Kyoto Encyclopedia of Genes and Genomes
KIAA1324	Estrogen-Induced Gene 121 Protein
KO	Knock out
LBD	Ligand-binding domain
Lep	Leptin
LEPR	leptin receptor
LFD	Low fat diet
LOH	Loss of heterozygosity
LP	Lateral prostate
M	Methionine
MAFA	MAF BZIP Transcription Factor A
MAPK	microtubule associated protein kinase
MCP-1	Monocyte chemoattractant protein – 1
MDV3100	Enzalutamide
MG	Mammary gland

Mogat1	Monoacylglycerol O-Acyltransferase 1
Msmb	Microseminoprotein Beta
MT2A	Metallothionein 2A
MTMR	MTM related proteins
mTORC2	mTOR Complex 2
MYOF	Myoferlin
NAFLD	Non-alcoholic fatty liver disease
NES	Normalized enrichment scorE
Nkx3.1	NK3 Homeobox 1
NNMT	Nicotinamide N-methyltransferase
NTD	Amino-terminal domain
OGTT	Oral glucose tolerance test
PAGE	Polyacrylamide gel electrophoresis
PBS	Phosphate-buffered saline
Pbsn	probasin
PCR	Polymerase chain reaction
PCSK1	Proprotein Convertase Subtilisin/Kexin Type 1
PDK1	Pyruvate Dehydrogenase Kinase 1
PH	Pleckstrin homology
PI	Phosphatidylinositol

PI(3,4)P2	Phosphatidylinositol 3,4-bisphosphate
PI(3,4,5)P3	Phosphatidylinositol (3,4,5)-trisphosphate
PI(4,5)P2	Phosphatidylinositol 4,5-bisphosphate
PI3K	Phosphoinositide 3-kinases
PI3P	Phosphatidylinositol 3-phosphate
PI4P	Phosphatidylinositol 4-phosphate
PI5P	Phosphatidylinositol 5-phosphate
PIK3CA	Phosphatidylinositol-4,5-Bisphosphate 3-Kinase Catalytic Subunit Alpha
PKC	Protein kinase C
PLA2G2A	Phospholipase A2 group IIA
PLC	Phospholipase C
PPARG	Peroxisome proliferator-activated receptor γ
PR	Progesterone receptor
PSA	Prostate-specific antigen
PTEN	Phosphatase and tensin homolog
PTPMT1	Protein Tyrosine Phosphatase Mitochondrial 1
PTT	Pyruvate tolerance test
PVDF	Polyvinylidene fluoride
RANKL/Tnfsf11	TNF Superfamily Member 11
RAPGEFL1	Rap Guanine Nucleotide Exchange Factor Like 1

RT-qPCR	Quantitative reverse transcription PCR
SDS	sodium dodecyl sulfate
SEM	Standard error of the mean
SGK3	Glucocorticoid-regulated kinase 3
SHIP2	SH2 domain-containing inositol 5'-phosphatase
siRNA	Small interfering ribonucleic acid
SMAα	Smooth muscle actin alpha
SREBP1/Srebf1	Sterol Regulatory Element Binding Transcription Factor 1
SYTL2	Synaptotagmin like 2
T2D	Type 2 diabetes
TARP	TCR gamma alternate reading frame protein
TBS	Tris-buffered saline
TCGA	The Cancer Genome Atlas
Tet	Tetracycline
TMEM55A	Phosphatidylinositol-4,5-Bisphosphate 4-Phosphatase 2
TMEM55B	Phosphatidylinositol-4,5-Bisphosphate 4-Phosphatase 1
TMPRSS2	Transmembrane serine protease 2
TNBC	Triple-negative breast cancer
Tnf	Tumor Necrosis FactoR
UGT2B17	UDP Glucuronosyltransferase Family 2 Member B17

UPR	unfolded protein response
Vldlr	Very Low Density Lipoprotein Receptor
WAT	White adipose tissue
WNT4	Wnt Family Member 4
WT	Wild-type

CHAPTER 1: INTRODUCTION

1.1. Phosphoinositide and phosphatidylinositol signaling

Phosphatidylinositol (PI) is an important lipid component of the cell membrane that activates essential metabolic processes and signal transduction. PI is an acidic phospholipid that consists of a glycerol backbone connected with two fatty acid chains inserted into the cytosolic layer of the cell membrane and esterified with phosphate connected to a water-soluble inositol head group (Figure 1-1). Phosphorylation of the inositol hydroxyl groups at D-3, D-4, or D-5 position creates various phosphoinositides with distinct signaling functions: PI3P, PI4P, PI5P, PI(3,4)P2, PI(4,5)P3, PI(3,5)P2, PI(3,4,5)P3 (Figure 1-2).

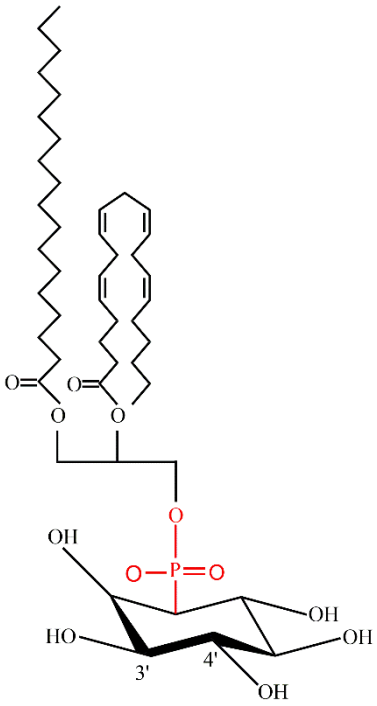

Figure 1-1. The structure of phosphatidylinositol.

Phosphoinositides are a family of phospholipids found in both the plasma and cytoplasmic membranes (1). They play an essential role in signal transduction, intracellular membrane trafficking, cytoskeleton remodeling, cell growth, and survival (2, 3). The maintenance of phosphoinositide homeostasis is critical for the cellular function. The conversion between different types of phosphoinositides is mainly dependent on phosphoinositide phosphatases and kinases (4, 5). Currently, there are 35 phosphatases have been identified in mammals (1). The inositol polyphosphate 3-phosphatases include myotubularin (MTM), MTM related proteins (MTMR), and phosphatase and tensin homolog deleted on chromosome 10 (PTEN). The inositol-4-phosphatases include four enzymes: INPP4A, INPP4B, TMEM55A, and TMEM55B, which preferentially dephosphorylate 4-phosphate. There are ten known 5-phosphatases, which include INPP5B, INPP5E, OCRL1, PIPP, SAC2, SHIP1/2, SKIP, and SYNJ1/2 (1). Some other phosphatases can remove 2 or more phosphate groups simultaneously. Changes or mutations of phosphoinositide phosphatases have been implicated in diabetes, cancer, cardiovascular, and neuronal diseases (2, 3, 6). Among phosphatidyl polyphosphate phosphatases, INPP4B and PTEN display the most significant structural and functional similarity.

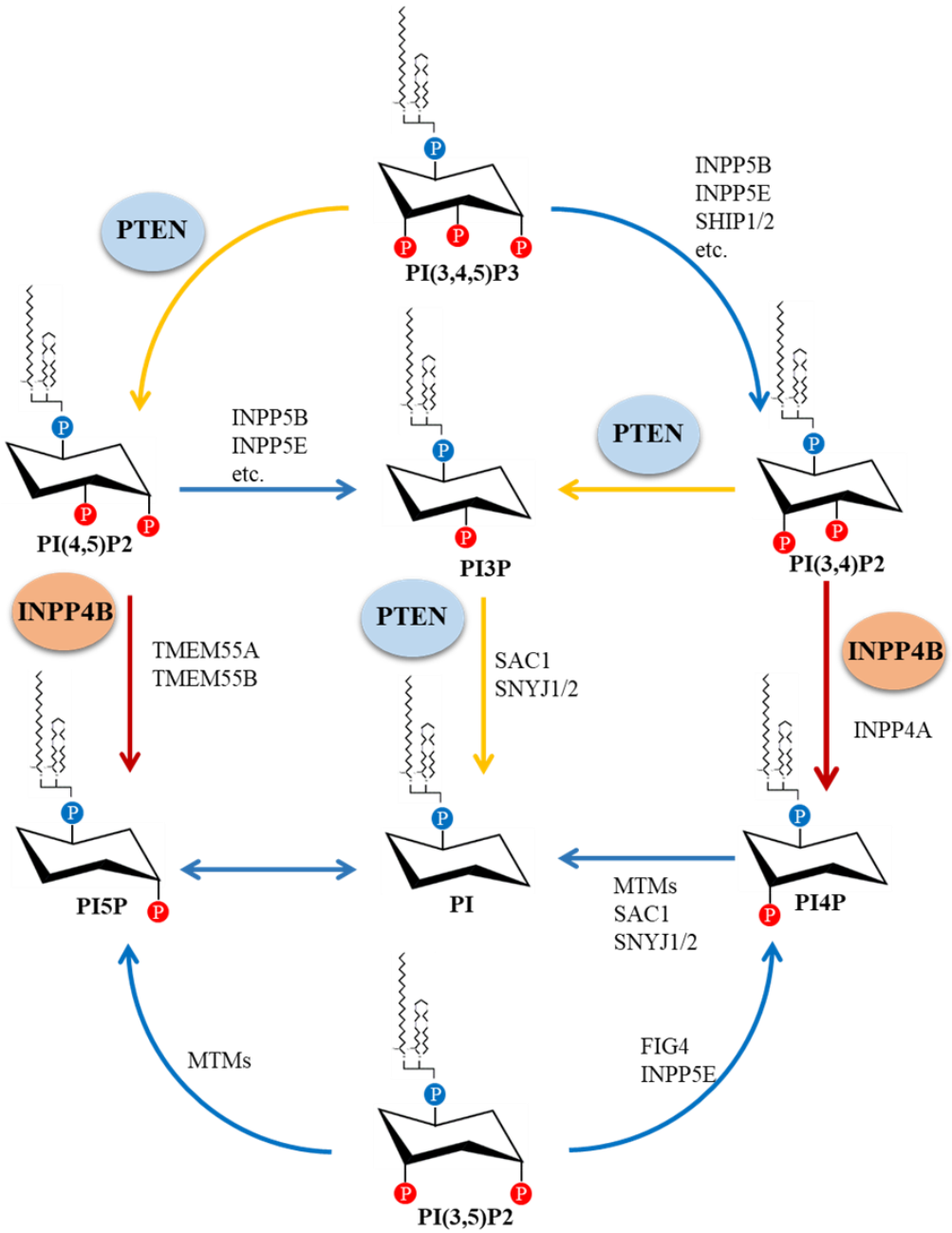

Figure 1-2. Major phosphoinositide interconversion diagram shows the structure of phosphatidylinositol and its various phosphorylated forms.

1.2. Inositol polyphosphate 3-phosphatase: PTEN

PTEN is the most well-described phosphoinositide phosphatase. PTEN functions as a phosphoinositol phosphatase that can hydrolyze the phosphate at D-3 position of the inositol ring of PI(3,4,5)P3, PI(3,4)P2, PI3P, and Ins(1,3,4,5)P4 (7, 8). Loss of heterozygosity of PTEN is observed in human cancers (2, 9). Somatic homozygous mutations of PTEN have been found in human glioblastoma, prostate, kidney, lung, endometrial, bladder, and breast cancer (10-13). The germline mutations of PTEN are associated with Cowden's disease (14). In the mouse model, the homozygous PTEN knockout causes embryonic lethality (15) while the heterozygous PTEN knockout results in the development of neoplasias in colon, prostate, uterus, and thyroid (15-17). Previous studies demonstrated that PTEN functions as a tumor suppressor by negatively regulating oncogenic PI3K/AKT pathways. The tumor suppressor function of PTEN mainly depends on lipid phosphatase activity. However, Jiang et al. have shown that PTEN directly dephosphorylated Insulin receptor substrate (IRS1), a mediator of insulin/IGF1 signaling, through protein tyrosine phosphatase activity (18).

The crystal structure analysis revealed that PTEN has an N-terminal dual-specificity phosphatase domain that consists of five standard central β sheets surrounded by six α helices. Carboxyterminal region contains a C2 domain formed by two antiparallel β sheets connected by two short α helices and a PDZ-binding domain (8, 19, 20) (Figure 1-3). The N-terminal domain includes a consensus dual-specificity phosphatase catalytic motif CX_5R that forms an active-site pocket to accommodate not only PI(3,4,5)P3 but also phosphoproteins (19). The C2 domain binds phospholipids while the PDZ-BD is involved in protein-protein interactions (8, 21).

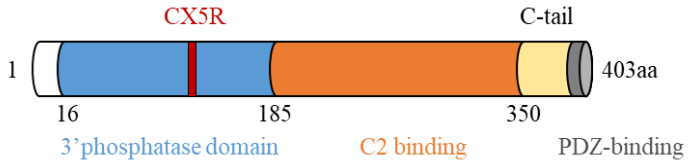

Figure 1-3. Introduction of PTEN functional domains. The human PTEN has four functional domains: N-terminal 3'phosphoase domain (blue) with catalytic motif (C124X5R) of dual-specificity phosphatase, a C2 binding domain (orange), a carboxyl-terminal tail domain (C-tail) (yellow), and a PDZ-binding domain (PDZ-BD) (grey).

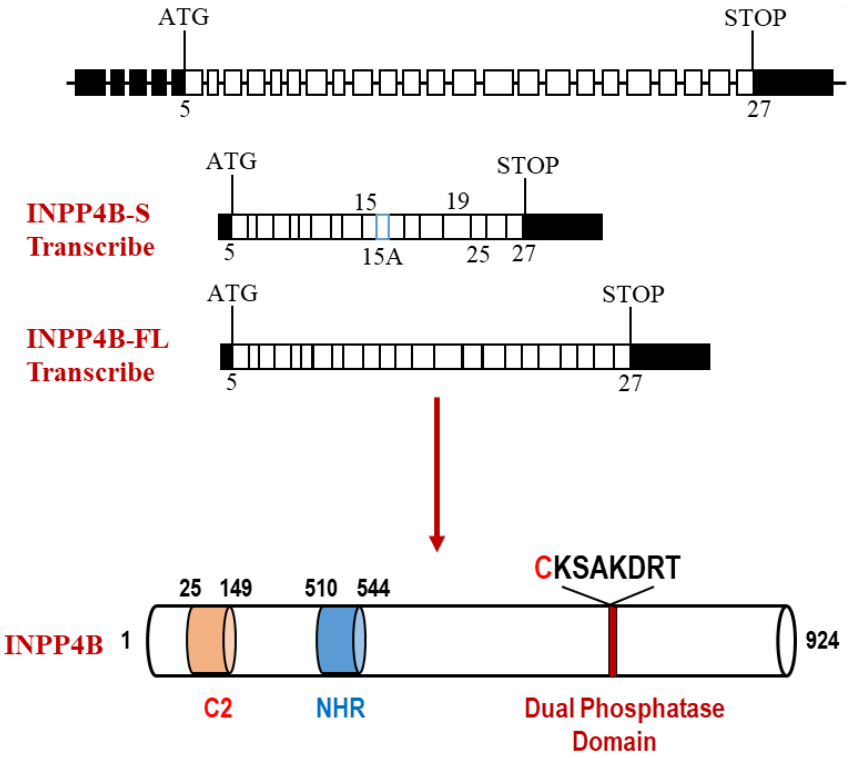

Figure 1-4. Introduction of INPP4B DNA locus, transcript, and protein domains.

1.3. Inositol polyphosphate 4-phosphatase: INPP4B

1.3.1. Gene locus, splice variants and patterns of protein expression of INPP4B

First INPP4 transcript was isolated from rat brain in 1995 (22) and subdivided into two classes, INPP4A and INPP4B. The INPP4B function was firstly reported by Norris et al. in 1997 (23). The human INPP4B gene is around 824 Kb and is located on chromosome 4q31.21, as seen in Figure I-4. Human INPP4B is comprised of 27 exons of which 23 are protein-coding (Ensembl). The coding region starts from exon 5 and ends in exon 27 (24) (Figure I-4). Croft et al. recently isolated a novel variant of INPP4B, called INPP4B-S; this variant incorporates extra 27 bp from the sequence between exon 15 and 16 whereas the exons 20-24 are spliced. The mouse *Inpp4b* gene is located on chromosome 8, and the mouse INPP4B protein has two isoforms INPP4Bα and INPP4Bβ that are produced by alternative splicing. The INPP4Bα distributed in the cytoplasm while INPP4Bβ localized to the Golgi apparatus (25). Both isoforms are similar to the human and rat homologs. The INPP4B is widely expressed in multiple human and murine tissues such as breast/mammary gland, ovary, adipose tissue, bladder, testis, prostate, etc. (Figure 1-5 A-B)

1.3.2. Biochemistry and structure of INPP4B

The human INPP4B is similar in structure to PTEN. It has a conserved C2 lipid-binding domain at the N terminus, an NHR2 domain, and a C-terminal dual phosphatase domain, as seen from Figure I4 (25, 26). The dual phosphatase domain allows INPP4B to function as a dual-specificity phosphatase, capable of dephosphorylation of both lipid and protein substrates (27). Multiple studies have shown that INPP4B preferentially binds with PI(3,4)P2, PI(4,5)P2, and Ins(1,3,4)P3 (23, 28, 29). However, low but biologically

significant levels of PI(3,4,5)P3 hydrolysis by INPP4B were observed in murine thyroids (31). Our lab has shown that INPP4B reduces the phosphorylation of tyrosines on the AKT (32). Guo et al. have shown that INPP4B dephosphorylates PTEN, which causes downregulation of PTEN in colon cancer (33).

Unlike PTEN, INPP4B mutations are not frequently observed in human cancers. Our lab previously generated the mutation of cysteine in the catalytic site CX_5R of INPP4B gene. The C842A mutation abolishes both lipid and phosphatase activity (28, 32) ( ). The K846M mutation completely abolishes lipid phosphatase activity but does not affect the phosphoprotein phosphatase activity (PTP) (32). The INPP4B D847E mutant ablates the PTP activity and significantly reduces the phosphatase activity of lipid substrates, PI(3,4)P2 and PI(4,5)P2 (32).

Table 1. Introduction of INPP4B mutation and corresponded activity

Mutation of INPP4B	Lipid phosphatase activity			Protein phosphatase activity
	PI(3,4)P2	PI(4,5)P2	I(1,3,4)p3	
C842A/S	Abolished	Abolished	Abolished	Abolished
K846M	Abolished	Abolished	Abolished	Remained
D847E	Abolished	Abolished	Reduced	Abolished
K843M	Abolished	Unchanged	Reduced	Increased

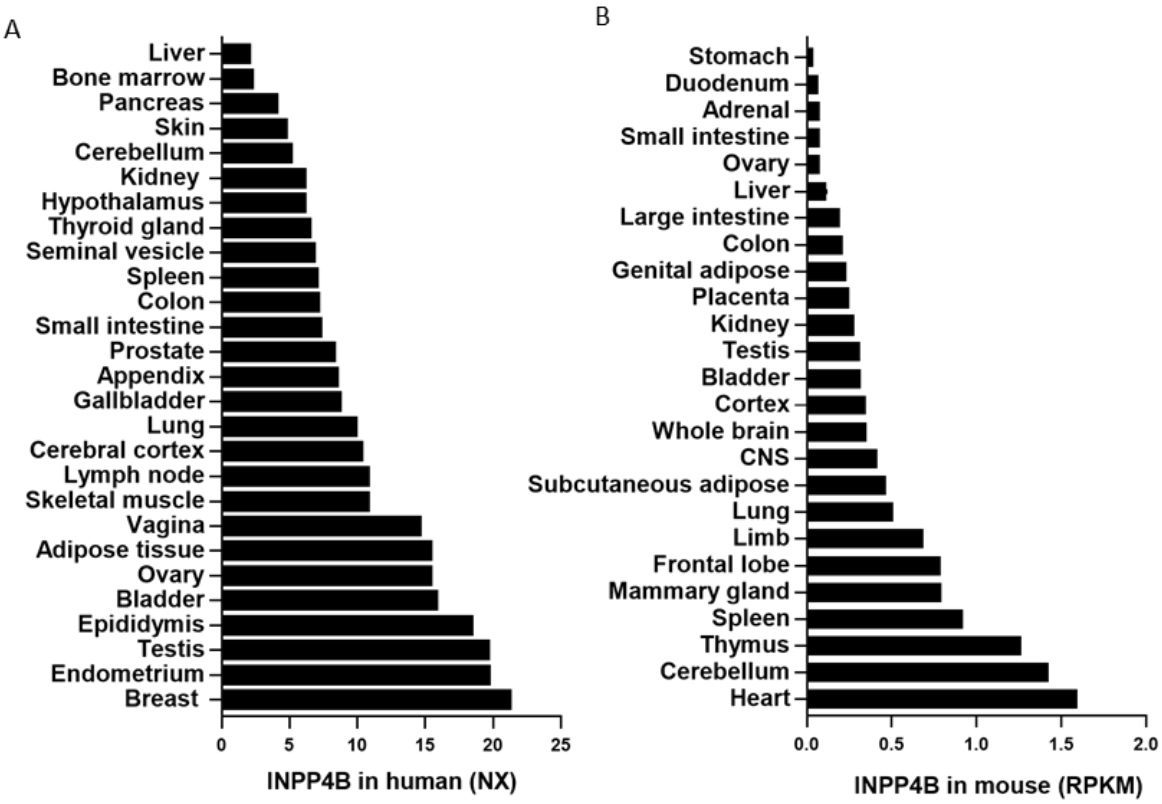

Figure 1-5. INPP4B expression in human and mouse tissues. (A) Comparative INPP4B expression in 27 human tissues were determined by RNA-sequencing. The RNA levels were presented in Consensus Normalized eXpression (NX) and data were acquired from The Human Protein Atlas (proteinatlas.org). (B) INPP4B expression in different mouse tissues from 123 mouse cell types and primary tissues (RPJNA66167) (30). Data were presented in Reads Per Kilobase of transcript (RPKM).

1.3.3. PI signaling network (Figure 1-6)

Class I PI3Ks synthesize the lipid messenger PI(3,4,5)P3. PTEN, dephosphorylates PI(3,4,5)P3, another lipid messenger that can activate the AKT pathway. PTEN is known as a tumor suppressor in prostate cancer not only because of the inhibition of AKT signaling, but also because the loss of PTEN in prostate cancer promotes the expression of androgen receptor (AR) and amplifies AR transcriptional activity. The activation of AR is essential for prostate development and initiation and progression of prostate cancer (34, 35). When PTEN is deficient in thyroid tumors, INPP4B suppresses tumor proliferation by dephosphorylating PI(3,4,5)P3 (31).

The two lipid substrates of INPP4B, PI(3,4)P2 and PI(4,5)P2, are important second messengers for AKT and PKC signaling (Figure I6). AKT is known as a serine/threonine protein kinase and an effector of PI3K signaling (it is activated in a PI3K-dependent manner) (36, 37). The PI3K products, PI(3,4,5)P3 and PI(3,4)P2, recruit AKT to the membrane by binding to the C-terminal pleckstrin homology (PH) domain (38), which results in the conformation change in AKT leading to the phosphorylation by PDK1/mTORC2 at Thr308 and Ser473 (39). The AKT pathway has more than 200 known protein downstream targets that are involved in protein synthesis, survival, migration, proliferation, and glucose metabolism (40, 41). The AKT signaling is oncogenic in numerous tissues such as lung, ovary, breast, and prostate (42-45). INPP4B dephosphorylates PI(3,4)P2 and inhibits oncogenic AKT pathway in breast, ovarian, thyroid, and prostate cancers (29, 31, 46, 47). Therefore, INPP4B is considered as a tumor suppressor in these epithelial cancers.

PI(4,5)P2 is another lipid substrate of INPP4B and is hydrolyzed by phospholipase C (PLC) into inositol triphosphate and diacylglycerol (DAG). DAG activates both conventional (α,β,γ) and novel (ε,δ,η,θ) kinases of the PKC family (48-50). The atypical PKC isoforms (ζ and ι/λ) are activated by lipid membrane components other than DAG (51). Protein levels of PKC α, ε, ζ are increased in prostate and other cancers (52). We have previously shown that INPP4B suppresses PKC signaling in prostate cancer cells and normal mouse prostate (53, 54).

In turn, Akt directly binds and phosphorylates AR on serines 213 and 791 (55-58). Phosphorylation of these sites affects AR activity in a cell-specific manner (56, 57). INPP4B regulates both Akt and PKC activity and is capable of dephosphorylating phosphoproteins opening a possibility for either direct or indirect regulation of AR phosphorylation and activity. To date, numerous publications suggest that INPP4B is playing essential roles in the prostate, breast, ovarian, and other cancers.

1.4. Prostate cancer and INPP4B role in prostate cancer

1.4.1. Prostate cancer requires androgen receptor (AR) for initiation and progression

Prostate cancer is the second most common male malignancy and the second leading cause of cancer death for men in America (59). In 2018, 164,690 men were diagnosed with prostate cancer, and around 18% of them have died (60). Localized prostate cancer is managed with radical prostatectomy. Once the cancer spreads beyond the prostate capsule, androgen-ablation therapy (ADT) is the first-line treatment (61). Effective at first, this treatment always leads to biochemical recurrence of castration-resistant prostate cancer (CRPC). The pathogenesis of prostate cancer progression mainly depends on the activation

of the AR signaling (62). Treatment with androgen receptor inhibitors such as enzalutamide (MDV3100) or abiraterone, prolongs patient survival but inevitably results in the emergence of adaptive AR signaling and resistance to castration therapies (63). Death from prostate cancer is due mainly to the development of metastatic castration-resistant prostate cancer (CRPC) (64). The high risk of advanced prostate cancer and the development of resistance after treatment underscore the importance to identify more effective targets for prostate cancer, especially for CRPC (60, 64, 65).

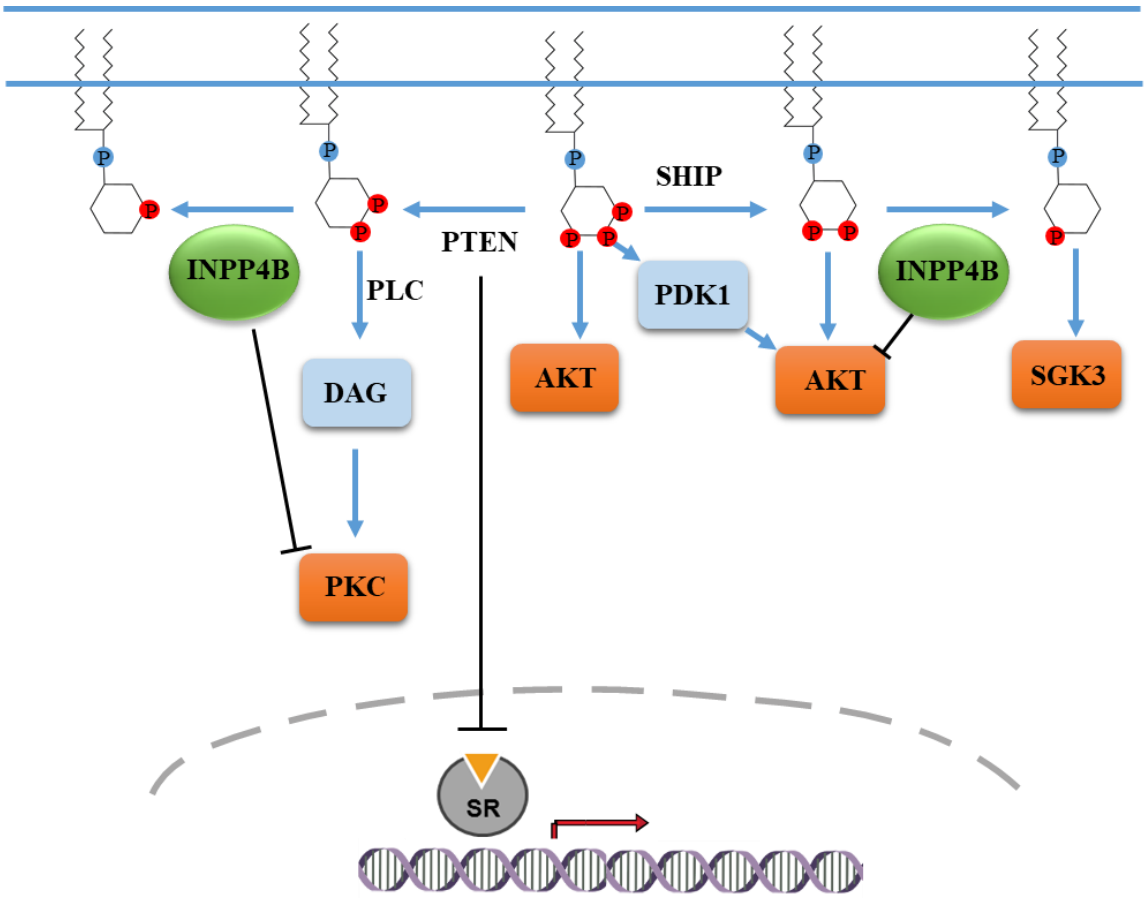

Figure 1-6. INPP4B signaling network. In response to the extracellular signals, PI3K, PI4K, and PI5K generate diacylglycerol derivatives (PI3P, PI(3,4)P2, PI(4,5)P2, PI(3,4,5)P3) that are important for the activation of downstream pathways including AKT and PKC pathways. The AKT and PKC pathways can phosphorylate the AR and change AR transcriptional activity. PTEN, 3'-phosphatase, terminates downstream signaling by dephosphorylating PI(3,4,5)P3. PTEN suppresses AR activity and AR stability through the AKT pathway. INPP4B, 4'-phosphatase dephosphorylates PI(3,4)P2 that activates AKT pathway, and PI(4,5)P2 that activates PKC pathway. Additionally, INPP4B enhances SGK3 activation by producing PI3P. SHIP, 5'-phosphatase converts PI(3,4,5)P3 to PI(3,4)P2.

1.4.2. AR structure and AR splice variants

The AR signaling is required for the development, function, and homeostasis of the prostate, as well as the initiation and proliferation of the prostate cancer. AR is a ligand-dependent transcription factor that regulates gene expression. The AR protein has an amino-terminal domain (NTD), a DNA binding domain (DBD), a hinge region, and a ligand-binding domain (LBD) (Figure 1-7) (66, 67). The classical action of AR signaling starts with the binding of androgen to LBD of AR, causing translocation of AR into the nucleus where AR dimerizes and binds to the androgens response element (ARE) in the promoter region of the target genes and recruits the other transcriptional coregulators to facilitate transcription(68).

Various mechanisms contribute to the development of CRPC. The AR signaling can be activated by altered expression of AR coregulators, overexpression of AR, gain-of-function mutations, and alternative splicing of AR mRNA (69-71). Expression of AR splice variants that lack ligand-binding domain in advanced prostate cancer stimulates AR activity during castration therapies (Figure 1-7). The lack of LBD allows these active isoforms to regulate gene expression independently of ligand. Another mechanism of antiandrogen resistance is upregulation of the glucocorticoid receptor (GR) (72). The ChIP-sequencing data revealed that AR and GR share highly overlapping cistrome profiles suggesting the GR activation can restore expression of a subset of AR target genes that are involved in cellular proliferation and resistance to therapies (72, 73). Additionally, the resistance can also be induced by overexpression of AR coregulators (74) or ligand-independent AR activation via cytokines or growth factors such as, IL6 or IGF1 (75). Thus, AR is a pivotal factor in prostate cancer initiation and its progression to CRPC (68).

1.4.3. The tumor-suppressive function of INPP4B in prostate cancer

A global analysis of copy number alteration, transcriptome, and mutation data from 181 primary prostate tumors and 37 metastatic tumors has revealed that INPP4B is lost in 8% of the primary tumors and 47% of the metastasis (76). Using prostate tissue microarrays, our laboratory has shown INPP4B protein level is reduced in human prostate cancer compared to healthy prostate specimens (47). Our laboratory is the first to demonstrate INPP4B tumor-suppressive function in prostate. We have shown that the loss of INPP4B is associated with accelerated biochemical recurrence in high proliferating prostate tumors (47). In prostate cancer cells, AR binds to INPP4B locus and induces INPP4B expression. INPP4B suppresses oncogenic AKT pathway, inhibit cell proliferation, migration, and invasion *in vivo* (47, 53, 77).

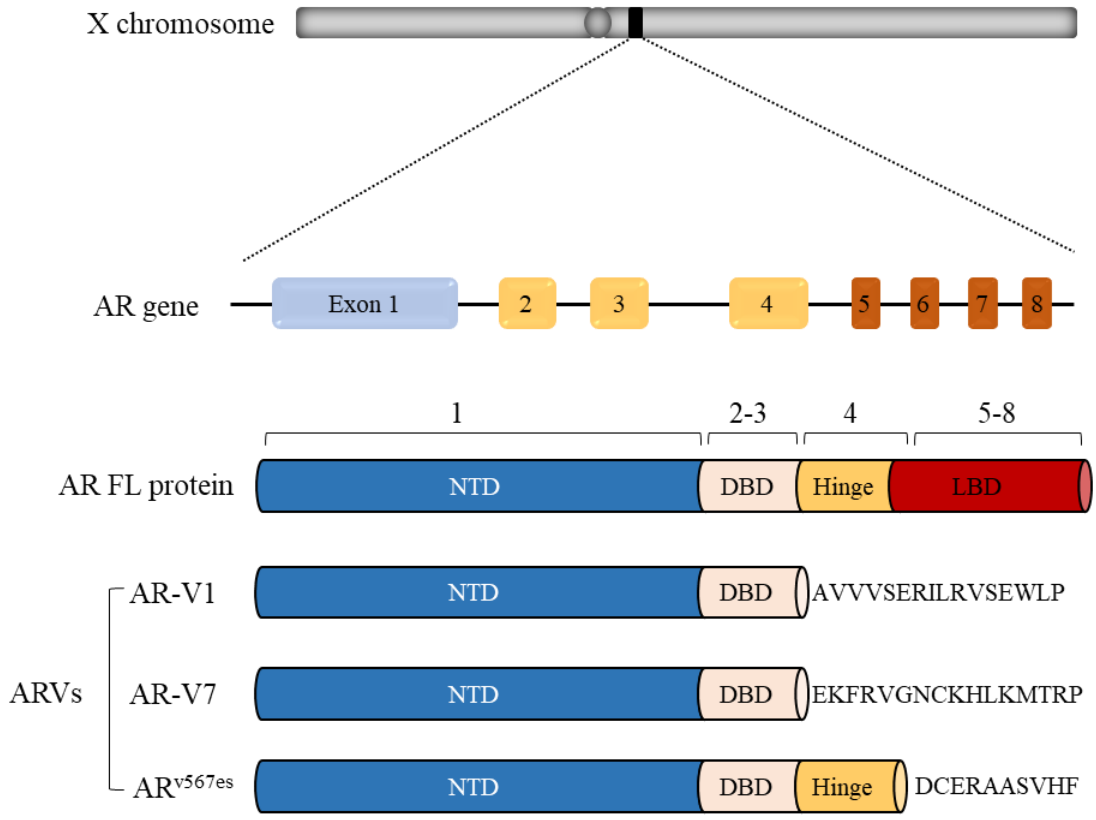

Figure 1-7. Organization of the AR gene and domains of the full length and splice variants' of AR protein.

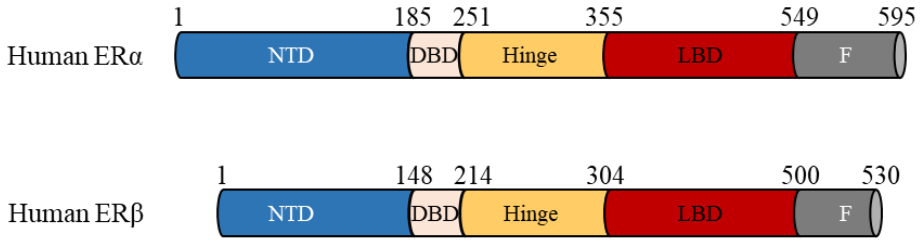

Figure 1-8. Structures of ERs.

1.5. Breast cancer and INPP4B role in breast cancer

1.5.1. Four major subtypes of breast cancer

Breast cancer has the second highest incidence and mortality rates in women after cutaneous cancers (CDC). Currently, four major molecular subtypes of breast cancer have been identified that exhibit distinct levels of expression of estrogen receptor α (ERα) and progesterone receptor (PR), and human epidermal growth factor receptor 2 (HER2). These subtypes include luminal A, luminal B, HER2-positive, and triple-negative breast cancer (Table 2) (78). The luminal A breast cancer has a relatively low proliferation rate, while the triple-negative breast cancer has the worst patient survival.

Table 2. Molecular subtypes of breast cancer

Subtypes	**Characteristics**			**Proliferation rate**	**INPP4B level**	**Therapies**
	ERα	PR	HER2			
Luminal A	+++	+++	-	Low (+)	+++	Hormone therapy
Luminal B	+	+	+/-	++	+~+++	Chemotherapy and hormone therapy
HER2 enriched	-	-	+	+++	+	Chemotherapy and treatment targeted to HER2
Triple-negative	-	-	-	++++	-	Chemotherapy

1.5.2. ERα and PR

ER are hormone receptors of the nuclear receptor family and has a similar structure as AR (Figure 1-8). The estrogen and ER complex bind to the estrogen-responsive element (ERE), recruit cofactor and regulate the expression of a subset of genes. The estrogen is important

to stimulate the development of normal breast and promote progression of breast cancer. Alternatively, the growth factors like EGF or IGF can phosphorylate ER to mediate ER-mediated transcriptional regulation (79). ERα and ERβ, encoded by ESR1 and ESR2 respectively, are two distinct estrogen receptors (ER). ERα and ERβ have distinct expression patterns and some structural differences in NTD and LBD (Figure I8). Indeed, ERα but not ERβ is required for the development of the mammary gland structure (80). More importantly, estrogen promotes proliferation in the presence of ERα but suppresses proliferation with ERβ that makes ERβ a potential therapeutic target (81).

Among breast cancer patients, more than 70% of breast cancers express ERα (82). Both luminal A and B breast cancers expresses ERα and PR but at different levels. ERα functions as an estrogen-activated transcription factor and regulates a variety of genes that govern cell proliferation and survival in cancerous and non-cancerous breast epithelial cells (83). Even though patients whose tumors are ERα-positive mostly benefit from ER antagonists and inhibitors of estrogen synthesis, both early or late relapses still occur. Some of the main mechanisms of resistance are the activation of signaling pathways such as PI3K/Akt and p44/42 MAPK which phosphorylate and activate ER independently of ligand binding (84-86).

Currently, both ERα and PR are used as biomarkers and targets in breast cancers. PR is an ERα regulated gene and has two isoforms PRA and PRB that are encoded by the same gene PGR. Progesterone mediated activation of PR is known to inhibit ERα activity and estrogen-induced tumor growth (87, 88). Depletion of PR does not affect the establishment of mammary gland structure but affects mammary ductal branching (89).

1.5.3. HER2 enriched breast cancer

Human epidermal growth factor receptor 2 (HER2) is a transmembrane receptor tyrosine kinase that regulates cell differentiation, proliferation, and survival. Even though HER2 does not have its own ligand, it is activated by dimering with other HER family members in breast cancer enriched with HER2 (90). Estrogen mediated activation of ER signaling can also activates HER signaling (91). HER2 is amplified in 15–20% of breast cancers (92). Specific treatments for HER2-enriched breast cancer include tyrosine kinase inhibitors (lapatinib) and recombinant humanized monoclonal antibodies that inhibit HER2 dimerization or binding to HER3 (pertuzumab or trastuzumab) (93).

The activation of HER2 signaling in breast cancer promotes tumor cell proliferation through various pathways including oncogenic PI3K/AKT/mTOR signaling and MAPK signaling (94). PTEN loss is considered as a potential predictor to evaluate whether patients could benefit from anti-HER2 treatments (95). INPP4B level is reduced in HER2-enriched breast cancers (96) suggesting a tumor-suppressive function of INPP4B in HER2-enriched cancer.

1.5.4. Triple-negative breast cancer (TNBC)

Approximately 10-20% of breast cancers are classified as TNBC characterized by high proliferative rate and relatively poor survival compared to the other types of breast cancers. TNBC is characterized by increased inflammatory infiltrates and a mesenchymal phenotype which are a characteristic of advanced breast carcinomas (97). TNBC is defined by the absence of ER, PR, and HER2, all of which are used as therapeutic targets. Therefore, chemotherapy is the primary established treatment for TNBC patients.

Currently, there are studies to explore novel approaches targeting damage and repair pathways, androgen-mediated signaling, PI3K pathway, among others (97, 98).

1.5.5. Paradoxical role of INPP4B in breast cancer

In human mammary epithelial cells, knockdown of INPP4B activates AKT pathway and facilitates cell motility, proliferation, anchorage-independent growth, and three-dimensional growth (29, 46). Overexpression of INPP4B in a xenograft mouse model suppresses tumor growth (29). INPP4B protein is highly expressed in luminal tumors (82). In $ER\alpha^{+}$ breast cancer, there is a tight correlation between INPP4B and ERα (46). In basal-like cancers, loss of INPP4B expression is 61% specific and 99% sensitive with the highest odds ratio at 108 among all other biomarkers (99). Loss of heterozygosity (LOH) of INPP4B is common in triple-negative breast cancer (46). This suggested that INPP4B is a marker for triple-negative breast cancer (46, 99). However, in a subset of breast cancer, INPP4B can play a tumor-promoting role. Gasser et al. have demonstrated that glucocorticoid-regulated kinase 3 (SGK3), a protein amplified in *PIK3CA* mutant breast cancers, is essential for the proliferation and migration of breast cancer cells (100, 101). SGK3 is a PI3K effector and overexpression of SGK3 activates AKT signaling. A product of INPP4B lipid phosphatase enzymatic activity, PI3P, activates SGK3. The knockdown of INPP4B abolishes SGK3 mediates cell growth (101).

1.6. Crosstalk between INPP4B regulated signaling and metabolic disorders

Currently, the known roles of INPP4B in normal physiology are restricted to regulation of osteoclastogenesis and protection from osteoporosis (28). No reports are published on the role of INPP4B in metabolic pathways. However, its direct downstream targets, Akt and PKC, are intricately involved in obesity-related metabolic disorders.

1.6.1. Metabolic disorders

The prevalence of obesity in the United States has been increasing for almost 50 years (102). Currently, more than two-thirds of adults are overweight or obese. The high caloric diet induced obesity is recognized as a leading cause of metabolic disorders and chronic inflammation which increase the risk of health complications including insulin resistance, cardiovascular disease, type 2 diabetes (T2D), non-alcoholic fatty liver disease (NAFLD), and even cancers (103, 104). All of these are affecting a large number of people and lead to increased morbidity and mortality rates (105, 106).

In 2015, around 35% of the US population were pre-diabetic or were diagnosed with diabetes. Taking into account the underreporting of these conditions, the prevalence of prediabetes and diabetes is likely more than 50% (107). The nutritional excess is a major cause of T2D that is universally represented by an insufficient insulin sensitivity and impaired blood glucose clearance. The hormone insulin is secreted by the beta cells of the pancreas, binds with insulin receptor (INSR) on the plasma membrane, and promotes the uptake of glucose into liver, muscle, and adipose tissues (108). The disruption of insulin signaling causes hyperglycemia, followed by hyperinsulinemia and subsequent T2D in mice and humans (109).

In normal condition, insulin suppresses adipocyte lipolysis, a metabolic process that breaks down triglycerides into fatty acid and glycerol (110). Rats fed with high fat diet develop insulin resistance associated with reduced insulin-mediated inhibitory action on lipolysis (111). This phenomenon causes the release of excessive fatty acid and glycerol from adipose tissue, promotes the hepatic glucose production, and eventually leads to the

elevated blood glucose (112, 113). Therefore, it is important to study the insulin signal transduction and the factors that induced insulin resistance.

1.6.2. AKT signaling under normal diet or high fat feeding conditions

To maintain the glucose homeostasis, insulin signaling suppresses gluconeogenesis in the liver through the AKT pathway. Under normal condition, insulin-mediated AKT pathway suppresses Foxo1 and down regulates key enzymes that are involved in gluconeogenesis (114, 115). With the feeding of high-fat diet (HFD), the insulin mediated inhibition of Foxo1 is abolished. The upregulated Foxo1 increases the level of gluconeogenesis leading to high blood glucose (112). On the other hand, AKT pathway is activated by insulin signaling and promotes de novo lipogenesis (DNL), a process of fatty acid synthesis. In diabetic models, the stimulation of DNL results in the development of NAFLD, characterized by the accumulation of ectopic lipid content in hepatocyte. The inhibition of AKT or AKT downstream target mTOR blocks the insulin-induced upregulation and activation of SREBP1 (116, 117). Overexpression of SREBP1, a primary transcriptional regulator of DNL, causes liver steatosis (118). From healthy state to T2D state, insulin resistance selectively lost regulation on gluconeogenesis whereas insulin signaling continues to active lipogenesis leading to hyperglycemia and hypertriglyceridemia (119) (120).

1.6.3. Activation of PKC pathways under obese conditions

The ectopic lipid accumulation in the insulin-resistant state can lead to abnormal activation of intracellular signaling pathways. PI(4,5)P2 is cleaved by PLC into diacylglycerol (DAG) and phosphoinositol. DAG is a lipid metabolite that binds and activates conventional PKCs and novel PKCs as mentioned in the previous section. Early reports link the accumulation

of DAG with insulin resistance. In turn, the activated PKC signaling further impairs insulin resistance (106). Studies have shown that in obese rodents with T2D, the level of PKCα, β, δ, ε, and ζ are significantly increased compared to lean rodents (121, 122). Dr. Shulman and his group demonstrated that the activation of PKCε is involved in the developing of hepatic insulin resistance (123). The whole-body or liver-specific inactivation of PKCδ enhances the insulin signaling and suppresses the gluconeogenetic and lipogenic function (124). Consistently, overexpression PKCs causes hepatic steatosis, insulin resistance, and glucose intolerance (124, 125). One potential mechanism contributing to the PKCs induced impairment of insulin signaling is that the PKC phosphorylates IRS-1 at S1101, which has been shown to block IRS-1 tyrosine auto-phosphorylation and activation of the AKT pathway (126).

1.7. INPP4B knockout (*Inpp4b*$^{-/-}$) mouse model

Mouse INPP4B protein shares 96% identity with human INPP4B and has the same functional domains (25). C2 lipid-binding domain of INPP4B is 91% identical between human and mouse (127). We used INPP4B knockout mouse model to investigate the role of INPP4B in normal physiology of lean and obese mice. The *Inpp4b*$^{-/-}$ mouse model was generated and kindly provided by Dr. Jean Vacher. The *Inpp4b*$^{-/-}$ mouse model was created by inserting LoxP sites into introns surrounding exon 11 of *Inpp4b* (Figure 1-9). Deletion of exon 11 during Cre-Lox germ line recombination led to frame shift in the mRNA and generation of STOP codon at 217 codon (28). Using this mouse model, Dr. Vacher's group described INPP4B as a negative regulator of the osteoclastogenesis and bone mass (28).

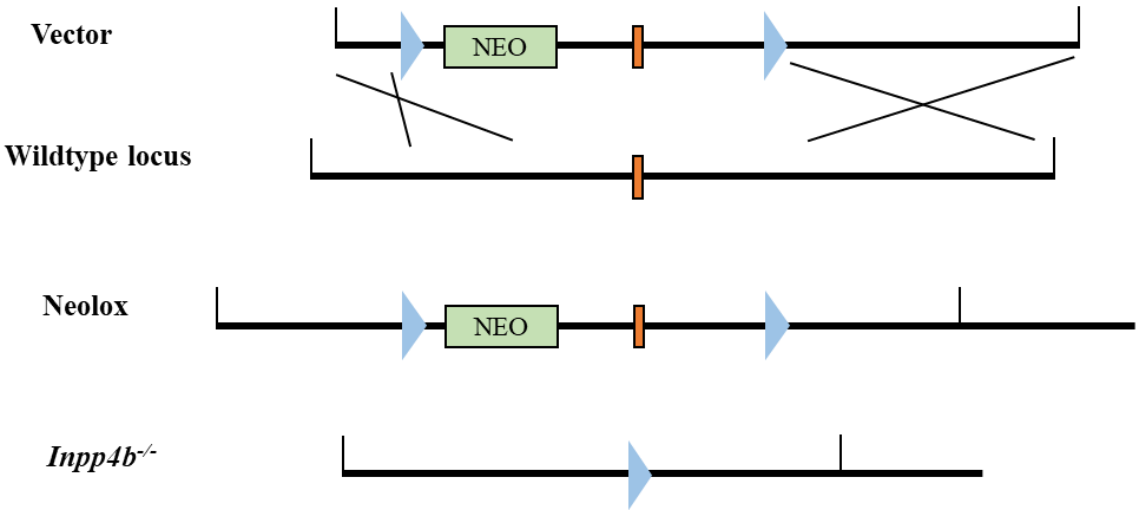

Figure 1-9. The diagram shows the generation of *Inpp4b*$^{-/-}$ mouse model.

1.8. OVERVIEW

Tumor suppressors are proteins that help control cell growth. The studies of tumor suppressor reveal potential mechanisms to inhibit tumor cell growth, which might contribute to the development of novel treatments. INPP4B and its enzymatic activity as a dual-specificity phosphatase were first described in 1997 (128). However, the physiological functions of INPP4B remained unknown until 2005, when an RNAi-based genetic screening revealed that INPP4B might be a suppressor of neoplastic transformation of the mammary epithelial cells (129). Multiple subsequent studies identified the tumor-suppressive function of INPP4B in different types of malignancies. Barnache et al. revealed that INPP4B was lost in malignant proerythroblasts with reduced AKT activation (130). Gewinner et al. first demonstrated that INPP4B is a tumor suppressor in breast and ovarian cancers (29). Our lab has described the tumor-suppressive function of INPP4B in prostate cancer (47). With the accumulation of evidence, INPP4B is now emerging as a tumor

suppressor in multiple epithelial cancers including prostate, breast, ovarian, thyroid, and bladder cancers (29, 31, 46, 47, 131) (Figure 1-10).

In our previous publications, we showed two of the INPP4B lipid substrates, PI(3,4)P2 and PI(4,5)P2, activate AKT and PKC signaling, respectively. INPP4B-mediated inhibition of tumor growth depends mainly on the suppression of oncogenic AKT pathway. In obese mice and humans, PKC signaling is activated in livers, skeletal muscles, and adipose tissues. Activation of PKC is tightly associated with the ectopic lipid accumulation and insulin resistance in liver and muscle of obese model (123). While there is ample evidence of INPP4B tumor suppressive function, its physiological roles in metabolism and homeostasis of healthy tissues are not known. Therefore, I set out to delineate the mechanisms of tumor suppressive functions of INPP4B in breast and prostate cancer models and INPP4B role in diet regulated metabolic processes.

In Chapter One, we investigated the relationship between INPP4B and AR signaling in prostate cancer cells and normal mouse prostate. Taylor et al. have previously shown the activation of AR signaling and loss of INPP4B or PTEN both happened in metastatic prostate cancer (132). Using prostate cancer cell lines, we showed that INPP4B regulates AR transcriptional activity partially through oncogenic signaling pathways Akt and PKC. Using an *Inpp4b*$^{-/-}$ mouse model, we observed that INPP4B suppressed on Akt and PKC signaling pathways and modulated AR transcriptional activity in the healthy mouse prostate. Our data demonstrated that INPP4B modulates AR activity in healthy prostate and its loss contributes to the oncogenic reprogramming of the AR-dependent transcriptome in prostate cancer.

In Chapter Two, we investigated INPP4B function in a mouse model of diet-induced obesity in males (DOI). We observed an accelerated weight gain in INPP4B deficient obese mice. We showed that in lean male mice, loss of INPP4B caused hyperglycemia and insulin resistance. Combined with HFD, *Inpp4b* loss led to type 2 diabetes represented by an increased level of blood insulin and glucose. More importantly(133), *Inpp4b* deficient male mice had an enhanced activation of SREBP1 in the liver which, along with the high-fat diet, caused increased expression and activity of PPARG and other lipogenic pathways, leading to liver steatosis. Additionally, we observed the development of high-grade prostatic intraepithelial neoplasia in HFD *Inpp4b*$^{-/-}$ mouse but not the HFD WT mouse prostates suggesting the synergetic function of INPP4B and HFD in prostates.

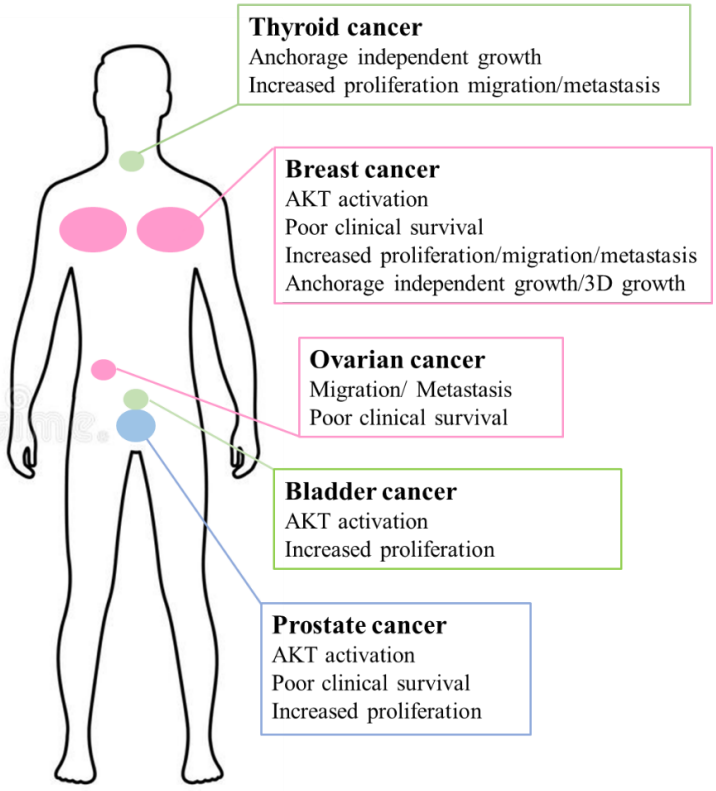

Figure 1-10. Role of INPP4B in human cancers. Each box shows when INPP4B is lost, the phenotype displayed by each type of cancer.

In Chapter Three, we explored the function of INPP4B in breast cancer cells and obese female mice. ERα and PR are steroid receptor that regulate mammary gland development homeostasis, neoplastic transformation and breast tumor progression. Using gene expression microarrays, we demonstrated INPP4B modulated ERα and PR transcriptional activities. Specifically, INPP4B loss reduced PR protein level and altered expression of PR target genes. Phenotypically, we observed reduced ductal branching of mammary gland in *Inpp4b*$^{-/-}$ female mice. Using the HFD treated wild-type female mice as controls, we showed *Inpp4b* deletion led to extensive weight gain and white adipose tissue (WAT) expansion in HFD female mice. Most importantly, we observed increased lipid content and development of fibrosis in livers of HFD *Inpp4b*$^{-/-}$ females suggesting that INPP4B protect obese female mice from developing NAFLD.

Overall, we demonstrated INPP4B regulates hormone receptor signaling in prostate and breast normal epithelium and cancer cells, stimulates mammary gland development in female mice, and protects obese male mice from developing prostatic epithelial neoplasia. As a metabolic regulator, INPP4B protect the mice from diet induced weight gain and metabolic diseases such as NAFLD, hyperglycemia, and T2D.

CHAPTER 2: THE ROLE OF INOSITOL POLYPHOSPHATE 4-PHOSPHATASE TYPE II IN PROSTATE CANCER CELLS AND NORMAL MOUSE PROSTATE

2.1. ABSTRACT

Activation and transcriptional reprograming of AR in advanced prostate cancer frequently overlaps with the loss of two tumor suppressors, INPP4B and PTEN, which are highly expressed in human and mouse prostate epithelium. While regulation of AR signaling by PTEN has been described by multiple groups, it is not known whether the loss of INPP4B affects AR activity. Using prostate cancer cell lines, we showed that INPP4B regulates AR transcriptional activity and oncogenic signaling pathways AKT and PKC. Analysis of gene expression in prostate cancer patient cohorts showed a positive correlation between INPP4B expression and both AR mRNA levels and AR transcriptional output. Using an *Inpp4b*$^{-/-}$ mouse model, we demonstrated that INPP4B suppresses AKT and PKC signaling pathways and modulates AR transcriptional activity in normal mouse prostate. It has been previously shown that the high fat diet activates AKT pathway in mouse prostate. We showed that the loss of INPP4B further increases AKT phosphorylation in dorsolateral and ventral lobes of mice fed with the high fat diet. Remarkably, levels of PTEN protein levels and phosphorylation of S380 were the same in *Inpp4b*$^{-/-}$ and WT males, suggesting that observed changes were due exclusively to the loss of INPP4B. Our data show that INPP4B modulates AR activity in normal prostate and its loss contributes to the AR-dependent transcriptional profile in prostate cancer.

2.2. INTRODUCTION

INPP4B has been identified as a tumor suppressor in ovarian, breast, thyroid, bladder, and prostate cancers (29, 46, 131, 134, 135). INPP4B functions as a dual specificity phosphatase, capable of dephosphorylation of both lipid and protein substrates similar to PTEN (127). Remarkably, both PTEN and INPP4B are lost in nearly half of all metastatic prostate cancers (132).

Preferred substrates for INPP4B lipid phosphatase activity are PI(3,4)P2, PI(4,5)P2, and Ins(1,3,4)P3 (31, 136). However, low but biologically significant levels of PI(3,4,5)P3 hydrolysis by INPP4B were observed in murine thyroids (31). Both PI(3,4,5)P3 and PI(3,4)P2 bind and activate the oncogenic AKT signaling pathway which facilitates cell survival, migration, and invasion in multiple malignancies including prostate cancer (41, 137). The INPP4B substrate PI(4,5)P2 is required for activation of both conventional (α,β,γ) and novel (ε,δ,η,θ) kinases of the PKC family (138, 139). PI(4,5)P2 is hydrolyzed by phospholipase C (PLC) into inositol triphosphate and diacylglycerol (DAG) which binds and activates PKC (48). A separate class of PKC, the atypical PKC isoforms (ζ and ι/λ) are activated by lipid components other than DAG [9]. Protein levels of PKC α, ε, ζ are increased in prostate and other cancers (140). We and others found that INPP4B suppresses PKC signaling in prostate, breast, and gastric cancer cells (136, 141, 142). The activation of the androgen receptor (AR) is essential for prostate development and for the initiation and progression of prostate cancer (34, 35). With prostate cancer progression the AR transcriptional profile changes from one of differentiation to proliferation (134). This change is due, in part, to the activation of cell signaling pathways and posttranslational modifications of AR. We and others have shown that the loss of INPP4B activates AKT signaling (29, 31, 134). In turn, AKT directly binds and phosphorylates serine 213 and 791

on AR (56-58). Phosphorylation of these sites affects AR activity in a cell specific manner (56, 57). In mice, a prostate specific *Pten*$^{-/-}$ knockout leads to AKT activation and nearly complete loss of the AR protein, which is partially reversed by treatment with AKT inhibitors (143). PKC was reported to phosphorylate AR on S213 and S578 increasing AR transcriptional activity and regulating its turnover (144). In mouse models, overexpression of PKCε led to prostate hyperplasia and intraepithelial neoplasia, in part, by stabilizing AR levels (145, 146).

In this report we investigated whether INPP4B modulates transcriptional activity and turnover of the full-length AR, and the AR splice variant, AR-V7. Unlike full length AR, AR-V7 was unable to induce INPP4B gene expression. Loss of INPP4B significantly altered a subset of AR, as well as AR-V7 target genes, without altering AR protein levels. We showed that INPP4B suppresses AKT and PKC signaling in independently derived prostate cancer cell lines. To test whether these signaling pathways were responsible for the change in AR activity, we used AKT and PKC specific inhibitors to mimic INPP4B expression. We determined that some, but not all changes in AR target gene expression are mediated by the activation of AKT and PKC. Similar to our observations in human prostate cancer cell lines, induction of prostate specific AR target genes was reduced in *Inpp4b*$^{-/-}$ mice. In the prostate, *Inpp4b* knockout mice expressed similar levels of AR, PTEN, and p-PTEN when compared to their wild-type (WT) littermates. Interestingly, the *Inpp4b* knockout mice displayed increased activity of AKT, PKCζ and PKCβII in the prostate, as indicated by increased phosphorylation levels. Our data indicate that INPP4B suppresses AKT and PKC signaling pathways and modulates AR transcriptional output in human and mouse models.

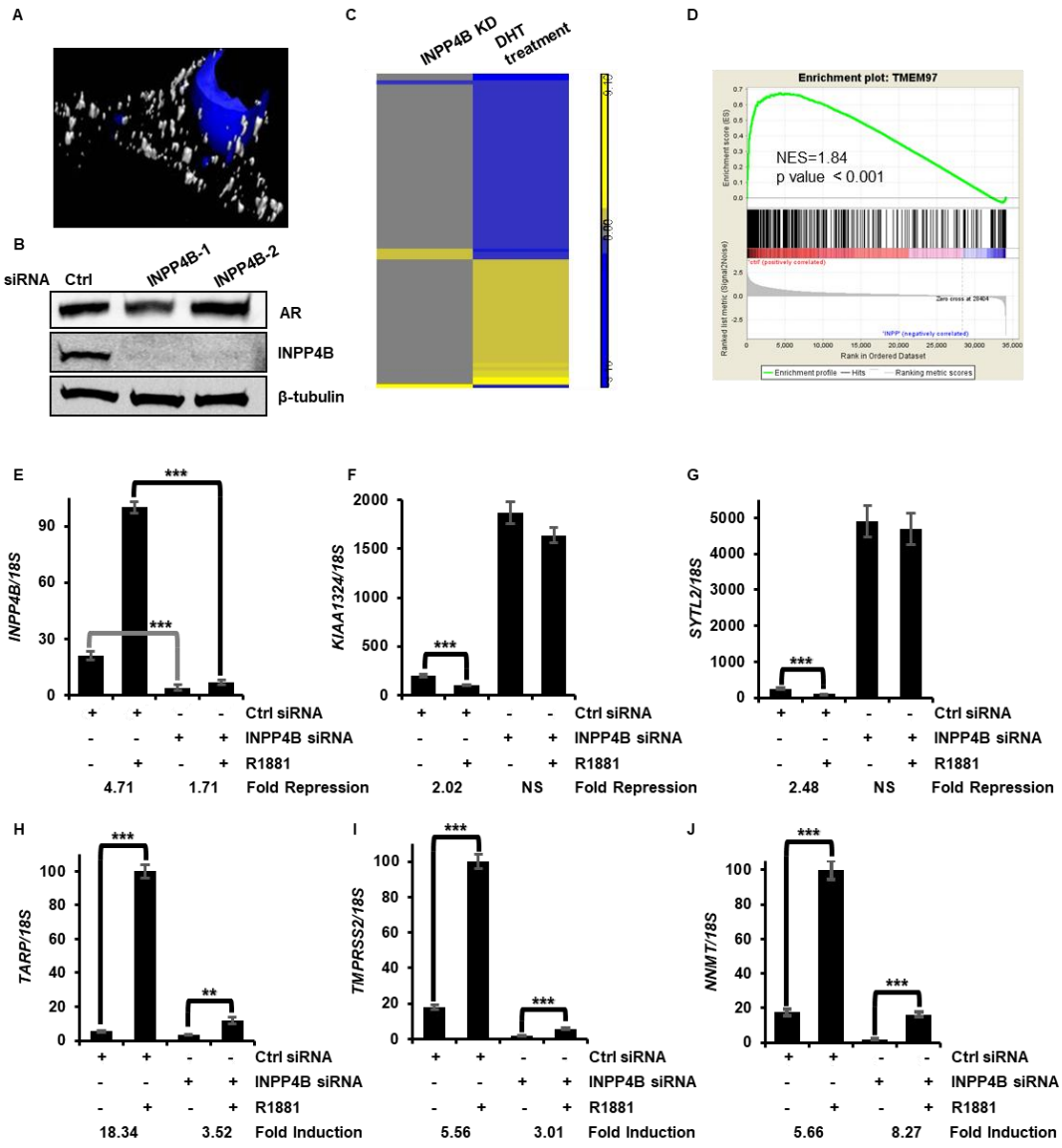

Figure 2-1. Loss of INPP4B changes AR transcriptional activity. (A) Three dimensional rendering of INPP4B distribution. Cells were fixed and stained with INPP4B primary and Alexa Fluor conjugated secondary antibodies (white). The nuclei were counterstained with DAPI (blue). (B) Early-stage LNCaP cells were transfected with either a control (Ctrl) or two independent INPP4B specific siRNAs (INPP4B-1, INPP4B-2) for 48 hours in medium supplemented with FBS. Protein levels of AR, INPP4B, and tubulin were compared by western blotting. (C). LNCaP cells were transfected as in (B). RNA was extracted and used in microarray analysis. Gene expression was compared to that of AR regulated genes in LNCaP cells. (D) GSEA analysis of INPP4B regulated genes using an AR transcriptional signature in LNCaP cells (GSE60721). (Normalized Enrichment Score = 1.84, p <0.001). E-J. LNCaP cells were cells were tandem transfected with either control or INPP4B siRNAs with 48 hour intervals. Forty eight hours later cells were placed in medium supplemented with 10% CSS and treated with either vehicle (ethanol) or 0.1 nM R1881 for 24 hours as indicated. RNA was analyzed for expression of *INPP4B* (E), *KIAA1324* (F), *SYTL2* (G),

TARP (H), *TMPRSS2* (I), and *NNMT* (J). Expression was normalized to *18S*. ** $p < 0.01$, *** $p < 0.001$.

2.3. RESULTS

2.3.1. Loss of INPP4B changes AR transcriptional output.

INPP4B depletion accelerates LNCaP cell proliferation, an androgen dependent feature of this prostate cancer cell line. To determine whether INPP4B modulates AR transcriptional activity we performed gene expression microarray analysis. Endogenous INPP4B is generally localized to the cell membrane and cytoplasm (Figure 2-1 A), while AR shuttles between the cytoplasm and nucleus (147). Two INPP4B specific siRNAs were used to knock down INPP4B in LNCaP cells (Figure 2-1 B). Forty-eight hours later INPP4B protein levels were nearly undetectable while AR protein levels were unchanged (Figure 2-1 B). We chose this time point to evaluate changes in transcript levels using Affymetrix microarrays (Figure 2-1 A). DHT-dependent AR output in LNCaP cells was previously reported by our laboratory (148). To determine whether INPP4B regulates AR target genes, we analyzed changes in the expression of the AR target genes in LNCaP cells transfected with either control or INPP4B specific siRNAs. A subset of AR target genes were significantly affected by the knockdown of INPP4B (Figure 2-1 C). To confirm INPP4B regulation of AR transcriptional activity we used gene set enrichment analysis (GSEA). An AR signature was created using our previously reported microarray analysis of AR target genes, GSE60721 (148). The analysis indicated that the AR signature is significantly represented among INPP4B regulated genes (Normalized Enrichment Score = 1.84, $p < 0.001$) (Figure 2-1 D). We next investigated whether INPP4B expression correlates with AR mRNA levels and AR signature in prostate cancer patients. As seen from Figure 2-2

A

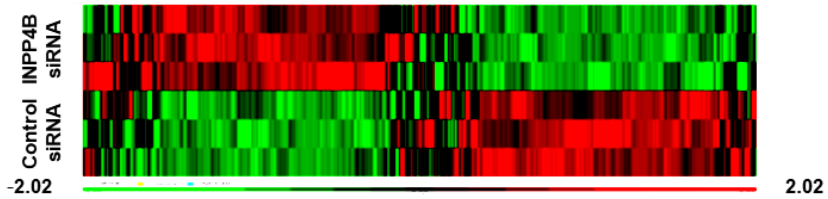

B

TCGA

	AR gene	Hieronymus signature	INPP4B gene	Nelson signature	PTEN gene
AR gene	1.00	NS	0.31	NS	NS
Hieronymus signature	NS	1.00	0.49	0.77	0.18
INPP4B gene	0.31	0.49	1.00	0.59	0.32
Nelson signature	NS	0.77	0.59	1.00	0.15
PTEN gene	NS	0.18	0.32	0.15	1.00

Taylor

	AR gene	Hieronymus signature	INPP4B gene	Nelson signature	PTEN gene
AR gene	1.00	0.70	0.25	0.68	0.35
Hieronymus signature	0.70	1.00	0.39	0.84	0.20
INPP4B gene	0.25	0.39	1.00	0.55	0.25
Nelson signature	0.68	0.84	0.55	1.00	NS
PTEN gene	0.35	0.20	0.25	NS	1.00

Pearson Correlation Coefficient

-1	-0.5	0	0.5	1

Figure 2-2**.** Correlations between INPP4B expression and AR expression and transcriptional output. (A) LNCaP cells were transfected with either control or INPP4B siRNAs and incubated in complete serum for 48 hours. RNA was extracted and analyzed using Illumina microarrays. Gene expression was clustered in biological replicates. (B) TCGA and Taylor cohorts were used to examine correlations between INPP4B, AR, and PTEN mRNAs and Nelson and Hieronymus AR signatures.

B, in both Taylor and TCGA cohorts there are statistically significant positive correlations between INPP4B and both AR mRNA and two AR signatures, Nelson and Hieronymus.To determine whether INPP4B regulates basal or androgen dependent gene expression, we knocked down INPP4B, treated cells with vehicle or 0.1 nM R1881, and compared the expression of three AR induced genes and three AR reduced genes in LNCaP cells. The three AR induced genes most strongly regulated by INPP4B were: T Cell Receptor Gamma Alternate Reading Frame Protein (*TARP*), Transmembrane Protease Serine 2 (*TMPRSS2*) and Nicotinamide N-Methyltransferase (*NNMT*) (Figure 2-3 A). Three AR suppressed genes most strongly regulated by INPP4B are; Estrogen-Induced Gene 121 Protein (*KIAA1324*), Synaptotagmin-Like 2 (*SYTL2*), Phospholipase A2, Group IIA (*PLA2G2A*) (Figure 2-3 B). Both induction and repression of these genes was reduced following INPP4B knockdown in medium supplemented with FBS (Figure 2-3 C-D). As seen in Figure 2-1 E, INPP4B siRNA significantly reduced INPP4B mRNA levels in cells cultured with CSS serum treated with vehicle or R1881. Since INPP4B is a primary AR target gene (134), its expression was increased with R1881 treatment. Following INPP4B knockdown, AR dependent repression of *KIAA1324* and *SYTL2* was abolished (Figure 2-1 F-G). While both basal and R1881-dependent induction of *TARP* and *TMPRSS2* were reduced (Figure 2-1 H-I), fold induction of *NNMT* was increased by INPP4B loss (Figure 2-1 J).

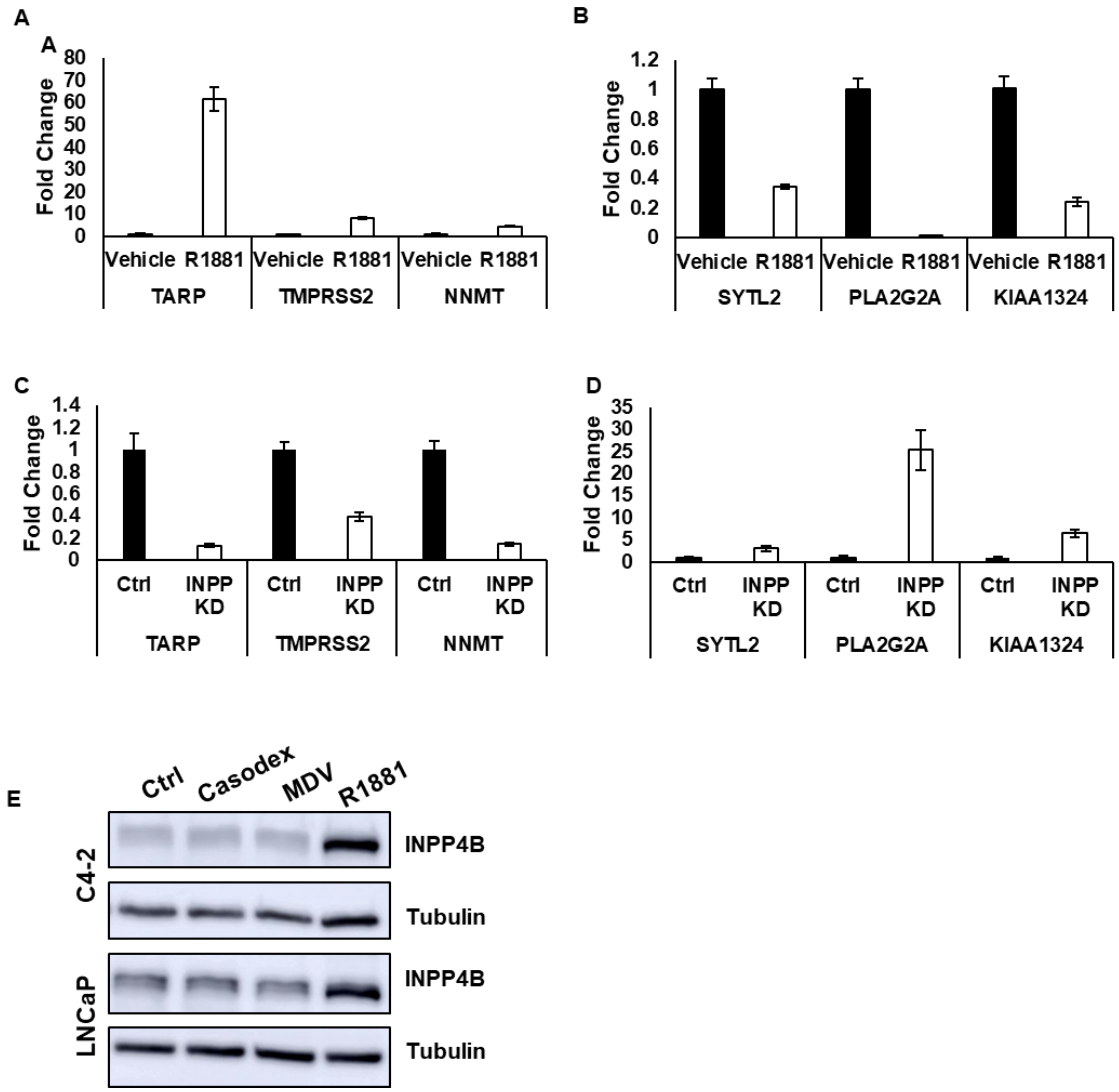

Figure 2-3**. INPP4B is required for optimal induction and repression of a subset of the AR target genes.** (A) LNCaP cells were plated in 10% CSS medium with either vehicle or 1nM R1881. Twenty-four hours post-treatment, mRNA was collected and expression of AR target genes, *TARP, TMPRSS2, NNMT*, was analyzed by RT-qPCR. (B) RNA from A was used to analyze expression of *SYTL2, PLA2G2A*, and *KIAA1324.* (C) LNCaP cells were plated in 10% CSS medium. Next day cells were transfected with control or INPP4B siRNA and treated with either control or vehicle for 48 hours. RNA was extracted and analyzed for expression of *TARP, TMPRSS2, NNMT* by RT-qPCR (D) RNA from C was used to compare expression of *SYTL2, PLA2G2A*, and *KIAA1324*. All gene expression levels were normalized for 18S. Differences in gene expression between treated and control cells was statistically significant ($p<0.01$) in all panels of this figure.

2.3.2. Reciprocal regulation of AR-V7 and INPP4B.

AR splice variants, including AR-V7, are expressed at the late stages of prostate cancer and correlate with poor prognosis (149, 150). We have previously shown that INPP4B expression is stimulated by androgens in LNCaP and VCaP cell lines and in primary prostate cancer patient derived xenografts (134, 136). We used the LNCaP$^{AR\text{-}V7/pHAGE}$ cell line which expresses an inducible AR-V7 variant (151) to test whether AR-V7 is able to upregulate expression of endogenous INPP4B. Similar to the parental LNCaP cell line, androgens increase expression of endogenous INPP4B (Figure 2-4 A) in LNCaP$^{AR\text{-}V7/pHAGE}$ cell line, while AR-V7 splice variant fails to induce INPP4B expression (Figure 2-4 A lanes 5 and 6). Moreover, AR-V7 suppresses INPP4B expression on mRNA levels (Figure 2-4 B, bars 1 and 2). Expression of AR-V7 in LNCaP$^{AR\text{-}V7/pHAGE}$, increased phosphorylation of AKT and PKCβII in media supplemented with either CSS or FBS (Figure 2-4 A). To test whether INPP4B modulates AR-V7 transcriptional activity we compared expression of EDN2, an AR-V7 specific target gene in the LNCaP$^{AR\text{-}V7/pHAGE}$ cell line (151). As seen from Figure 2-4 C, INPP4B knockdown significantly decreased the induction of EDN2. These results suggest that INPP4B modulates AR-V7 transcriptional activity and that, unlike full-length AR, AR-V7 is unable to induce INPP4B expression. Since AR-V7 has many target genes in common with full length AR, we tested whether *NNMT*, *TARP*, *TMPRSS2*, *KIAA1324*, and *SYTL2* were regulated by both AR-V7 and INPP4B in LNCaP$^{AR\text{-}V7/pHAGE}$ cell line. Similar to the parental LNCaP cell line, INPP4B knockdown reduced basal transcription of NNMT without changing the ability of AR-V7 to induce its expression (Figure 2-4 D). Both basal and AR-V7 - dependent regulation of *TARP*, *TMPRSS2*, *KIAA1324*, and *SYTL2* required INPP4B expression (Figure 2-4 E-H).

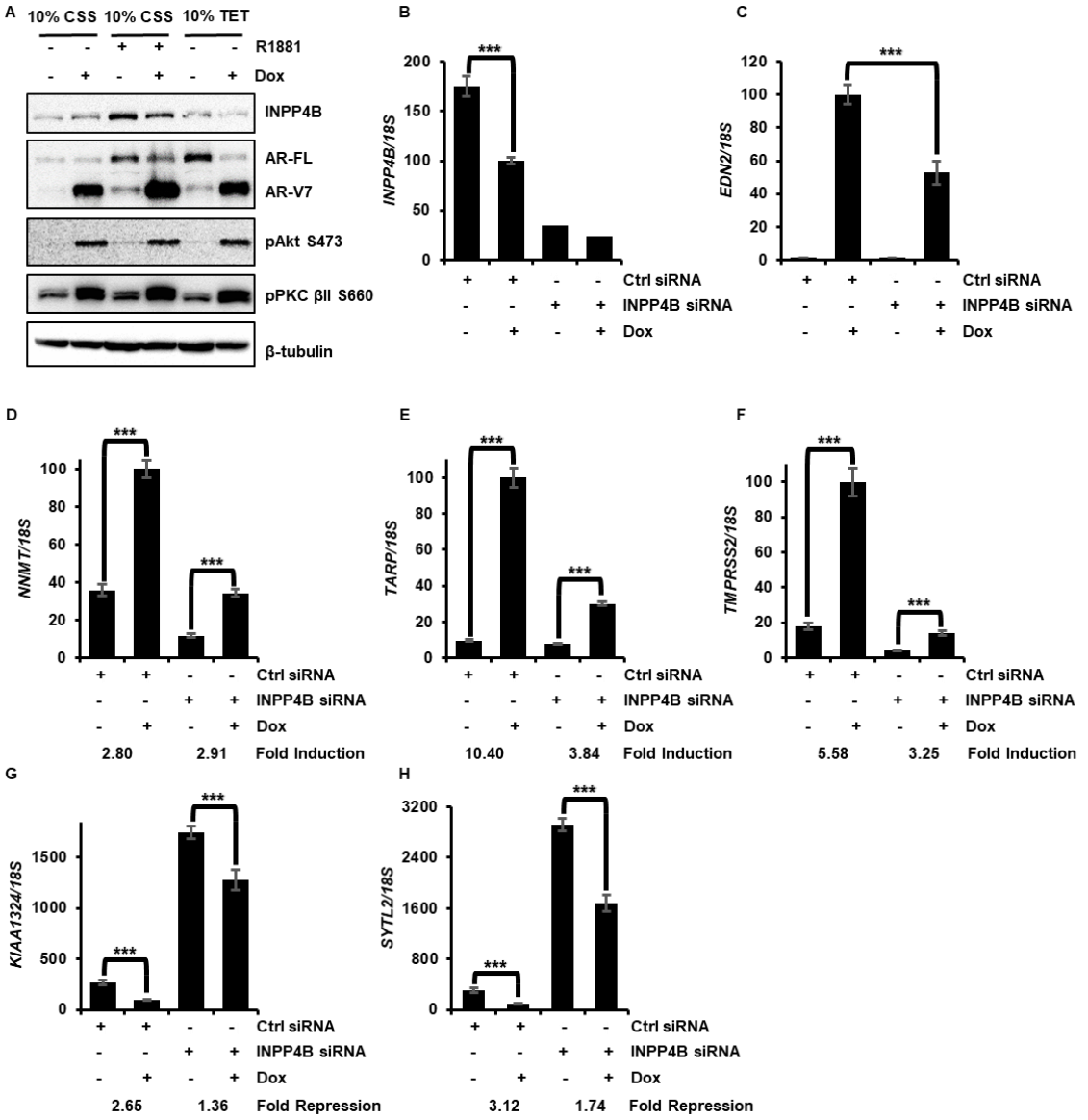

Figure 2-4**.** Reciprocal regulation of AR-V7 and INPP4B. (A) LNCaP $^{AR\text{-}V7/pHage}$ cells were placed in medium with 10% CSS or 10% TET FBS serum for 24 hours and treated with 50 ng/ml Dox or 1nM R1881 as indicated for an additional 36 hours. Protein level of INPP4B, AR-FL, AR-V7, pPKC βII, and tubulin were assessed by Western blotting. (B, C) LNCaP $^{AR\text{-}V7/pHage}$ cells were transfected with control or INPP4B siRNA and maintained in medium supplemented with 10%TET serum. Forty-eight hours later cells were transfected again with control or INPP4B siRNAs and treated with either vehicle or 25ng/ml Dox for additional 24 hours. Gene expression of *INPP4B* (B) and *EDN2* (C) were analyzed by RT-qPCR using *18S* as a control. LNCaP $^{AR\text{-}V7/pHage}$ cells were tandem transfected with either control or INPP4B siRNAs with 48 hour intervals. Forty-eight hours later cells were placed in medium supplemented with 10% CSS with or without 30ng/ml Dox for 24 hours as indicated. RNA was analyzed for expression of *NNMT* (D), *TARP* (E), *TMPRSS2* (F), *KIAA1324* (G), and *SYTL2* (H). ** $p < 0.01$, *** $p < 0.001$.

2.3.3. INPP4B regulates AR transcriptome via inhibition of PI3K/AKT and PKC signaling pathways.

Based on the disparate spatial distribution of INPP4B and AR, we tested whether INPP4B regulation of the AR transcriptome includes intermediate signaling pathways. We and others have reported INPP4B regulation of the AKT pathway (29, 32, 33, 46, 134) and in our previous reports we showed that overexpression of INPP4B in the PC3 cell line reduces phosphorylation of PKCβII and PKCζ (136). As seen in Figure 2-5 A-C, INPP4B knockdown increased phosphorylation of PKCζ on Thr410 (2.52 fold ± 0.77; 1.84 fold ± 0.19) and PKCβII on Ser660 (2.23 fold ± 0.09; 1.70 fold ± 0.04) in the androgen sensitive cell lines LNCaP and VCaP, respectively, and upregulates phosphorylation levels of PKCζ (1.89 fold ± 0.30) in the C4-2 cell line. As previously shown, INPP4B knockdown increased pAKT levels in LNCaP cells (134). We confirmed that under our experimental conditions, pAKT levels are increased 48 hours after INPP4B knockdown in LNCaP and C4-2 cell lines (Figure 2-5 B-C). Since INPP4B suppresses both AKT and PKC pathways, we tested whether their inhibitors could phenocopy the INPP4B regulation of AR induced and repressed genes. Both induction and repression of these genes was reduced following INPP4B knockdown (Figure 2-3 C-D). AZD5363 and bisindolymaleimide I (BIM-I) were used to test whether INPP4B regulates AR transcriptional activity through the AKT and PKC pathways, respectively. The inhibitor activity was confirmed by decreased phosphorylation of the downstream target S6 protein (Figure 2-5 D). Similar to INPP4B expression in control siRNA treated cells, PLA2G2A mRNA was reduced following BIM-I and AZD5363 treatment and expression of KIAA1324 was decreased by PKC inhibitor (Figure 2-5 E-F). AZD5363 increased expression of TARP and NNMT, as did expression

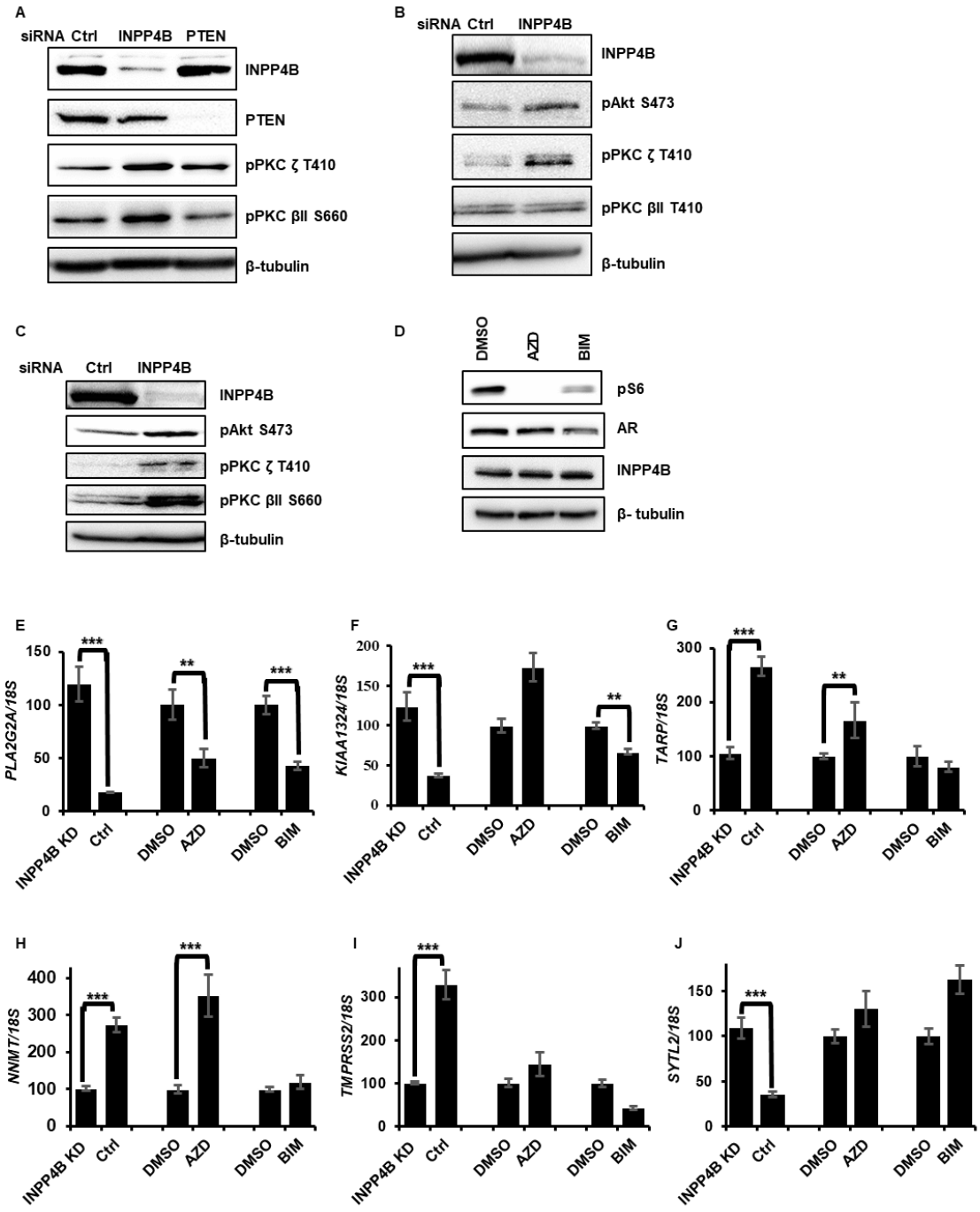

Figure 2-5. Suppression of AKT and PKC signaling contributes to INPP4B regulation of AR transcriptional activity. (A) VCaP cells were transfected with control, INPP4B, or PTEN specific siRNAs individually. Proteins were extracted and assayed for levels of INPP4B, PTEN, pAKT, pPKC βII, pPKC ζ, and β-tubulin by Western blotting. (B) C4-2 cells were transfected with control or INPP4B siRNAs for 48 hours in medium supplemented with 10% FBS. Cellular lysates were assayed for INPP4B, pAKT, pPKC βII, pPKC ζ, and tubulin by western blotting. (C) LNCaP cells were transfected and assayed in parallel with B. (D) LNCaP cells were plated in complete medium

and treated with indicated inhibitors for 8 hours. Protein extracts were assayed for AR, INPP4B, pS6, and tubulin levels by Western blotting. (E-J) LNCaP cells were plated in medium supplemented with 10% CSS with either vehicle or 1nM R1881. Twenty four hours later cells were treated with vehicle (DMSO), 5uM AZD5363, or 2uM BIM-I for additional 8 hours. In parallel, LNCaP cells were transfected with control or INPP4B siRNA for 48 hours in 10% CSS medium supplemented with 1nM R1881. RNA was purified, reverse transcribed, and expression levels of AR regulated genes *PLA2G2A* (E), *KIAA1324* (F), *TARP* (G), *NNMT* (H), *TMPRSS2* (I) and *SYTL2* (J) compared by RT-qPCR. Expression levels were normalized to *18S*. ** represents $p < 0.01$; *** represents $p < 0.001$.

of INPP4B (Figure 2-5 G-H). However, lack of concordant regulation of TMPRSS2 and SYTL2 (Figure 2-5 I-J) suggests additional modes of INPP4B regulation of AR activity.

2.3.4. INPP4B signaling in the normal mouse prostate.

To investigate the function of INPP4B in the normal prostate we used an *Inpp4b*$^{-/-}$ mouse model with deletion of exon 11 (28) which results in a frame shift at codon 213 and the generation of a stop signal at codon 217 (Figure 2-6 E). As expected, no expression of INPP4B was detected in the prostates of *Inpp4b*$^{-/-}$ mice and immunohistochemical analysis confirms the lack of INPP4B protein in prostate epithelial cells (Figure 2-7 A-B). Mutant male mice were fully fertile and displayed no difference in body, prostate, and testis weights (Figure 2-6 A-C). The ratio of seminal vesicles versus body weight showed modest but statistically significant increase in *Inpp4b*$^{-/-}$ mice compared to age-matched WT males (Figure 2-6 D).

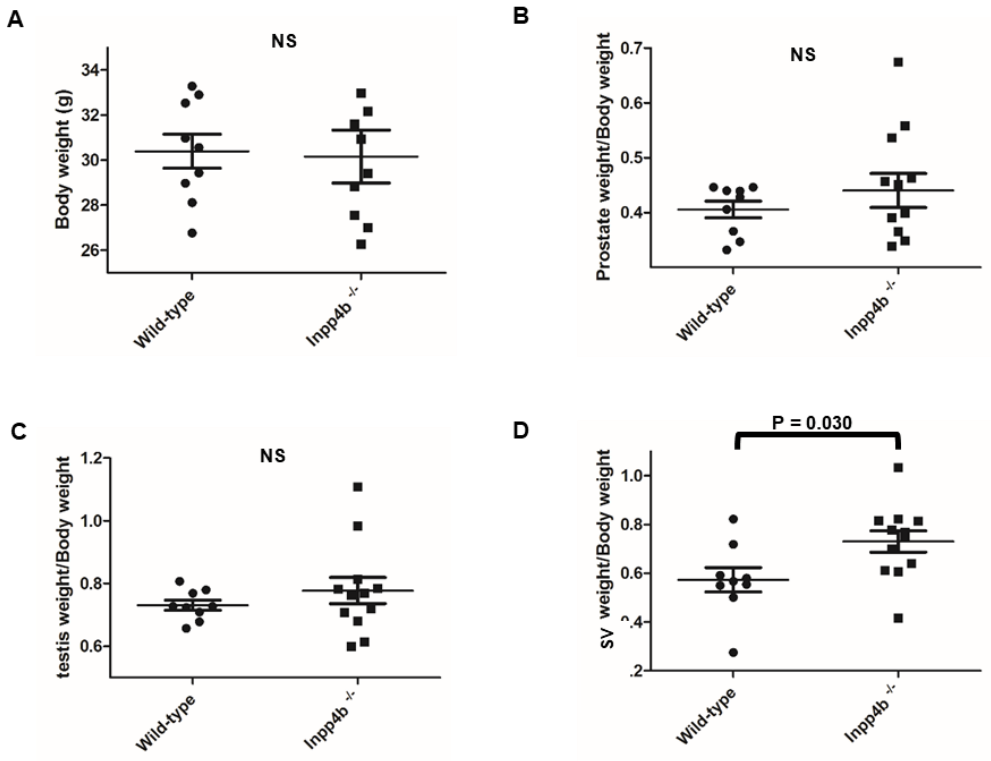

E

INPP4B 170 GEIEDGDTDHITTDVQGQKCALMYESTAPESLSGKENLPFMNAVLRNPVCKLYR

INPP4B$^{-/-}$ GEIEDGDTDHITTDVQGQKCALMYESTAPESLSGKENLPFMNAETRS*

F

	GSE46473		GSE46799		GSE24691		GSE76822	
Gene	FC	P value	FC	P value	FC	P value	FC	P value
Msmb	Not measured		**-13.09**	**0.0000**	**-15.03**	**0.0000**	1.53	0.7140
Pbsn	Not measured		**-45.57**	**0.0000**	**-22.16**	**0.0000**	**40.22**	**0.0004**
Nkx3.1	Not measured		**-23.75**	**0.0000**	**-7.16**	**0.0000**	**25.11**	**0.0002**
Clu	9.06	0.00061	Not measured		**14.93**	**0.0000**	10.4	0.0855
Apof	Not measured		-1.06	0.4570	1.02	0.8290	1.90	0.3910
Inpp4b	Not measured		1.18	0.0243	1.03	0.5690	1.00	0.9400

Figure 2-6**.** Body and urogenital organ weight comparison of 2 month old WT and *Inpp4b*$^{-/-}$ male littermates. Two month old WT (N=9) and *Inpp4b*$^{-/-}$ (N=12) male littermates were euthanized and their body, prostate, testis, seminal vesicle weight determined. (A) Body weight. (B) Prostate weight normalized to body weight. (C) Testis weight normalized to body weight. (D) Seminal vesicle weight normalized to body weight. (E) *Inpp4b*$^{-/-}$ mouse prostate cDNA was amplified, sequenced, translated and aligned with WT mouse protein sequence NP_001019788. * signifies stop codon. (F) Fold change and significance of *Msmb, Pbsn, Nkx3.1, Apof, Clu,* and *Inpp4b* expression caused by prostate specific *Pten* deletion in gene sets GSE46473, GSE46799, GSE24691 and GSE76822.

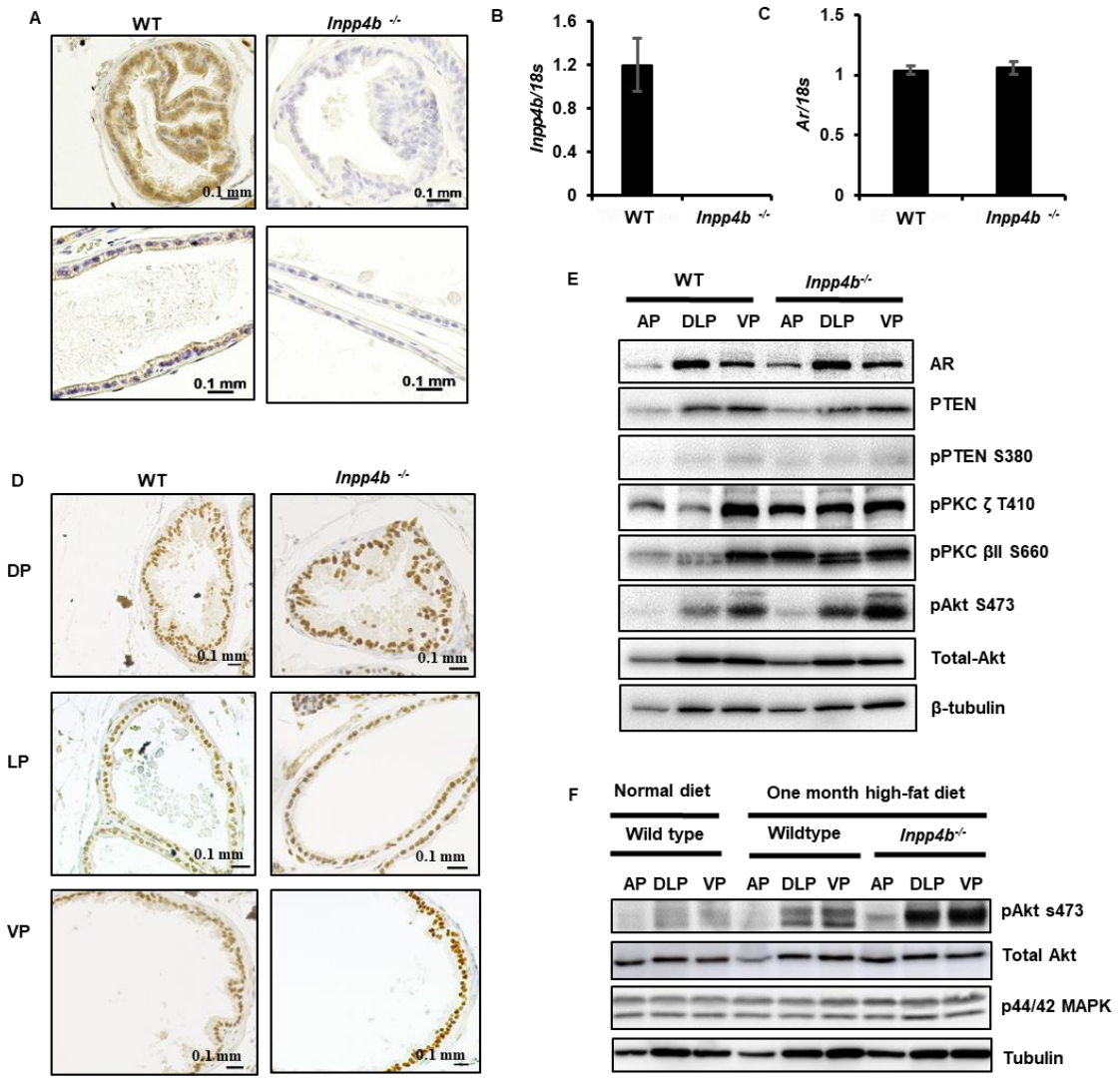

Figure 2-7. Loss of INPP4B in mouse prostate activates PKC and AKT signaling without changing AR levels. (A) Prostates from the 2 month old WT or *Inpp4b*$^{-/-}$ littermate males were dissected, fixed in paraffin, sectioned, and stained with INPP4B antibodies and counterstained with hematoxylin. (B-C) RNA was extracted from prostates of WT (N=11) or *Inpp4b* $^{-/-}$ (N=11) littermates. Expression of *Inpp4b* (B) and AR (C) and was compared by RT-qPCR. Gene expression was normalized for 18S. (D) Slides from A were stained with AR antibody and counterstained with hematoxylin (E) Individual prostate lobes, anterior (AP), dorsolateral (DLP), and ventral (VP), from four prostates of WT or *Inpp4b*$^{-/-}$ littermates were pooled, protein extracted, and analyzed for AR, total PTEN, pPTEN, pPKC ζ, pPKC βII, pAKT, total AKT, and tubulin levels by Western blotting. (F) Mice fed either normal chow or high-fat diet one month before euthanasia. AP, DLP, and AP prostate lobes of WT or *Inpp4b*$^{-/-}$ were dissected and samples were pooled from 3 mice of the same genotype. Protein was extracted and analyzed for pAKT, total AKT, p44/42 MAPK, and tubulin levels by Western blotting.

Consistent with our observations in prostate cancer cell lines, AR mRNA and protein levels did not change in *Inpp4b*$^{-/-}$ mouse prostates compared to those of the WT mice (Figure 2-7 C-E). Anterior (AP), dorsolateral (DLP), and ventral (VP) prostate lobes of WT and *Inpp4b*$^{-/-}$ mice had similar expression of AR protein (Figure 2-7 D-E). We observed an increase of pPKCβII (3.98 fold ± 1.01) and pPKCζ (2.83 fold ± 0.39) in AP and increase of pPKCβII (2.11 fold ± 0.24) and pPKCζ (2.28 fold ± 0.26) in DLP of the *Inpp4b*$^{-/-}$ mice compared to the WT controls (Figure 2-7 E). Increase in pAKT levels in DLP (1.519 fold ± 0.084) and VP (1.508 fold ± 0.199) occurred without change in PTEN protein and phosphorylation levels. It was previously shown that high fat diet causes increase in pAKT levels in mouse prostate (152, 153). We investigated whether INPP4B inhibits oncogenic AKT signaling in prostates of mice maintained on high fat diet. Consistent with previous results, one-month exposure to 58% fat diet elevated pAKT levels in prostates of WT mice (Figure 2-7 F). In *Inpp4b*$^{-/-}$ mice, the pAKT levels were further increased in DLP and VP tissues (Figure 2-7 F).

2.3.5. INPP4B regulates AR transcriptional activity in normal mouse prostate.

To investigate whether INPP4B modulates AR target gene expression, we selected three genes strongly induced by AR and three genes regulated by PTEN in the mouse prostate (143, 154). In previous reports, DHT supplementation of castrated mice significantly induced Microseminoprotein β (*Msmb*), Apolipoprotein F (*Apof*), and NK3 Homeobox 1 (*Nkx3.1*) (154). We show that INPP4B was required for their optimal expression (Figure 2-8 A-C). Expression of the AR and PTEN regulated genes probasin (*Pbsn*) and clusterin (*Clu)* was similar in the prostates of WT and *Inpp4b*$^{-/-}$ age-matched males. Interestingly, *Pten* knockout in the mouse prostate did not alter INPP4B mRNA levels in two

independent microarray profiles (Figure 2-6 F). In human prostate cancer samples, however, a weak but significant positive correlation was observed between INPP4B and PTEN mRNA levels in TCGA and Taylor cohorts. This data suggests that INPP4B regulates a subset of AR target genes and the PKC and AKT signaling pathways in the mouse prostate. These changes are due specifically to the loss of INPP4B as the levels of total and phosphorylated PTEN did not change. Thus, the phosphatases INPP4B and PTEN participate in separate and nonredundant functions and exhibit a lack of reciprocal regulation in the mouse prostate.

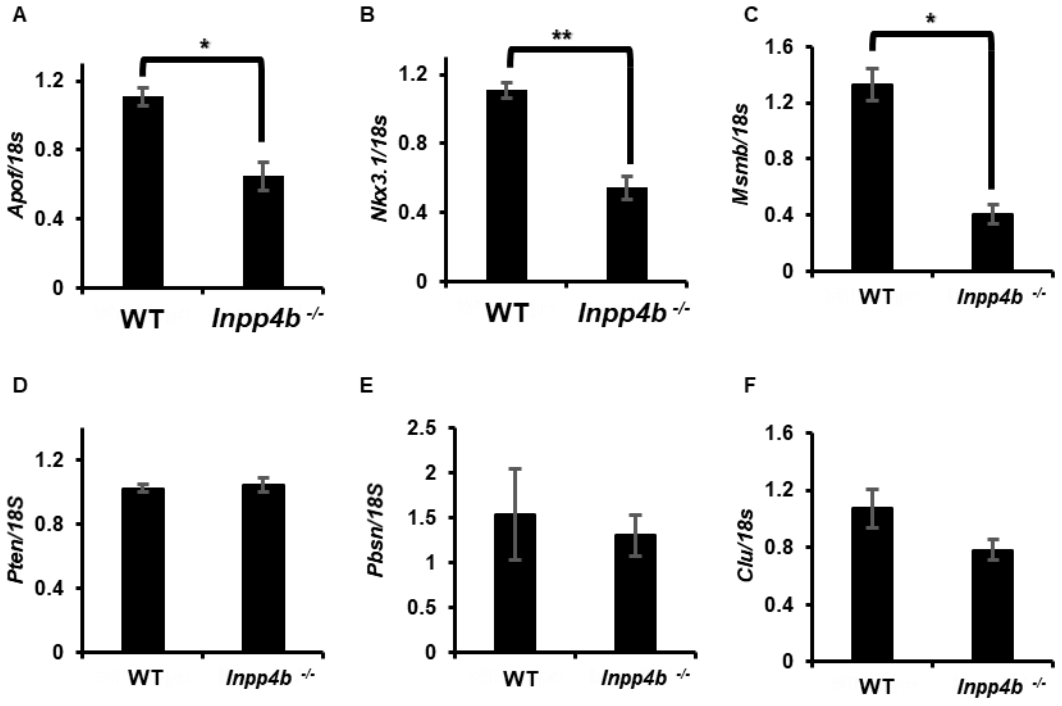

Figure 2-8**.** INPP4B is required for optimal expression of a subset of AR target genes in mouse prostate. Whole prostates were dissected from 2 month old WT (N=11) and *Inpp4b*$^{-/-}$ (N=11) littermates. RNA was extracted, reverse transcribed, and expression levels of *Apof* (A), *Nkx 3.1* (B), *Msmb* (C), *Pten* (D), *Pbsn* (E) and *Clu* (F) were compared by RT-qPCR. Expression levels were normalized for 18S expression.

2.4. Discussion:

Prostate cancer is dependent on AR signaling for its initiation and progression. During this progression, AR signaling undergoes significant reprogramming to acquire predominantly proliferative and pro-survival functions (155). The loss of PTEN and/or activation of PI3K/AKT signaling in prostate cancer leads to the loss of AR protein and a corresponding decrease in AR transcriptional output (143, 156). On the other hand, ERG and ETV1 expression in PTEN deficient prostate cancers reactivate AR transcriptional output (157). Both PTEN and INPP4B are members of a dual specificity phosphatase family that dephosphorylates lipids and phosphoproteins. Taylor et al reported similar copy number alterations for both INPP4B and PTEN with prostate cancer progression (132). Our group showed a decline in INPP4B protein levels in prostate cancer and a correlation of INPP4B loss with biochemical recurrence (134). Thus we investigated how losing INPP4B affects AR signaling.

We used the LNCaP cell line which expresses high levels of INPP4B and AR and is also dependent on androgens for its proliferation (158). In LNCaP cells, INPP4B knockdown modulated ability of AR to activate and repress target genes (Figure 2-1 F–J). Supporting this observation, the AR transcriptional signature is significantly represented among genes regulated by INPP4B in the LNCaP cell line (Figure 2-1 D). Importantly, statistically significant correlations between INPP4B expression and AR mRNA levels and transcriptional output were observed in the TCGA and Taylor cohorts. While it is well established that PTEN regulates AR transcriptional output in prostate cancer, INPP4B correlations with AR signatures were stronger than those of PTEN (Figure 2-2 B) in both cohorts.

Loss of INPP4B and gain of AR splice variant expression occurs most frequently in advanced stages of prostate cancer (132, 159). We used a well characterized LNCaP$^{AR\text{-}V7/pHAGE}$ cell line which retains endogenous full length AR and INPP4B expression and signaling to investigate reciprocal regulation of INPP4B and AR-V7 (151, 160). Consistent with its oncogenic function, AR-V7 is unable to induce expression of the tumor suppressor INPP4B and may in fact reduce INPP4B expression (Figure 2-4 A-B). INPP4B however, retains its ability to regulate AR-V7 transcriptional activity (Figure 2-4 C-H).

While AR shuttles between the nucleus and the cytoplasm in both a ligand dependent and independent manner (147, 161), INPP4B has been shown to localize mostly to cytoplasmic and membrane compartments (46, 136). This localization could be due in part to the INPP4B C2 domain that binds phosphatidylinositol polyphosphates, a lipid component of cellular membranes (162). Similar to observations in mammary epithelium and PC3 cells (46, 136), INPP4B shows focal extranuclear localization in LNCaP cells (Figure 2-1 A). Membranes contain the INPP4B lipid substrates PI(3,4)P2 and PI(4,5)P2 which activate AKT and PKC respectively. Activation of PKC has been linked to AR phosphorylation and prostate cancer progression (140, 163, 164) and was shown to regulate angiogenesis, apoptosis, cell proliferation, invasion, and metastasis (163, 165-167). The PI3K/AKT signaling pathway is activated in nearly half of primary prostate tumors and in all metastatic prostate tumors (132). AKT regulation of AR signaling is well described both *in vitro* and *in vivo* (57, 58, 143, 156). We and others have shown that both these pathways are suppressed by INPP4B in multiple cell models (29, 33, 134) including LNCaP cells (Figure 2-5 A-C). Since both AKT and PKC phosphorylate AR and regulate its activity (56-58, 144) we tested whether these kinases mediate some of the INPP4B dependent

changes in AR transcriptional activity. We reasoned that if treatment with inhibitor mimicked the effect of INPP4B on gene expression, the corresponding kinase might contribute to the INPP4B regulation of AR transcriptional activity. As seen from Figures 3E-3F, expression of KIAA1324 and PLA2G2A is lower in the presence of INPP4B. BIM-I and AZD5363 decreased expression of KIAA1324 and PLA2G2A, respectively, implicating PKC and AKT in the regulation of these genes. Both INPP4B and AZD5363 treatment increase expression of TARP and NNMT (Figure 2-5 H-J), suggesting that AKT mediates INPP4B-dependent induction of these genes. However, INPP4B regulation of SYTL2 and TMPRSS2 are due to mechanisms other than inhibition of PKC and PI3K/AKT signaling. This could be attributed to INPP4B protein phosphatase (32, 33) or other activities. We have shown that INPP4B can dephosphorylate AKT on pTyr residues, and Guo et al have shown that INPP4B can bind to and dephosphorylate PTEN on Ser380/Thr382/Thr383 residues (32, 33). Importantly, phosphorylation of AKT on Tyr176 and Tyr 284 positively correlates with prostate cancer progression and inversely correlates with patient survival, (168) suggesting a role for INPP4B protein phosphatase activity in prostate cancer progression.

To validate INPP4B regulation of AR activity *in vivo* we used an *Inpp4b* knockout mouse (28). Deletion of exon 11 in this model causes a frame shift leading to the addition of four amino acids after Ala 212 and protein truncation (Figure 2-6 E). Using antibodies to the INPP4B amino terminus we did not detect any signal (Figure 2-7 A), suggesting that even if the N-terminal portion of INPP4B is translated, it is not abundant in prostate epithelium. Male *Inpp4b*$^{-/-}$ mice are fertile and their prostates are histologically normal (Figure 2-7 A and D). Similar to our observations in prostate cancer cell lines, loss of INPP4B changed

neither mRNA nor protein levels of AR (Figure 2-7 C-E). However, we detected significant increase of pAKT in the dorsolateral and ventral prostate lobes and increased pPKCζ and PKC βII in the anterior and ventral prostate lobes of *Inpp4b*$^{-/-}$ versus age-matched WT males. Of note, the dorsolateral section of the mouse prostate is considered a functional model for the human prostate peripheral zone, the site of origin for most prostate cancers. Obesity is a risk factor for prostate cancer, especially in African American men (169). Here we show that loss of INPP4B exacerbates activation of oncogenic AKT pathway in mouse prostate caused by consumption of high fat diet.

Since levels of total and phospho-Pten S380 remained the same, PTEN is unlikely to have contributed to these changes (Figure 2-7 E). To determine whether INPP4B knockout modulates AR transcriptional activity *in vivo* we tested the levels of expression of AR target genes in the mouse prostate (154). As shown in Figure 2-6 F, prostate specific *Pten* knockout affected expression of a number of AR target genes (143, 156). Similar to PTEN, *Inpp4b* knockout reduced expression of *Apof, Nkx3.1*, and *Msmb* mRNAs. Unlike prostate specific *Pten* knockouts, we observed no induction of *Clu* or a decline in *Pbsn* mRNA levels in *Inpp4b*$^{-/-}$ prostates. Thus, differential regulation of AR target genes and AR protein levels signify nonredundant functions of INPP4B and PTEN in prostate epithelium. In this report we show that INPP4B loss reprograms the AR transcriptional output and activates PKC and AKT signaling *in vitro* and *in vivo*. INPP4B is lost at slightly higher rate than PTEN with prostate cancer progression (132) and is a strong predictor of recurrence (134). Our data shows that tumors that lack INPP4B have different mechanisms of progression from those with PTEN loss and may require a different therapy.

2.5. Materials and Methods

Cell culture and reagents

The human prostatic carcinoma cell lines, LNCaP and VCaP, were purchased from ATCC (Manassas, VA) and maintained under ATCC-recommended conditions. C4-2 cells were obtained from UroCor (Oklahoma City, OK) and maintained in RPMI 1640 (Thermo Fisher Scientific, Waltham, MA) supplemented with 10% fetal bovine serum (FBS). All experiments were performed during first 6 passages after purchasing cell lines from ATCC. FBS and charcoal stripped serum (CSS) were purchased from Sigma-Aldrich (St. Louis, MO). LNCaP$^{AR\text{-}V7/pHAGE}$ was described previously (151) and was maintained in RPMI 1640 supplemented with tetracycline-screened FBS (TET FBS) (GE Healthcare, Chicago, IL) and geneticin (Thermo Fisher Scientific). LNCaP$^{AR\text{-}V7/pHAGE}$ cells were treated with 25 ng/ml or 50 ng/ml Doxycycline (Dox) (Clontech Laboratories, Mountain View, CA) to express inducible AR-V7. R1881 was purchased from Perkin Elmer (Waltham, MA). The following cell signaling inhibitors were used: AZD5363 (Selleckchem, Houston, TX) and BIM-I (AdipoGen, San Diego, CA).

Immunofluorescence

LNCaP cells were grown on etched coverslips and fixed and processed as previously described (136). Fixed cells were incubated with INPP4B primary antibody (Cell Signaling, Danvers, MA) at 1:1000 dilution in 4°C overnight and Alexa Fluor conjugated anti-rabbit secondary antibody (Thermo Fisher Scientific) at 1:1000 dilution at 4°C for 1 hour. Cells were counterstained with DAPI (Sigma) and visualized using Axio Imager 2 (Zeiss, ST Petersburg, FL). Three dimensional rendering was performed using AxioVision LE software (Zeiss).

siRNA transfections

Noncoding control, INPP4B, and PTEN siRNAs were transfected at 50-100pmol siRNA per well in 6 well cell culture plate using Lipofectamine RNAiMAX Reagent (Thermo Fisher Scientific) as recommended by manufacturer. All siRNAs used in this manuscript are listed in Table 3.

Table 3. siRNA sequences.

siRNA	stock number	Sense	Antisense
non coding control	4390843		
non coding control	4390844		
PTEN	custom made	CCAUUACAAGAUAUACAAU	AUUGUAUAUCUUGUAAUGG
PTEN	custom made	AAACAUUAUUGCUAUGGGA	UCCCAUAGCAAUAAUGUUU
INPP4B	custom made	GAGCCUGAACUGCAUUAUU	AAUAAUGCAGUUCAGGCUC
INPP4B	s16826	CGAUGUCAGUGACACUUGA	UCAAGUGUCACUGACAUCG
INPP4B	104699	GGAAACAGGGUCCUCUUUC	GAAAGAGGACCCUGUUUCC
FOXA1		GCACUGCAAUACUCGCCUU	AAGGCGAGUAUUGCAGUGC

Microarray Analysis

LNCaP cells were transfected with noncoding control or INPP4B specific siRNAs using Lipofectamine RNAiMAX Reagent. After transfection, cells were maintained in complete medium for 48 hours. RNA was extracted using Tri reagent (Molecular Research Center, Cincinnati, OH). RNA was quantified, evaluated for quality, and analyzed using the Illumina Human HT-12v4 expression Beadchip platform exactly as described in our previous publication (136).

Gene Set Enrichment Analysis (GSEA)

GSEA analysis was performed using JAVA program http://software.broadinstitute.org/gsea as previously described (148, 170). AR signature

was generated from LNCaP which includes 422 genes significantly changed ($p<0.01$) after 48 hours of DHT treatment (GSE60721) (148).

Correlation with published AR signatures and key genes in prostate cancer cohorts

Previously published signatures of prostate cancer cells transcriptional response to androgen were derived from the Gene Expression Omnibus (GEO), termed Hyeronimus and Nelson AR signatures (171, 172) . We downloaded gene expression datasets from multiple previously reported human prostate cancer specimen cohorts: Taylor et al. (132), and The Cancer Genome Atlas (TCGA) (173). Within each dataset, we utilized the expression of each gene to calculate its respective z-score for each sample, relative to the normal prostate gland specimens available in that cohort. For each of two published androgen-induced signatures, Nelson and Hieronymus, we computed the sum z-score for each sample (the z-scores of downregulated genes were subtracted from the z-scores of upregulated genes), as described previously (132). Finally, for each pair of genes or signatures we computed the Pearson Correlation Coefficient R and associated p-value using the R statistical system.

Western blotting

Proteins were extracted from cultured cells as previously described (136). Mouse prostate tissue was homogenized in ice-cold RIPA buffer with protease and phosphatase inhibitors. Cleared lysates were diluted to 4 µg/µl and 10-25 µg of protein was resolved on SDS-PAGE. The proteins were transferred on nitrocellulose or PVDF membranes (GE Healthcare). Blots were blocked in 5% BSA (Millipore Sigma, Billerica, MA), incubated with primary antibodies against INPP4B, AR, pAKT S473, pPKC ζ T410, pPKC β S660, PTEN, total AKT, pS6 S235/236, and β-tubulin at 4°C overnight (Table 4). Blots were

washed and incubated with HRP conjugated secondary antibodies (Promega, Madison, WI) for 1 hour. Signal was generated using SuperSignal West Pico Chemiluminescent HRP Substrate (Thermo Fisher Scientific) and captured by Gel Logic 2000 imaging system with Carestream Molecular Imaging software (Carestream, Rochester, NY).

Table 4. Antibodies used in CHAPTER 2.

Antibody	cat #	concentration	RRID
phospho-Akt S473	Cell signaling #4051	1:1000	AB_331158
Total Akt	Cell signaling #4691	1:1000	AB_915783
phospho-PKCζ T410	Cell signaling #2060	1:1000	AB_561487
phospho-PKCβII S660	Cell signaling #9371	1:1000	AB_2168219
β-Tubulin	Millipore #05-661	1:5000	AB_309885
PTEN	Cell signaling #9188	1:1000	AB_2253290
AR	Millipore #06-680	1:1000	AB_310214
PKCε	R&D systems AF5134	1:1000	AB_2171918
AR-V7	Cell signaling #68492	1:1000	AB_2799747
pS6 S235/236	Cell signaling #4857	1:1000	AB_2181035

Gene expression analysis

RNA was prepared from prostate cancer cells or mouse prostate using Tri Reagent (Molecular Research Center). RNA concentration was determined using NanoVue Plus (GE Healthcare BioSciences, Piscataway, NJ). RNA was reverse transcribed using Verso cDNA synthesis Kit (Thermo Fisher Scientific). cDNA was used as a template for Real Time PCR using master mix, primers, and probes from Universal ProbeLibrary (Table 5) (Roche, Basel, Switzerland). Amplification and analysis was done using Roche 480 LightCycler (Roche).

Table 5. Primers and corresponding probes used in CHAPTER 2.

Human gene primers and corresponding probe sets			
Gene	Forward primers	reverse primers	Probe
KIAA1324	ggcaccgttaacttcgaatact	tggcactggtcattctgaac	67
PLA2G2A	ccgcactcagttatggcttc	agtgacacagcagcgatcc	53
NNMT	tgtgtgatcttgaagggaacag	cttgaccgcctgtctcaac	63
SYTL2	gcccgagctctttaaccaat	tccagattgccaaagtctcc	17
TARP	gacaattgttcaaaagatgcaaa	gatgatggcaaaatagaccaca	15
TMPRSS2	ctgatcacaccagccatgat	tatcccctatcagccaccag	44
INPP4B	tgtctgatgctgacgctaaga	ccacaaaccaatccagcaa	41
EDN2	gtcctcatctcatgcccaag	tagacgcactccttgtcgag	17
PSA	tccgtgacgtggattggt	cagggttgggaatgcttct	75
FOXA1	gtggctccaggatgttagga	gagtaggcctcctgcgtgt	---
FKBP5	ggatatacgccaacatgttcaa	ccattgctttattggcctct	---
RASSF3	gacgccgaggacttcttctt	tgctgaggtaactgtgggttt	---

Mouse gene primers and corresponding probe sets			
Gene	Forward primers	reverse primers	Probe
Ar	ccagtcccaattgtgtcaaa	tccctggtactgtccaaacg	58
Inpp4b	acagcaccagaaagtctgagc	ctttctgacatctgctcacgga	89
Apof	tctcaatggccggactgtat	aggatgagtcggaggctatg	17
Nkx3.1	cgactgaacccgagtctgat	aatcacctgagtgtgagagaagg	5
Msmb	cgtggtgttcatgtgacaaaa	ctcaaaggcctagtagcgttg	62
Pten	aggcacaagaggccctagat	ctgactgggaattgtgactcc	60
Probasin	tcatcctcctgctcacactg	gctaagtaaattgtttgccaagg	47
α-Clusterin	caatcctgcccaggctaac	ctgctctgtcagcctctcg	1
Pbsn	tcatcctcctgctcacactg	gctaagtaaattgtttgccaagg	47
Apof	tctcaatggccggactgtat	aggatgagtcggaggctatg	17
Msmb	cgtggtgttcatgtgacaaaa	ctcaaaggcctagtagcgttg	62

ChIP assay

LNCaP cells were cultured in RPMI medium supplemented with 10% FBS until 90% confluency. The medium was changed to 10% CSS RPMI. After 24 hours, cells were treated with vehicle, 20 nM R1881, and 25 ng/ml Dox for 18 hours. At the end of the treatment, 32% formaldehyde was added to the cells to crosslink proteins to DNA. After 30min, wash the cells with 1X PBS and harvest the cells. The cells pellets were resuspended in SDS lysis buffer. The cell lysate was sonicated 30s for 10 times using Bioruptor sonicator at 4 °C. The lysate was centrifuged and the supernatant was diluted 10 times using ChIP dilution buffer. The lysate was then incubated with AR, AR-V7, and Igg antibodies overnight at 4 °C. The Protein G and A conjugated beads (Thermo Fisher) were washed with TE buffer and the beads suspension was incubated lysates at 4 °C for 2 hours. The beads were washed with low salt wash buffer, high salt wash buffer, and TE buffer. The beads were washed with elution buffer to acquire the extracts. The extracts were reverse crosslinking by incubating with 1M $NaHCO_3$ at 65˚C for 6 hrs. DNA was extracted with QIAGEN PCR purification kit and DNA products were used for RT-qPCR using primers in Table 6. All buffers mentioned in this section were listed in Appendix with detailed recipes.

Table 6. Primers used in ChIP assay.

INPP4B chr4:143,516,774	tcttcttcccacctgactattttc	gccatgttttcaggtcatca
PSA enhancer	tctaggtcccgatcgactgt	tgagcgctgccttattctg
INPP4B intron2	aggtgagctacaagcaaggaa	tctgaataactcatgatattgggaaa
INPP4B enhancer	attggtggctcaaaatccaa	gcaagagaaagaagatacaaaacca

Animal Studies

Animals were housed at AAALAC certified barrier facility at Florida International University. All procedures were reviewed and approved by the Institutional Animal Care and Use Committee at FIU and conducted in accordance with the National Academy of Science Guide for Care and Use of Laboratory Animals. C57BL/6 *Inpp4b*$^{-/-}$ mice was kindly provided by Dr. Vacher (Institut De Recherches Cliniques De Montreal, Canada), and bred with FVB for at least three generations. Genotyping procedure was described in original publication (28). Two month old male mice were euthanized, weighed, their urogenital organs dissected and weighed, prior to RNA and protein extraction or formaldehyde fixation and paraffin embedding. For short-term high-fat diet treatment, 6 weeks old WT or *Inpp4b*$^{-/-}$ males were fed with control chow (LabDiet 5V75, St. Louis, MO) or high-fat diet (58% fat diet, TestDiet 58R3, St. Louis, MO) for one month before euthanasia.

Immunohistochemistry (IHC)

Whole prostates were fixed in 4% formaldehyde (Electron Microscopy Sciences, Hatfield, PA) overnight and embedded in paraffin. Sections (7 μm) were deparaffinized in xylene and rehydrated in ethanol. Antigen was retrieved by heating slides in 0.01M sodium citrate buffer (pH 6.0) (Fisher Scientific, Hampton, NH). Endogenous peroxidase was blocked by 1% hydrogen peroxide (Fisher Scientific) followed by incubation in 5% BSA for 45min. Slides were incubated with primary antibodies for INPP4B (Santa Cruz Biotechnology) or AR (Santa Cruz Biotechnology) at 1:800 dilution in TBS-T overnight. ABC kit (Vector Laboratories, Burlingame, CA) and Peroxidase substrate kit (DAB) (Vector Laboratories) were used to visualize the staining as suggested by manufacturer. Slides were rinsed with

tap water and counterstained with hematoxylin (EMD Millipore). All images were acquired by AxioCam camera and were processed by AxioVision LE software (Zeiss).

Statistical analysis

Comparisons of mean levels of expression of specific mRNAs and combination indices (CI) were done as previously described (32). Student t-tests were used to test for inequality of means from two independent samples. P-values less than 0.05 were considered to be statistically significant. Values are present as mean ± SEM. All experiments were repeated at least three times, unless stated otherwise. Biological triplicates were used for every point in individual experiment for evaluating changes in gene expression in cell lines.

CHAPTER 3: INPP4B PROTECTS FROM METABOLIC DISEASE AND ASSOCIATED DISORDERS.

3.1. Abstract

A high fat diet and obesity have been linked to the development of metabolic dysfunction and the promotion of multiple cancers. The causative cellular signals are multifactorial and not completely understood. In this report, we show that INPP4B signaling protects mice from diet-induced metabolic dysfunction. INPP4B suppresses AKT and PKC signaling in liver by dephosphorylating PI(3,4)P2 and PI(4,5)P2 respectively thereby improving insulin sensitivity. INPP4B loss results in proteolytic cleavage and activation of the of key regulator of de novo lipogenesis and lipid storage, SREBP1. Combined with the high fat diet, SREBP1 increases expression and activity of PPARG and other lipogenic pathways, leading to obesity and non-alcoholic fatty liver disease (NAFLD). *Inpp4b*$^{-/-}$ male mice fed high fat diet had type II diabetes, expansion and inflammation of adipose tissue, characteristic of metabolic dysfunction. In turn, systemic and localized inflammation drives the development of high-grade prostatic intraepithelial neoplasia. Thus, INPP4B is required for metabolic health and protects from metabolic disorder associated prostate neoplasms.

3.2. Introduction

In 2017, overconsumption and unhealthy diets contributed to 11 million deaths globally. Diet associated deaths from cancers and diabetes were ranked second and third behind cardiovascular disease (174). The National Center for Health Statistics reported in 2016 that over 80% of adult males aged 20 years and older were overweight or obese. Among this age group, 70% of obese men and 30% of normal weight men will develop metabolic

dysfunction (175).The consumption of a high-fat diet (HFD) is recognized as a leading cause of obesity, metabolic dysfunction, elevated chronic inflammation (103) and cancer mortality (104). Major indicators of metabolic dysfunction include elevated glucose levels, insulin resistance, and the expansion of mesenteric and omental adipose tissues (176). Importantly for men, an HFD and resulting obesity are tightly associated with lower urinary tract syndromes, including benign prostatic hyperplasia (BPH) (177), accelerated progression of prostate cancer; and decreased prostate cancer patient survival rates (178, 179).

Increasing evidence suggests that non-alcoholic fatty liver disease (NAFLD) is the best clinical indicator of metabolic dysfunction in both obese and lean individuals (180, 181). Hepatic lipid storage is a result of dysregulation of insulin signaling. Activation of the insulin receptor in liver, muscle, and fat cells leads to the activation of PI3K/AKT signaling pathways (182). High levels of circulating diacylglycerols (DAG) associated with HFD activate PKC, which, in turn, phosphorylates and inhibits the insulin receptor, lowering insulin sensitivity (106). In both mice and men, obesity elevates DAG levels and activates PKC signaling in multiple tissues, leading to the development of NAFLD and insulin resistance. Clinically, the levels of DAG and PKCε activation are the strongest predictors of insulin resistance in obese men (183).

Importantly, an HFD is not exclusively responsible for metabolic syndrome since some obese individuals maintain a healthy metabolic profile (106, 184, 185). There are a number of variants in several genes that can modulate the effects of known determinants of metabolic health. Polymorphisms in peroxisome proliferator-activated receptor γ (*PPARG),* adiponectin (*ADIPOQ),* leptin receptor (*LEPR*), and insulin receptor substrate 2

(*IRS2*) have been linked to obesity and type 2 diabetes mellitus (T2D) (186-189). However, the specific signaling pathways that are disrupted during the initiation of metabolic dysfunction are still not known.

INPP4B dephosphorylates both membrane lipids and phosphoproteins (32). We have shown that INPP4B suppresses the AKT and PKC pathways (32, 53, 134), which are major mediators of metabolic dysfunction, suggesting a role for INPP4B in the regulation of metabolic health. We tested this hypothesis using *Inpp4b*$^{-/-}$ male mice to compare their metabolic fitness to that of the wild type males. We found that INPP4B has diet-dependent and independent actions in mouse liver, adipose tissue, pancreas, and prostate. When fed a low-fat diet (LFD), three-month old *Inpp4b*$^{-/-}$ males developed liver steatosis associated with hyperglycemia. When fed an HFD, in addition to liver steatosis, *Inpp4b*$^{-/-}$ males also developed type II diabetes (T2D), inflammation of the visceral white adipose tissue (WAT) and prostate, and PIN. Thus, the loss of INPP4B results in metabolic dysfunction by increasing hepatic lipogenesis, elevating systemic and local inflammation, and promoting the neoplastic transformation of the prostates in obese males.

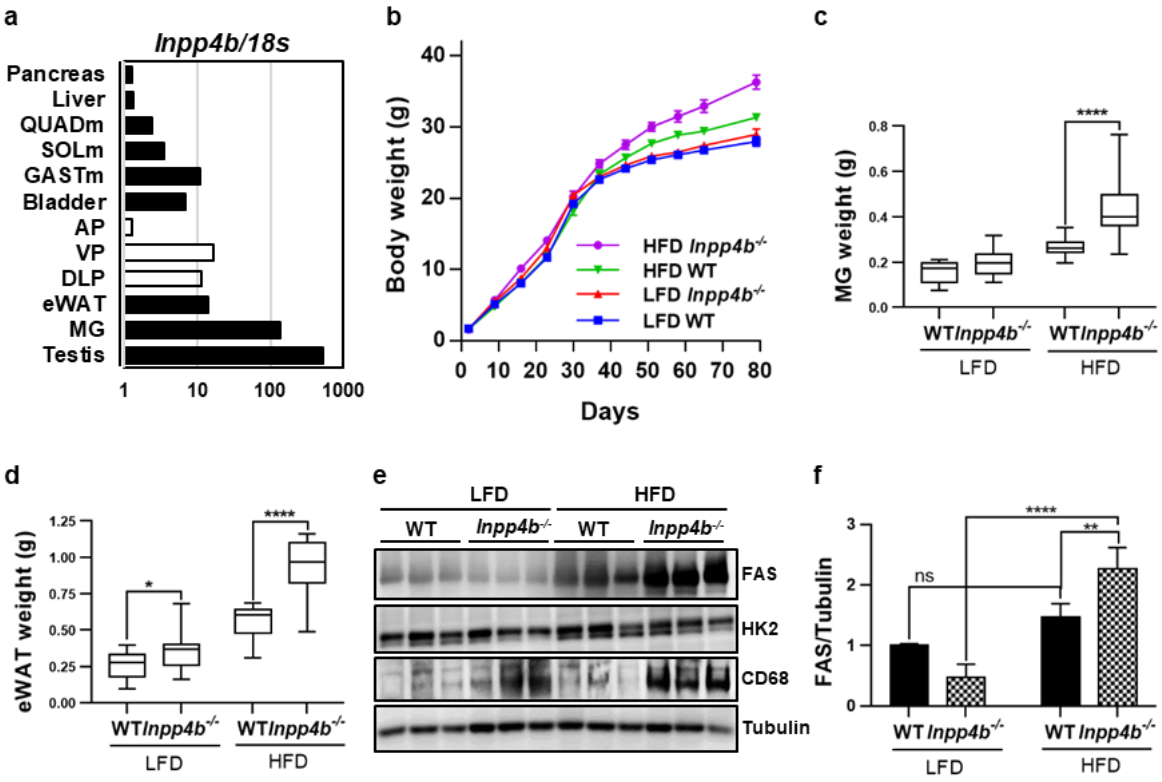

Figure 3-1. *Inpp4b* knockout accelerates adipose tissue expansion in mice on a high-fat diet. (a) mRNA expression of INPP4B in mouse tissues. (b) Body weight of LFD WT (N = 14), LFD *Inpp4b*$^{-/-}$ (N = 12), HFD WT (N = 9) and HFD *Inpp4b*$^{-/-}$ (N = 10) mice were recorded every week. Weight of mammary gland (c) and epididymal adipose tissue (eWAT) (d) were compared in the indicated groups at 12 weeks of age. (e) Protein lysates from eWAT were analyzed for FAS, HK2, CD68, and tubulin using western blotting. (f) Quantification of FAS protein level from (e). The FAS levels were normalized to tubulin and are shown as fold change.

3.3. Results

3.3.1. Accelerated weight gain in Inpp4b deficient male mice fed high fat diet.

Inpp4b expression was detected in multiple tissues (25). Analysis of mouse tissues showed that the highest expression of *Inpp4b* is in the testis, mammary gland fat pad, epididymal white adipose tissue (eWAT), muscle, and the ventral and dorsolateral lobes of the prostate. Lower levels of *Inpp4b* mRNA were also detected in the pancreas and liver (Figure 3-1 a), indicating that *Inpp4b* is expressed in major organs involved in insulin resistance. *Inpp4b*$^{-/-}$ males fed with an HFD gained significantly more weight than age-matched wild type (WT) controls (Figure 3-1 b). At three months of age, obesity in *Inpp4b*$^{-/-}$ males was not accompanied by changes in body length, blood pressure, or heart rate (Figure 3-2 a – c). A comparison of two representative depots of visceral WAT, the #4 mammary fat pad, and eWAT, revealed a significant weight increase in the HFD-fed *Inpp4b*$^{-/-}$ males versus the WT males (Figure 3-1 c – d). In eWAT, neither diet nor *Inpp4b* knockout altered the protein levels of HK2, an enzyme that mediates the commitment step of glycolysis (Figure 3-1 e, Figure 3-2 d). Expression of fatty acid synthase (*Fasn*) mRNA was increased with HFD (Figure 3-1 e) and the FASN protein levels were further increased in eWAT of HFD treated *Inpp4b*$^{-/-}$ mice (Figure 3-1 e – f), suggesting a role for INPP4B in lipid accumulation. Expression of *Inpp4b* was not affected in eWAT tissue by the HFD (Figure 3-2 f). Thus, the loss of INPP4B combined with an HFD treatment activated lipogenesis and led to significant adipose expansion.

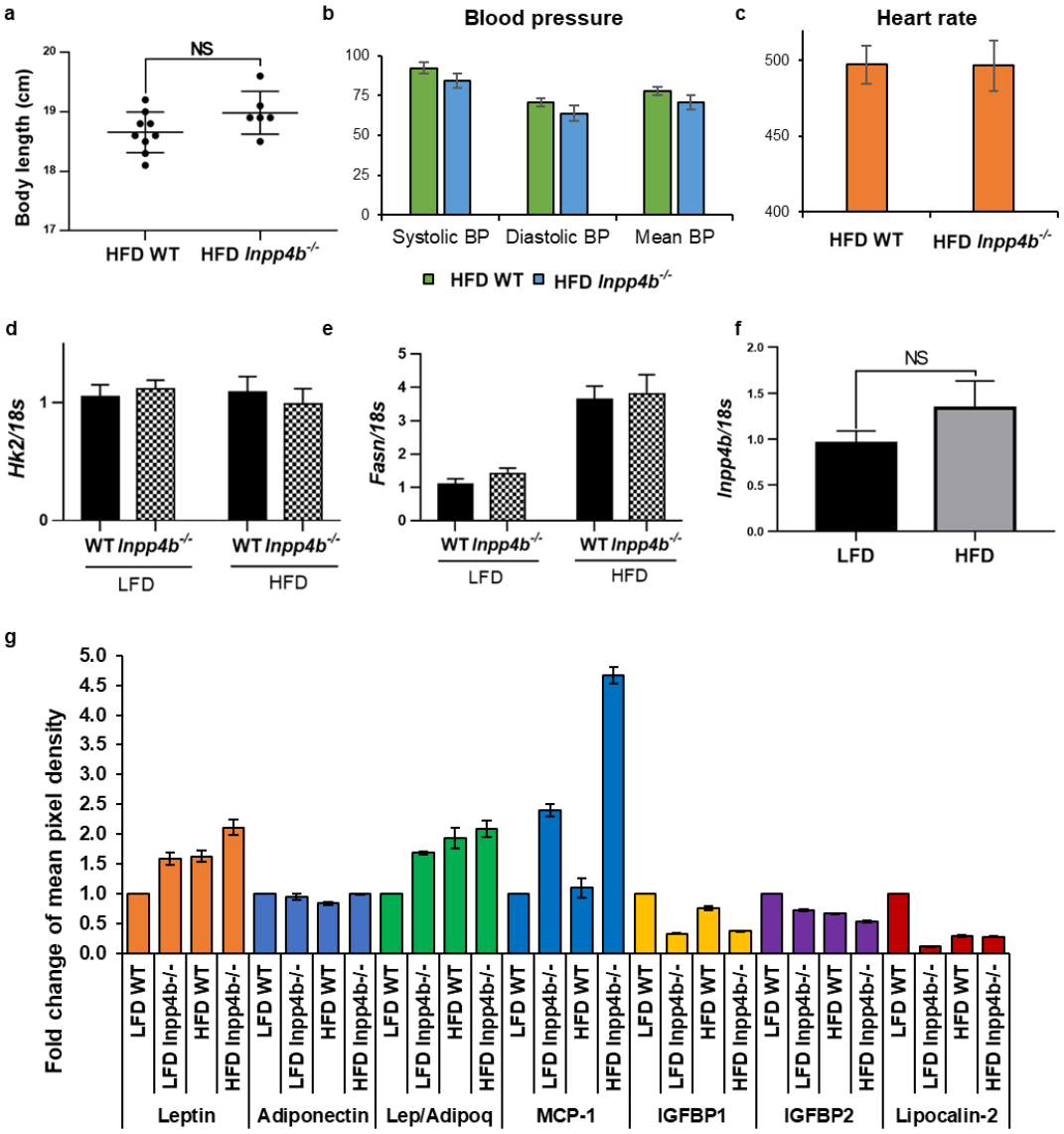

Figure 3-2. Morphometric and metabolic response to HFD and INPP4B loss. (a-c) Body length (a), blood pressure (b), and heart rate (c) were measured for HFD WT (N = 9) and HFD *Inpp4b*$^{-/-}$ mice (N = 10). (d-e) RNA was extracted from eWAT of LFD WT (N = 13), LFD *Inpp4b*$^{-/-}$ (N = 11), HFD WT (N = 9), and HFD *Inpp4b*$^{-/-}$ (N = 10) mice and analyzed for *Hk2* (d) and *Fasn* (e) expression by qRT-PCR using *18S* as an internal control. (f) The expression levels of *Inpp4b* in eWAT were determined in LFD WT and HFD WT mice by qRT-PCR and normalized to *18S* expression. (g) Semi-quantification of levels of Leptin, Adiponectin, Leptin/Adiponectin, MCP-1, IGFBP1, IGFBP2, and Lipocalin-2 in the eWAT of LFD WT, LFD *Inpp4b*$^{-/-}$, HFD WT and HFD *Inpp4b*$^{-/-}$ are presented as fold change of relative pixel density. Signal intensity in LFD WT mice was designated as 1. Protein extracts from 5 mice were combined in each group and used for the adipokine array.

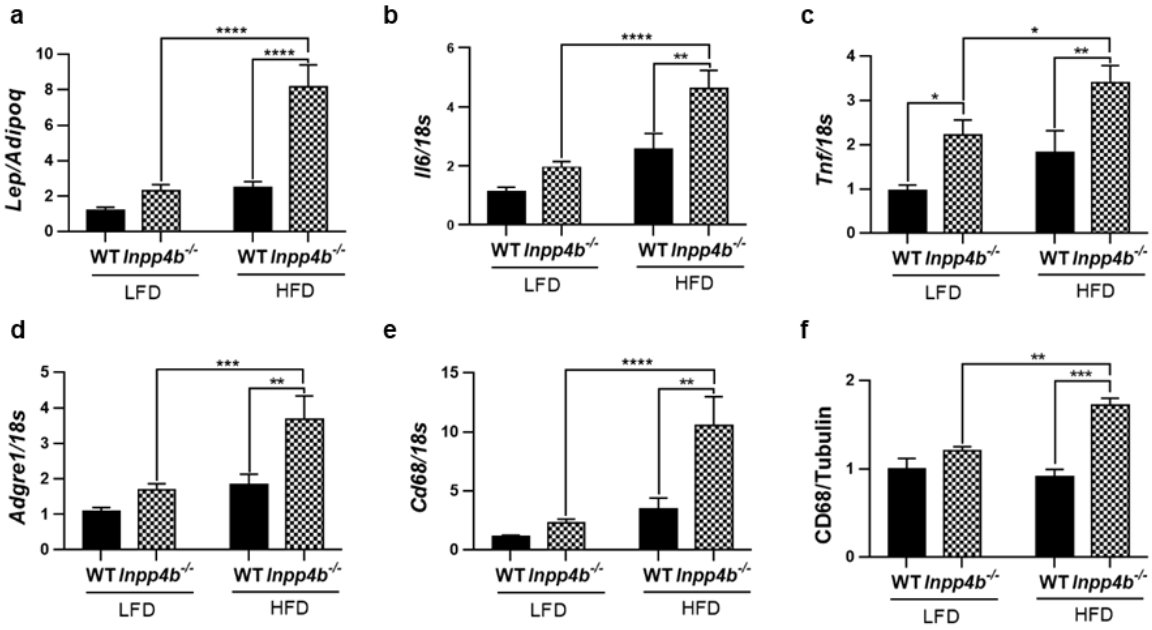

Figure 3-3. *Inpp4b* knockout accelerates inflammation in mice on a high-fat diet. (a-f) RNA was extracted from mouse eWAT of LFD WT, LFD *Inpp4b*$^{-/-}$, HFD WT, and HFD *Inpp4b*$^{-/-}$ mice. The expression levels of *Lep/Adipoq* (a), *Il6* (b), *Tnf* (c), *Adgre1* (d), and *Cd68* (e) were assayed by qRT-PCR using *18S* as an internal control. (l) Quantification of CD68 protein levels from Figure 3-1 e. Average expression in LFD WT mice was designated as 1. (*p < 0.05, **p < 0.01, ***p < 0.001, ****p < 0.0001)

3.3.2. High levels of inflammatory cytokines and expression of macrophage markers in visceral fat of *Inpp4b* deficient male mice.

WAT secretes a broad variety of adipokines and cytokines that modulate inflammation and insulin signaling (190-193). We tested whether INPP4B regulates the inflammatory status of adipose tissue in HFD-fed males. Strikingly, the eWAT of HFD-fed *Inpp4b*$^{-/-}$ mice had a significantly increased ratio of leptin to adiponectin expression (Figure 3-3 g) and elevated expression of the inflammatory cytokines *Il6* and *Tnf* (Figure 3-3 h – i). The adipose tissue in HFD-fed knockout males showed an increased expression of the macrophage markers *Adgre1* and *CD68* (Figure 3-3 j – k). The highest protein levels of CD68 were observed in the eWAT of the HFD *Inpp4b*$^{-/-}$ group, suggesting that the INPP4B

deficiency promotes the inflammatory response of adipose tissue in the diet-induced obesity (Figure 3-3 l). As shown in Figure 3-3 g – l, both HFD and INPP4B loss contributed to increases in inflammation and infiltration markers in the adipose tissue.

Using adipokine arrays, we compared the protein levels of 40 adipokines from the eWAT of WT and *Inpp4b*$^{-/-}$ mice fed with LFD or HFD (Figure 3-2 g). The array analysis confirmed the increased leptin/adiponectin ratio at the protein level. Consistent with the increased presence of CD68^{+} cells, the eWAT from *Inpp4b*$^{-/-}$ mice expressed significantly higher levels of the proinflammatory chemokine, monocyte chemoattractant protein – 1 (MCP-1), which promotes macrophage infiltration and is known to be increased in obese diabetic mice (194, 195). Adipose expansion and inflammation are downregulated by INPP4B in obese animals, suggesting a protective role for INPP4B from metabolic syndrome.

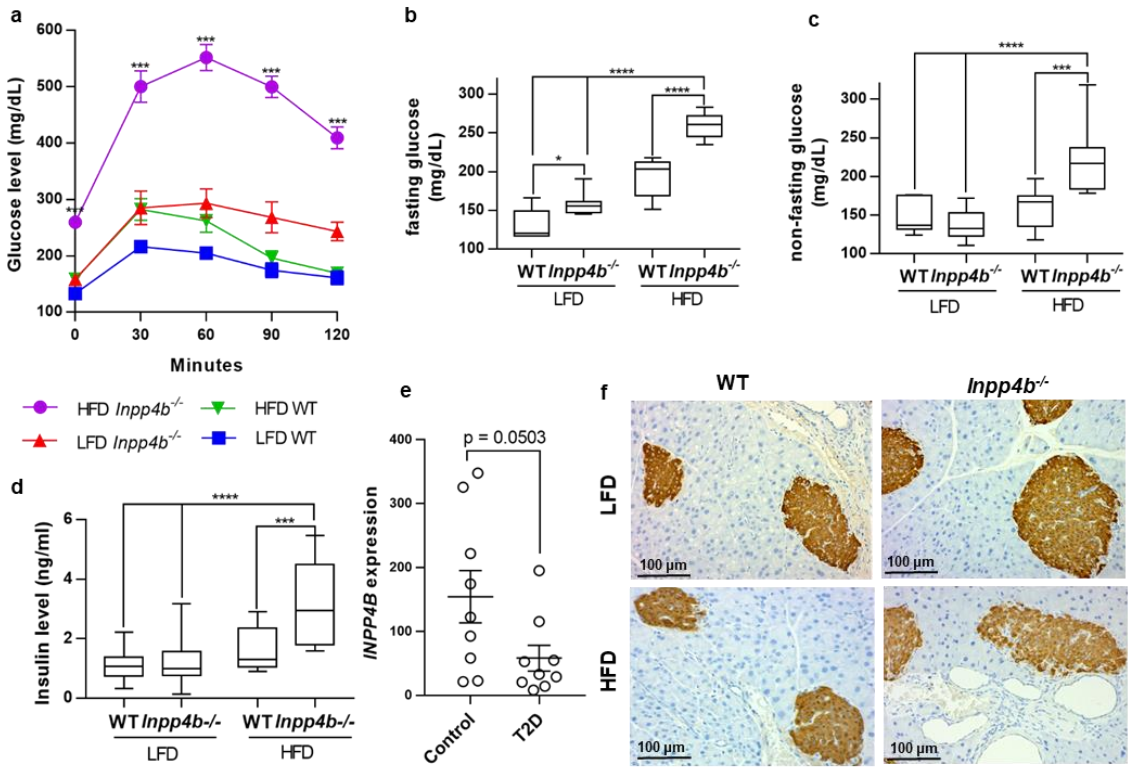

Figure 3-4. INPP4B protects mice from hyperglycemia and diabetes. (a) Oral glucose tolerance test of LFD WT (N = 7), LFD *Inpp4b*$^{-/-}$ (N = 7), HFD WT (N = 9) and HFD *Inpp4b*$^{-/-}$ (N = 6) mice following a 2 g/kg oral glucose challenge. Blood glucose levels were measured after 6 hours of fasting (b) or in non-fasted (c) LFD WT, LFD *Inpp4b*$^{-/-}$, HFD WT and HFD *Inpp4b*$^{-/-}$ mice. (d) Blood insulin level was measured using mouse insulin ELISA in the indicated groups. (e) INPP4B expression in livers of subjects with or without type II diabetes (T2D) were exported from GSE15653. (f) Pancreas sections from LFD WT, LFD *Inpp4b*$^{-/-}$, HFD WT and HFD *Inpp4b*$^{-/-}$ mice were stained for insulin and counterstained with hematoxylin. (*p < 0.05, ***p < 0.001, ****p < 0.0001)

3.3.3. *Inpp4b* deficient mice develop hyperglycemia on normal low fat diet and type 2 diabetes on high fat diet.

The expansion and increased inflammation of adipose tissue suggested that *Inpp4b*$^{-/-}$ animals are insulin resistant. In fact, in an independently conducted QTL analysis in mice, Mu *et al.* have shown an association between the *D8Mit195* locus, mapped immediately next to the *Inpp4b* gene, and elevated plasma glucose levels (LRS=10.4, LOD=2.3) (196). The increase in the *Lep/Adipoq* ratio observed in HFD *Inpp4b*$^{-/-}$ group, is characteristic to obese diabetic mice and men (197, 198). Glucose tolerance tests revealed that WT HFD-fed mice had an elevated fasting blood glucose level compared to the lean WT males. Upon administration of an oral glucose bolus to WT males, serum glucose levels rose higher in HFD group than in LFD but recovered to normal after 120 minutes. When fed with either LFD or HFD, *Inpp4b*$^{-/-}$ mice had elevated fasting glucose levels and they were unable to fully clear it after 120 minutes (Figure 3-4 a – b). The rapid rise to extremely high fasting glucose levels and the inability to clear blood glucose in obese *Inpp4b*$^{-/-}$ males were consistent with obesity-induced T2D (199). Circulating, non-fasting glucose and insulin levels were also significantly elevated in HFD-fed mutant animals compared to every other group (Figure 3-4 c – d). Despite normal levels of circulating insulin in LFD *Inpp4b*$^{-/-}$ males, the rate of hepatic gluconeogenesis was increased, confirming that lean knockout males developed hyperglycemia (Figure 3-5 a). Similar to our HFD *Inpp4b*$^{-/-}$ male mice, gene expression analysis in the livers of nondiabetic (N = 9) and T2D obese individuals (N = 9) (GSE15653) revealed that INPP4B expression was decreased in the obese, diabetic group (Figure 3-4 e) (200). As expected, pancreatic islets were positive for insulin staining by IHC (Figure 3-4 f). Consistent with the increase in blood insulin levels, the expression

of proinsulin convertase, *Pcsk1*, was increased in the pancreata of LFD-fed *Inpp4b*$^{-/-}$ mice and in both HFD-fed groups (Figure 3-5 b). Both HFD and *Inpp4b* knockout decreased expression of the peptide hormone cholecystokinin (*Cck*), an appetite suppressant and stimulant of pancreatic enzyme secretion (201) (Figure 3-5 c). The markers of pancreatic β-cell viability and inflammation, *Furin* and *Il6*, and the unfolded protein response (UPR), *Mafa*, did not significantly change (Figure 3-5 d – f) at 3 months of age. Our results and results from other groups suggest that INPP4B is a metabolic modulator that protects from diet induced T2D.

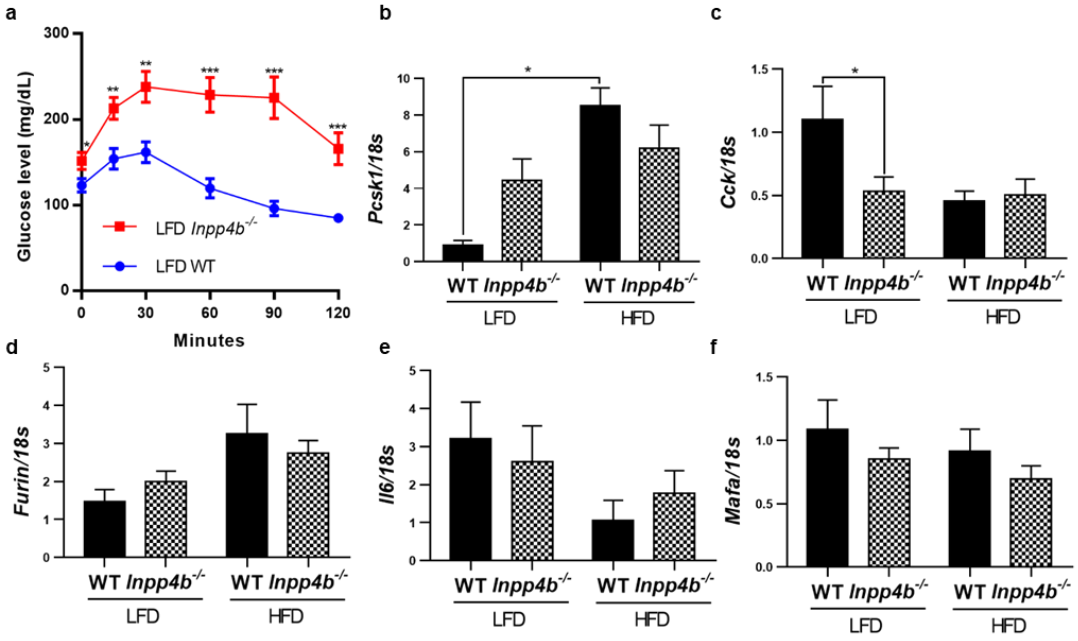

Figure 3-5**.** Development of hyperglycemia in LFD *Inpp4b*$^{-/-}$ males. (a) For the pyruvate tolerance test, sodium pyruvate was injected intraperitoneally at 1.5 g/kg to age-matched LFD WT and LFD *Inpp4b*$^{-/-}$ mice (N = 8 per group). (b-f) RNAs were extracted from mouse pancreas of LFD WT, LFD *Inpp4b*$^{-/-}$, HFD WT, and HFD *Inpp4b*$^{-/-}$ mice. The expression levels of *Pcsk1* (b), *Cck* (c), *Furin* (d), *Il6* (e), and *Mafa* (f) were assayed by qRT-PCR. (*p < 0.05)

3.3.4. Loss of INPP4B leads to NAFLD.

NAFLD is the best predictor of insulin resistance (180). To determine whether insulin resistance in *Inpp4b*$^{-/-}$ mice is associated with NAFLD, we first compared the liver weights in WT and *Inpp4b*$^{-/-}$ males fed LFD or HFD. Strikingly, the liver weights were significantly elevated in *Inpp4b*$^{-/-}$ knockouts independent of the diet (LFD $p = 0.0422$, HFD $p = 0.0374$) (Figure 3-6 a). Morphometric quantification of H&E stained slides revealed severe steatosis in the livers of all *Inpp4b*$^{-/-}$ mice (LFD groups: $p = 0.0111$, HFD groups: $p = 0.0004$) (Figure 3-6 b – c). Livers in knockout animals featured all major histological characteristics of NAFLD, such as accumulation of fat (Figure 3-6 d), microvesicular and macrovesicular steatosis, hepatocellular hypertrophy, inflammatory cell aggregates, pyknotic nuclei, and Mallory bodies (Figure 3-6 e) (202). Liver triglyceride amounts were significantly increased in *Inpp4b*$^{-/-}$ mice compared to WT controls in both LFD ($p = 0.0478$) and HFD ($p < 0.0001$) groups (Figure 3-7 a). In the livers of WT FVB male mice, the HFD caused modest increases in the expression of *Inpp4b* and *Cd68*, a marker of infiltrating macrophages (Figure 3-7 b – c). In human liver, INPP4B was detected in the cytoplasm and cell membrane of normal hepatocytes and its protein levels decreased in primary and especially metastatic hepatocellular carcinoma (203) which undergo significant metabolic reprogramming. Similar to the mouse liver, hepatic *INPP4B* expression in patients with NAFLD was significantly reduced compared to healthy controls (GSE126848) (204) and there was a highly significant correlation between steatosis score and *INPP4B* mRNA levels (Figure 3-6 f – g). Thus, the loss of INPP4B in mice is similar to the decline in *INPP4B* expression observed in steatotic livers of NAFLD patients (204).

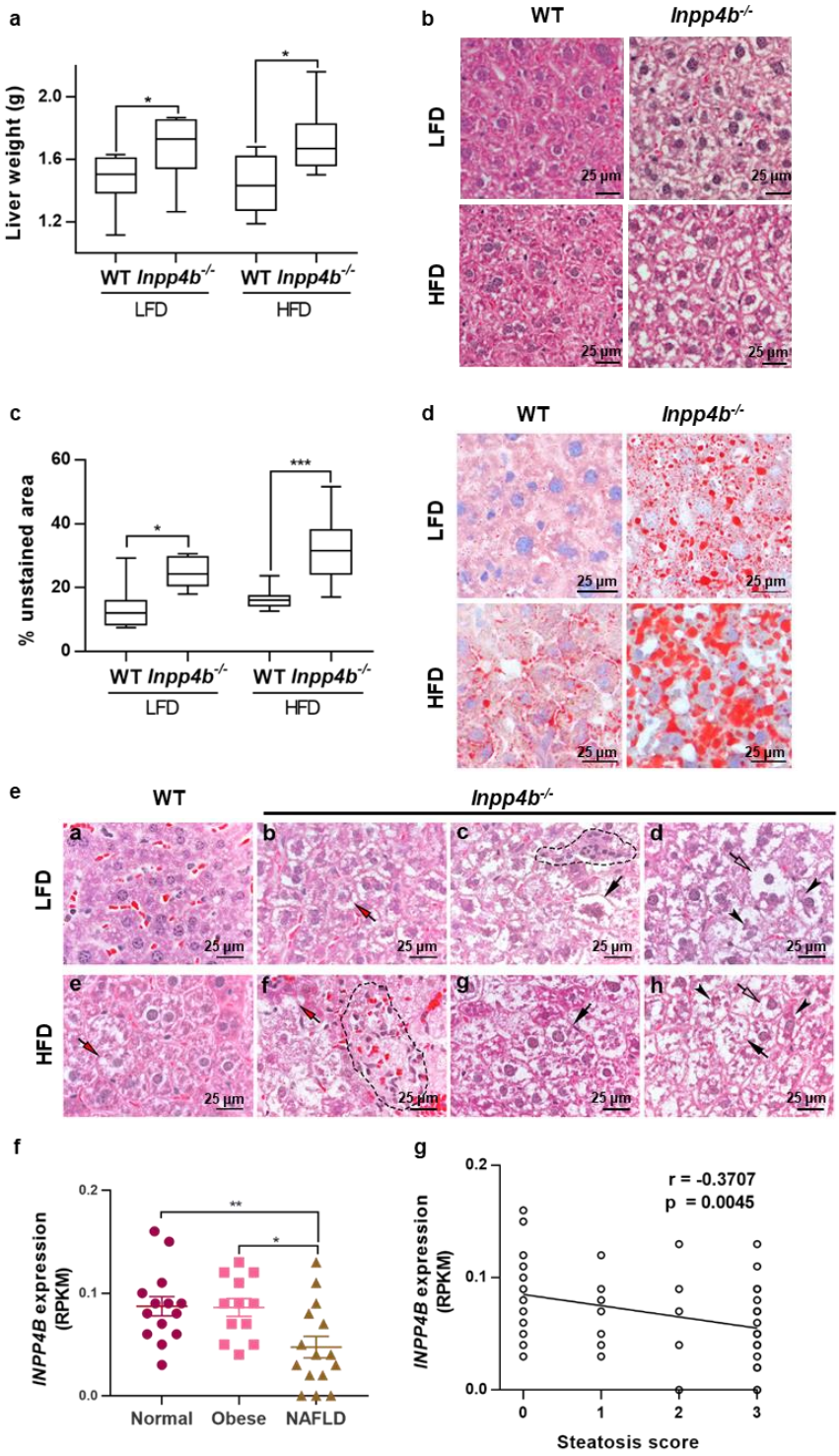

Figure 3-6. INPP4B protects mice from liver steatosis. Livers were dissected from LFD WT (N = 11), LFD *Inpp4b*$^{-/-}$ (N = 13), HFD WT (N = 9), and HFD *Inpp4b*$^{-/-}$ (N = 10) mice. (a) Liver weights in four experimental groups. (b) Representative H&E staining of liver sections from designated experimental groups used for steatosis analysis. (c) Morphometric quantification of the unstained area on H&E stained liver sections. (d) Representative images of the Oil Red O/ hematoxylin

staining of frozen liver sections in designated groups. (e) Characteristic features of hepatocellular steatosis in livers of HFD and LFD *Inpp4b*$^{-/-}$ males. Examples of hypertrophy (open arrow), inflammatory cell aggregates (dash line), Mallory bodies (arrowhead), macrovesicular steatosis (red arrow), and microvesicular steatosis (black arrow) in LFD and HFD *Inpp4b*$^{-/-}$ mice. (f) INPP4B expression in RPKM (Reads Per Kilobase Million) in normal liver tissue (N = 14), obese (N = 12 patients), and NAFLD (N = 15 patients) in GSE126848 dataset. (g) Correlation between INPP4B expression with the steatosis score in patients with NAFLD or NASH. Data were exported from GSE126848. (*p < 0.05, **p < 0.01, ***p < 0.001)

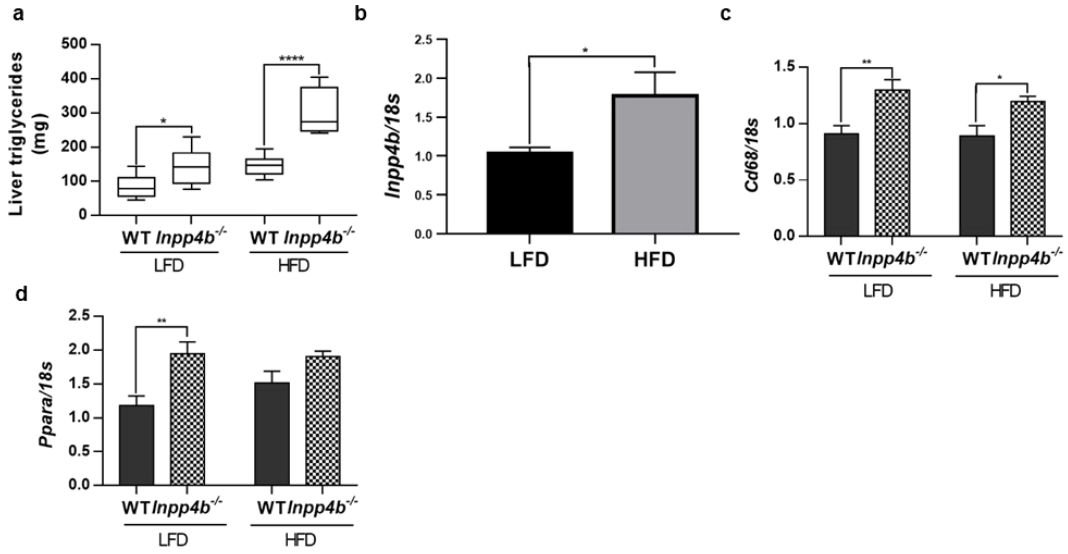

Figure 3-7**.** Aberrant lipid storage in livers of *Inpp4b*$^{-/-}$ males. (a) The amounts of total triglycerides in liver were measured in LFD WT (N = 8), LFD *Inpp4b*$^{-/-}$ (N = 8), HFD WT (N = 6) and HFD *Inpp4b*$^{-/-}$ (N = 4) mice. (b) RNAs were extracted from mouse livers and the expression level of *Inpp4b* was determined in LFD WT and HFD WT mice using qRT-PCR and normalized to *18S*. The expression levels of *Cd68* (c) and *Ppara* (d) were analyzed by qRT-PCR in groups with the indicated diets and genotypes. (*p < 0.05, **p<0.01, ****p<0.0001)

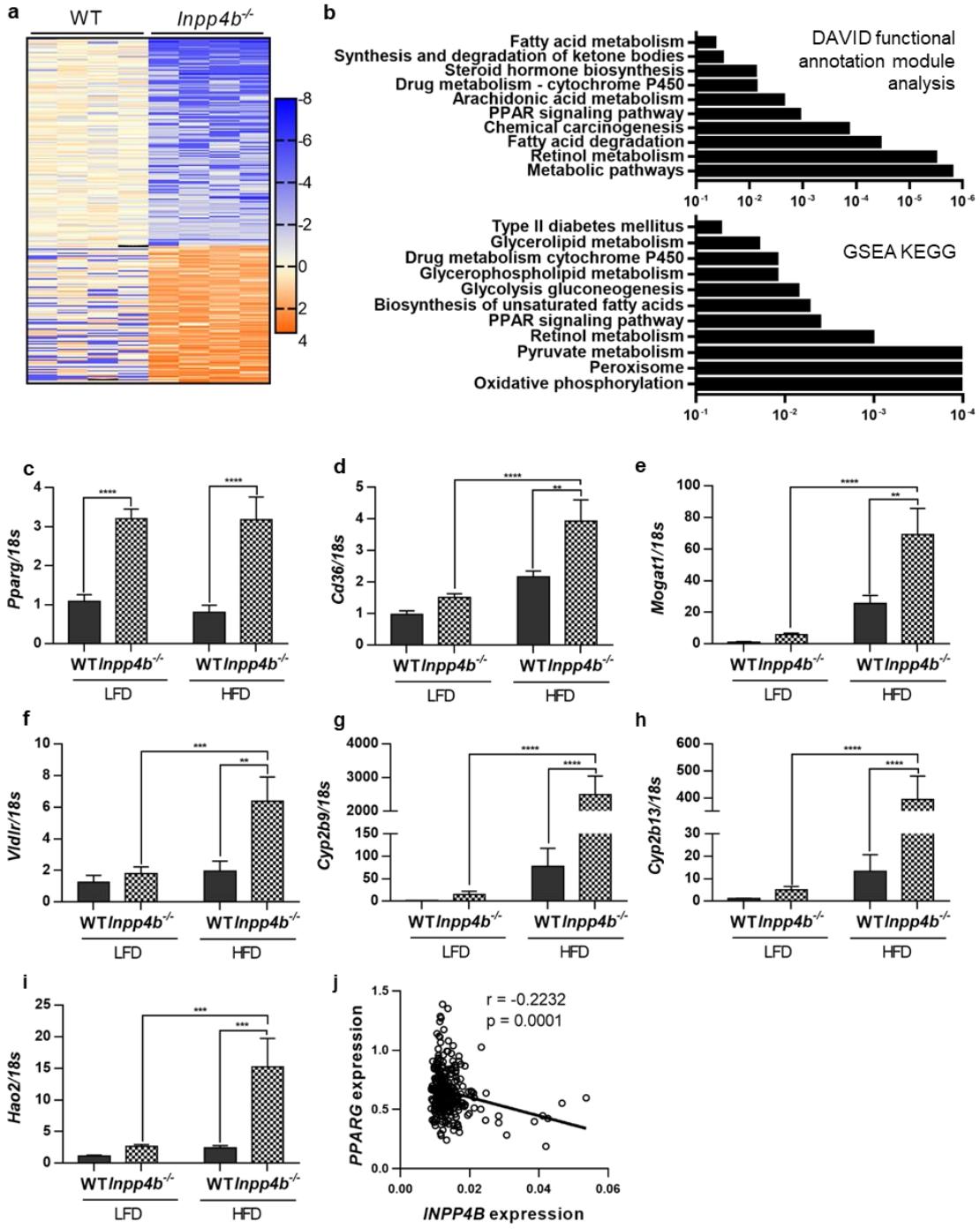

Figure 3-8. INPP4B regulates metabolic and PPAR pathways in mouse liver. (a) RNA were extracted from livers of HFD WT (N=4) and HFD *Inpp4b*$^{-/-}$ (N=4) mice and were submitted for RNA sequencing. The changes in gene expression were compared between HFD WT and HFD *Inpp4b*$^{-/-}$ mice. (b) KEGG pathway functional enrichment analysis were done using DAVID functional annotation module (top) or GSEA (bottom). The vertical axis represents the KEGG pathway terms significantly enriched by the differentially expressed gene with the loss of INPP4B

in mouse liver. The horizontal axis shows the logarithmic scale of p value. (c-i) RNA from LFD WT (N = 10), LFD *Inpp4b*$^{-/-}$ (N = 12), HFD WT (N = 8), and HFD *Inpp4b*$^{-/-}$ (N = 10) mice were analyzed for *Pparg* (c), *Cd36* (d), *Mogat1* (e), *Vldlr* (f), *Cyp2b9* (g), *Cyp2b13* (h), and *Hao2* (i) by qRT-PCR using *18S* as an internal control. (j) Correlation between INPP4B expression and PPARG expression in 289 human liver samples (GSE24335). (**p < 0.01, ***p < 0.001, ****p < 0.0001)

3.3.5. NAFLD in *Inpp4b*$^{-/-}$ males is caused by increased lipogenesis, WAT inflammation, and activation of AKT and PKC signaling.

To determine the molecular pathways that protect WT mice on HFD from NAFLD, we performed RNA-seq analysis of liver samples from WT and *Inpp4b*$^{-/-}$ males on an HFD. Analysis of differentially expressed genes (DEG) with DAVID functional annotation module and Gene Set Enrichment Analysis (GSEA) revealed that *Inpp4b* deletion affected lipid and glucose metabolisms, drug detoxification, peroxisome biogenesis, and expression of T2D associated genes (Figure 3-8 a – b). Lipid metabolism and peroxisome biogenesis are known targets of the PPAR family of transcription factors (203, 205, 206). PPARG is a transcriptional regulator of fatty acid uptake and storage, while PPARA activity stimulates fatty acid oxidation. Expression of *Pparg* increased in both LFD and HFD-fed *Inpp4b*$^{-/-}$ males compared to WT controls (Figure 3-8 c). Correspondingly, expression of PPARG target genes regulating lipid delivery, internalization, triglyceride synthesis, and fatty acid metabolism increased in *Inpp4b*$^{-/-}$ livers (Figure 3-8 d – g). Strikingly, a group of genes involved in sexually dimorphic drug and lipid metabolism, *Cyp2b9, Cyp2b13, Hao2* (GSE 89091) (207), were strongly downregulated by INPP4B and their expression strongly increased in livers of knockout males (Figure 3-8 g – i). *Ppara* expression was modestly increased in LFD *Inpp4b*$^{-/-}$ group only (Figure 3-7 d), potentially contributing to partial NAFLD resistance in lean knockout animals. Similar to *Inpp4b*$^{-/-}$ mice, liver samples

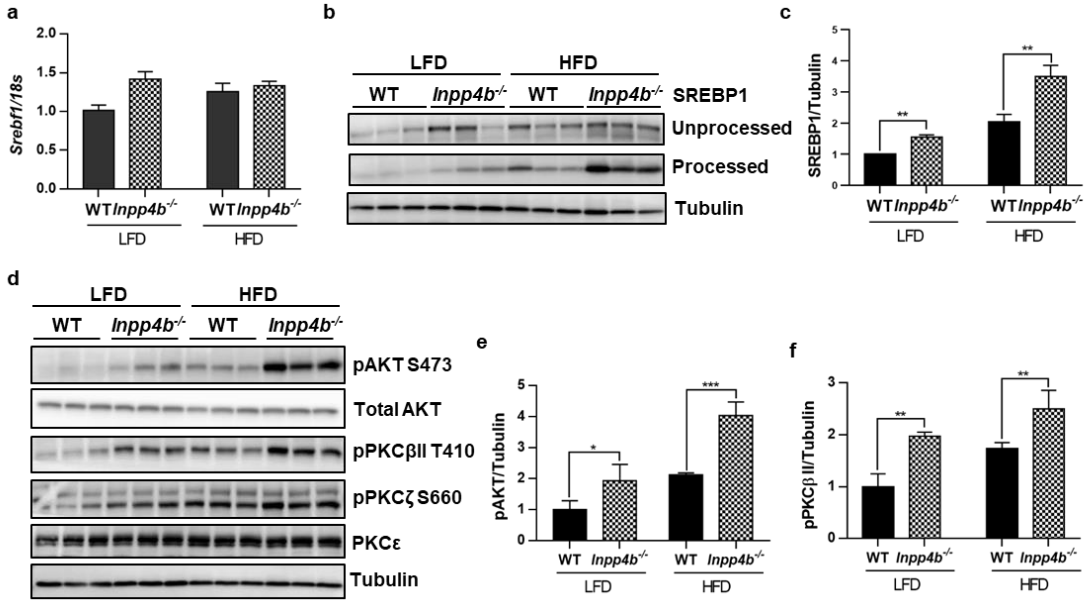

Figure 3-9. INPP4B regulates lipogenesis and AKT and PKC signaling pathways in mouse liver. (a) RNA from Figure 4(c-i) were analyzed for *Srebf1* by qRT-PCR using *18S* as control. (b) Proteins were extracted from livers of LFD WT, LFD *Inpp4b*$^{-/-}$, HFD WT, and HFD *Inpp4b*$^{-/-}$ mice and used to compare levels of unprocessed SREBP1, processed SREBP1, and tubulin by Western blotting. (c) Quantification of processed SREBP1 levels were presented as an average of four independent samples. The protein levels were normalized to tubulin and were shown in fold change from LFD WT. (d) Protein lysates from (b) were analyzed for pAKT, total AKT, pPKCβII, pPKCζ, pPKCε, and tubulin using western blotting. (e-f) Quantification of pAKT and pPKCβII protein levels from (d). (*$p < 0.05$, **$p < 0.01$, ***$p < 0.001$)

collected in the course of Roux-en-Y gastric bypass surgery from 1008 obese patients (GSE24335) exhibited a highly significant negative correlation between *INPP4B* and *PPARG* expression (208) (Figure 3-8 j). Thus, expression data in mice and men support our finding that INPP4B downregulates PPARG levels in liver. Disparate spatial localization of these proteins suggests the existence of an intermediate regulatory protein. SREBP1 is a transcriptional activator of many lipogenic enzymes, including *Pparg* (209, 210). Based on our RNA-seq analysis, the levels of *Srebf1* mRNA did not significantly increase in *Inpp4b*$^{-/-}$ livers (Figure 3-9 a). However, activation of SREBP1 requires proteolytic cleavage and nuclear translocation (211, 212). Comparison of the precursor (125 kDa) and transcriptionally active (55 kDa) forms of SREBP1, showed a significant increase of the 55 kDa form due to both *Inpp4b* knockout and HFD treatment (Figure 3-9 b – c). SREBP1 proteolysis is induced by a variety of signals, including insulin, Akt, retinoids, PKC, and its own activated form (211, 212). Thus, the activation of insulin, retinol, Akt, and PKC signaling pathways in obese knockout males stimulates proteolytic cleavage of SREBP1 in the livers of HFD *Inpp4b*$^{-/-}$ group activating expression of *Pparg* and other lipogenic enzymes and leading to the development of hepatosteatosis.

3.3.6. HFD causes neoplastic changes in prostates of *Inpp4b*$^{-/-}$ mice.

Inpp4b$^{-/-}$ mice on regular chow have the same weight as the WT animals and do not develop tumors in the first 4 months of age; some hyperplastic changes developed only in one year old animals (54). The increased leptin/adiponectin ratios and adipose inflammation are risk factors for the development of prostate cancer in men (213, 214) and were observed in in HFD *Inpp4b*$^{-/-}$ males. We tested whether significant metabolic dysfunction triggered by the HFD would lead to an earlier and more severe prostate phenotype in knockout male mice.

Indeed, all *Inpp4b*$^{-/-}$ males (N = 11) developed high grade PIN by 11 weeks of age, while none of the WT males on the same diet did. Anterior prostate (AP), dorsolateral prostate (DLP), and ventral prostate (VP) lobes exhibited various degrees of epithelial expansion and loss of polarity. The most extensive histological changes were observed in DLP glands, including epithelial and basal layer expansion, piling up of epithelial cells, loss of polarity, nuclear atypia, and a discontinuous fibromuscular layer around individual glands (Figure 3-10 a – b). Androgen receptor activity, cell signaling, and inflammation are among the factors most strongly contributing to neoplastic transformation of the prostate (215). The levels of AR and PTEN were not significantly altered by INPP4B loss on either diet. While the HFD led to increased macrophage infiltration in the prostates of both WT and mutant males, there was no difference between both genotypes in *Cd68* expression (

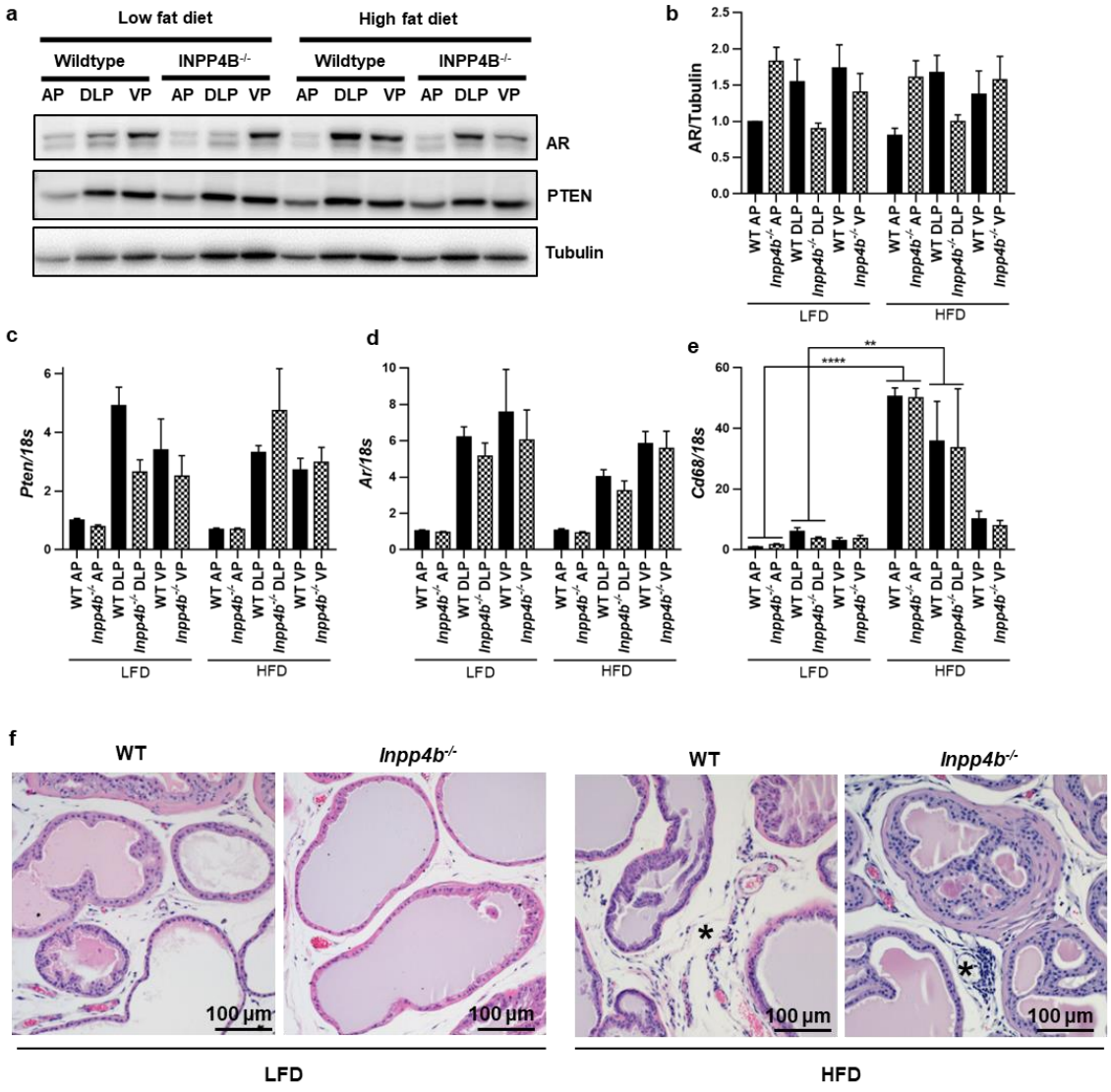

Figure 3-11 a – e). Consistently, inflammatory infiltrate was observed in the prostate stromae of obese WT and knockout males (

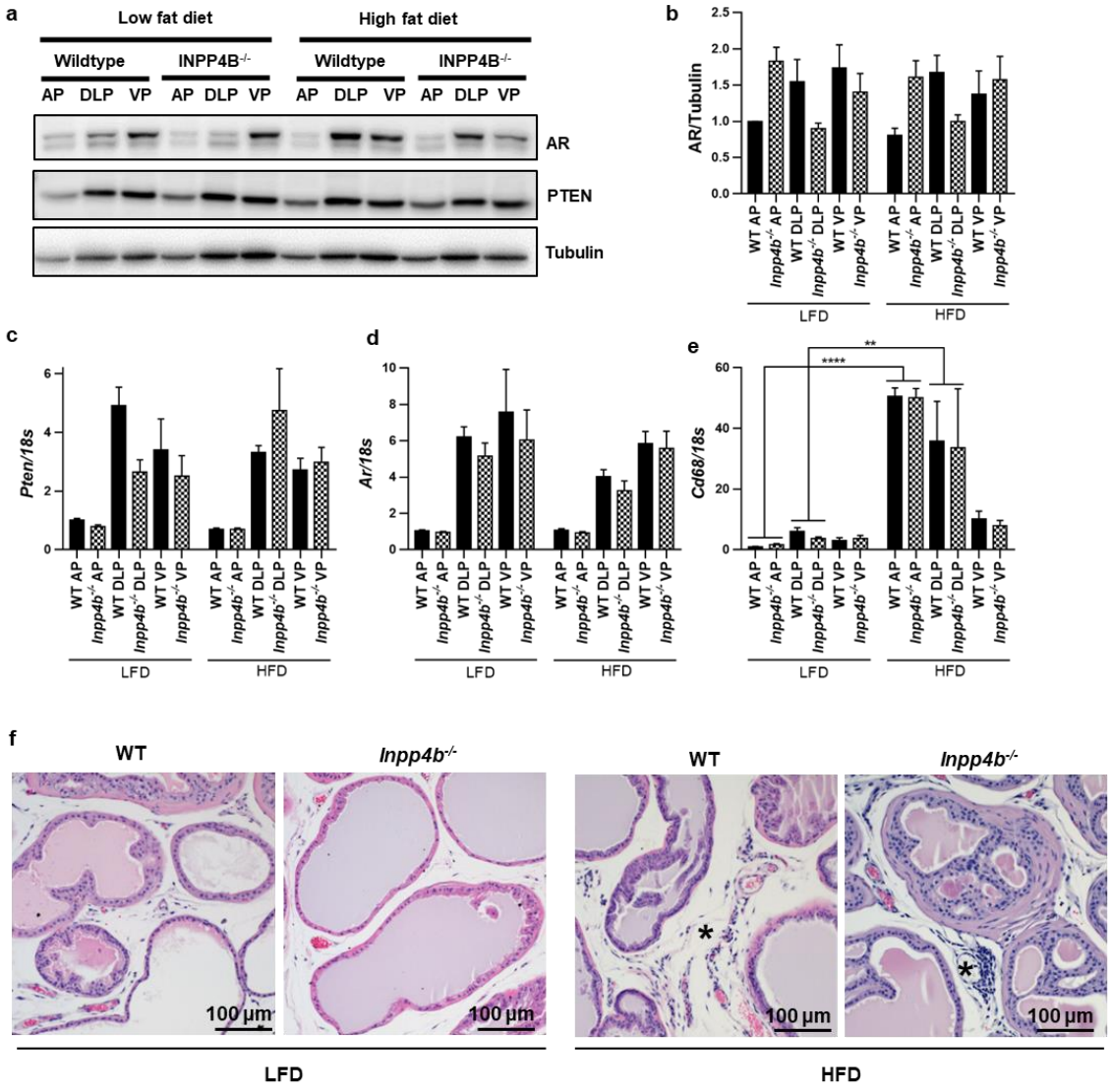

Figure 3-11 f, marked with *****). Staining with the Ki67 antibody indicated increased cellular proliferation in the prostates of HFD *Inpp4b*$^{-/-}$ males (Figure 3-12 a). While AR protein levels did not change, its transcriptional activity was affected. Expression of AR-induced target genes, *Pbsn*, *Apof*, *Nkx3.1*, and *Msmb*, were significantly decreased in the DLP of LFD *Inpp4b*$^{-/-}$ males (Figure 3-10 c - f). HFD further decreased expression of AR target genes *Nkx3.1* and *Msmb* (Figure 3-10 e – f). However, we observed no change in the ability of AR to repress transcription of its target gene *Igfbp3* (Figure 3-10 g). Levels of pAkt were

increased in prostates of LFD *Inpp4b*$^{-/-}$ mice; no further increase was detected in HFD-treated groups (Figure 3-12 c – d). Similarly, levels of PKCβII and pPKCζ were slightly increased in DLP and VP lobes of LFD *Inpp4b*$^{-/-}$ males and treatment with HFD did not further increase the signal (data not shown).

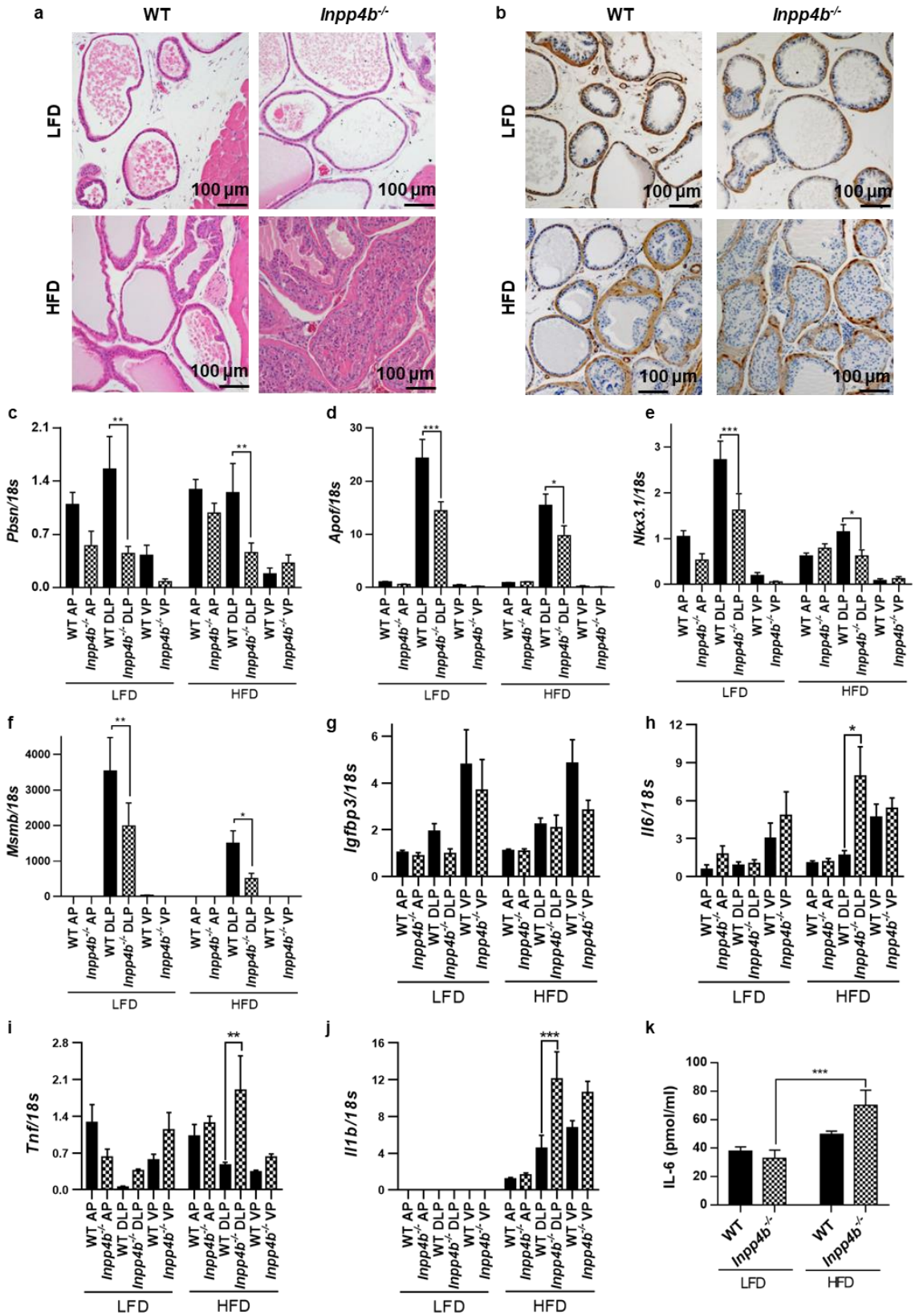
a
WT
Inpp4b-/-
LFD
HFD
100 µm
b
WT
Inpp4b-/-
LFD
HFD
100 µm
c
Pbsn/18s
d
Apof/18s
e
Nkx3.1/18s
f
Msmb/18s
g
Igfbp3/18s
h
Il6/18s
i
Tnf/18s
j
Il1b/18s
k
IL-6 (pmol/ml)
WT AP
Inpp4b-/- AP
WT DLP
Inpp4b-/- DLP
WT VP
Inpp4b-/- VP
LFD
HFD
WT
Inpp4b-/-

Figure 3-10**.** Loss of *Inpp4b* leads to the development of PIN and inflammation in obese males. (a) H&E staining of prostates from LFD WT, LFD *Inpp4b*$^{-/-}$, HFD WT, and HFD *Inpp4b*$^{-/-}$ males. (b) Representative tissue sections from LFD WT, LFD *Inpp4b*$^{-/-}$, HFD WT, and HFD *Inpp4b*$^{-/-}$ prostates were stained for α-SMA and counterstained with hematoxylin. Anterior prostate (AP), dorsolateral prostate (DLP) and ventral prostate (VP) were dissected from LFD WT, LFD *Inpp4b*$^{-/-}$, HFD WT, and HFD *Inpp4b*$^{-/-}$ mice. (c-j) RNA was extracted and the expression levels of *Pbsn* (c), *Apof* (d), *Nkx3.1* (e), *Msmb* (f), *Igfbp3* (g), *Il6* (h), *Tnf* (i), and *Il1b* (j) were compared by qRT-PCR using *18S* as an internal control. (k) Protein levels of IL-6 in mouse dorsolateral prostates were measured using IL-6 ELISA. (*$p < 0.05$, **$p < 0.01$, ***$p < 0.001$)

3.3.7. HFD leads to prostate inflammation in *Inpp4b*$^{-/-}$ males.

Inflammation plays a key role in the etiology of prostate cancer (216). We tested whether the development of prostate neoplasms in the HFD *Inpp4b*$^{-/-}$ males was accompanied by inflammation. In the dorsolateral lobe of the prostates of obese males, *Il6* and *Tnf* mRNA levels were significantly increased in *Inpp4b*$^{-/-}$ mice when compared to WT (Figure 3-10 h – i). As expected, expression of the potent pro-inflammatory cytokine, *Il1b*, was undetectable in the prostates of LFD mice. Consumption of HFD induced the expression of *Il1b* in the prostates in both genotypes. Specifically, in the DLP, the loss of INPP4B resulted in a significant increase in *Il1b* expression when compared to WT (Figure 3-10 j). Protein levels of the proinflammatory cytokine IL6 were significantly increased in the DLP of HFD fed *Inpp4b*$^{-/-}$ mice (Figure 3-10 k). While there are anatomical differences between mice and humans, the mouse DLP is considered most similar to the human peripheral zone, the site of origin of most human prostate cancers (217). It is also important to note that in the prostate, the dorsolateral region features the highest expression of *Inpp4b* (Figure 3-12 b), suggesting a physiological function for INPP4B protein in that lobe.

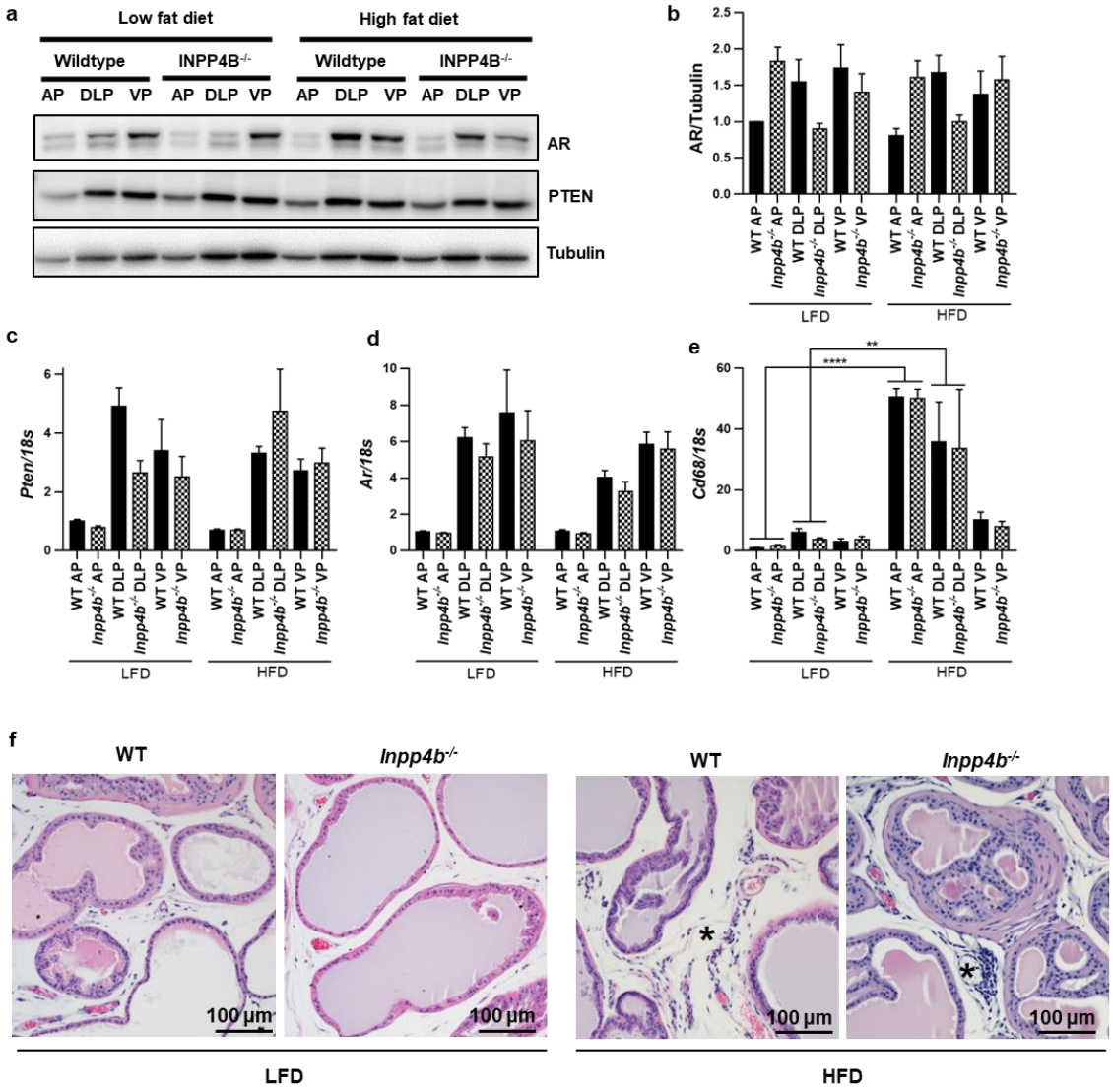

Figure 3-11. Prostate-specific levels of AR, PTEN and inflammation in WT and *Inpp4b*$^{-/-}$ males. (a) Protein levels of AR, PTEN, and tubulin in AP, DLP, and VP of LFD WT, LFD *Inpp4b*$^{-/-}$, HFD WT and HFD *Inpp4b*$^{-/-}$ mice were assayed by western blotting. (b) Quantification of AR protein levels were done using tissues from five individual mice in the indicated groups; representative western blot is shown in (a). (c-e) RNAs were analyzed for *Pten* (c), *Ar* (d) and *Cd68* (e) expression by qRT-PCR and normalized to *18S*. (f) H&E staining showed immune cell infiltration (labeled as *) in the prostates of WT and knockout males fed with HFD. (**p < 0.01, ****p<0.0001)

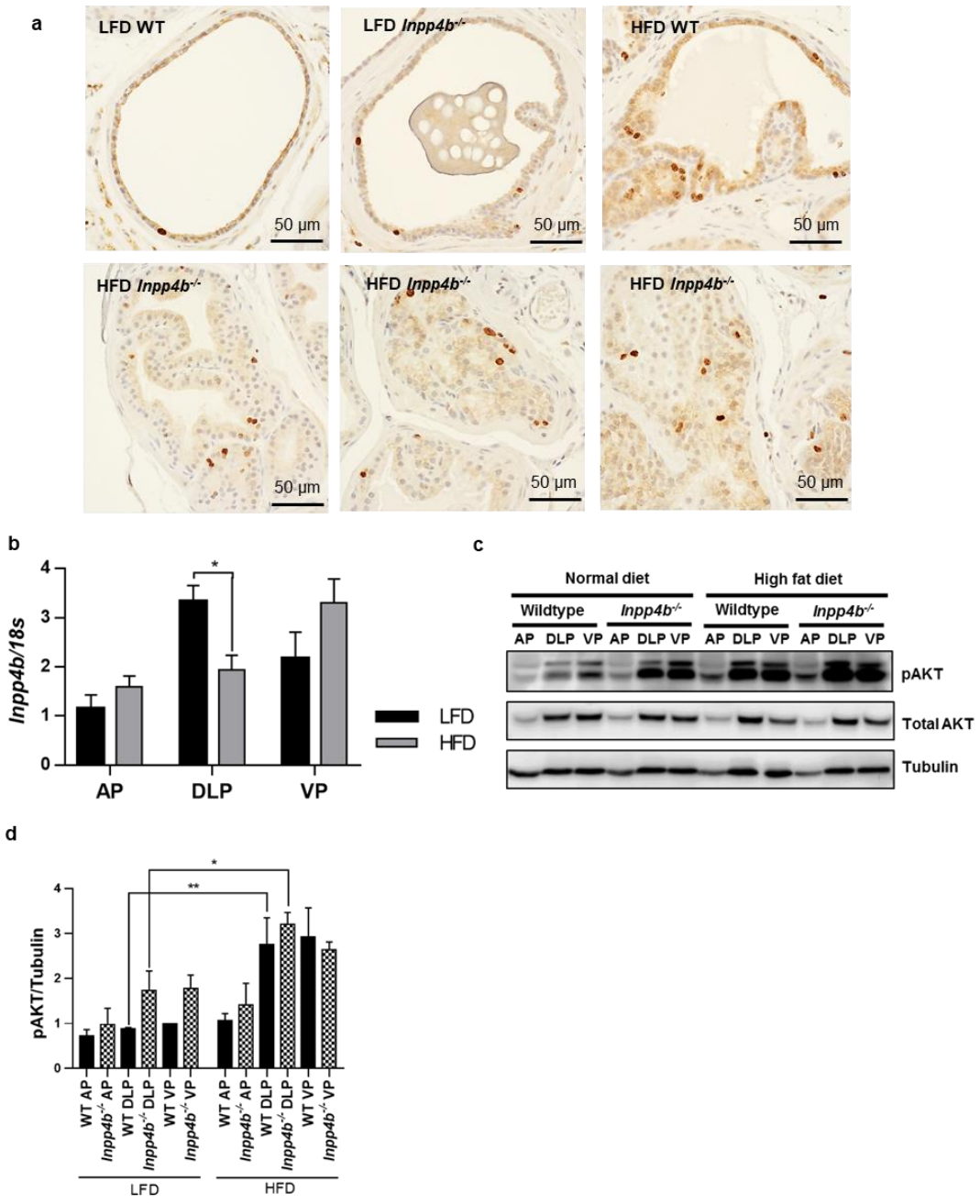

Figure 3-12. Loss of INPP4B promotes proliferation in prostatic epithelial cells in obsess male mice. (a) Representative prostate tissue sections from LFD WT, LFD *Inpp4b*$^{-/-}$, HFD WT, and HFD *Inpp4b*$^{-/-}$ prostates were stained for Ki67 and counterstained with hematoxylin. (b) RNAs were analyzed for INPP4B expression in AP, DLP and VP of WT mice fed with LFD or HFD. (c) Protein levels of pAkt, total Akt, and tubulin were assayed in indicated groups by western blotting. (d) Quantification of protein levels of pAkt from the western blot in (c). The averages were calculated from six individual mice. The protein levels were normalized to tubulin and shown as fold change. (*p<0.05, **p<0.01)

3.4. Discussion

Metabolic dysfunction is the cause of significant morbidity and mortality due to diabetes, cardiovascular abnormalities, and an increased risk of cancer-associated incidence and mortality. Though epidemiological links between increased calorie consumption, cancer, and diabetes are well established, less is known about the specific genes that protect some obese individuals from metabolic dysfunction and neoplasia. In this report, we show that INPP4B is required for metabolic health in lean male mice and protects obese mice from diabetes and prostate neoplasia.

INPP4B has been shown to play a tumor suppressor role in prostate, breast, and other cancers (29, 46, 129, 134), however, *Inpp4b*$^{-/-}$ mice do not develop malignancies (31). Significant metabolic changes were detected in *Inpp4b*$^{-/-}$ males at three months of age and these changes were exacerbated by HFD. Loss of INPP4B-dependent regulation of Akt and PKC pathways led to accelerated weight gain in *Inpp4b*$^{-/-}$ males fed with HFD. Hepatic Akt and PKC signaling is required for insulin sensitivity (106), thus we observed inefficient glucose clearance in both LFD and HFD *Inpp4b*$^{-/-}$ animals (Figure 3-4). *Inpp4b*$^{-/-}$ mice developed hyperglycemia on an LFD and T2D on an HFD. Direct hepatic insulin action and activated Akt and PKC signaling induce proteolytic cleavage of the SREBP1 precursor protein into a mature transcription factor (211, 212) which regulates expression of *Pparg* and other lipogenic enzymes. Consistently, we found that INPP4B loss and HFD cooperatively induced SREBP1 cleavage and increased expression of *Pparg* and other lipogenic transcripts (Figure 3-8). As a direct result of these transcriptional changes, we observed the development of hepatosteatosis, WAT expansion and inflammation in *Inpp4b*$^{-/-}$ males which were exacerbated by HFD. It is important to note, that the *Inpp4b*$^{-/-}$

mouse model closely models human NAFLD, as there was downregulation of hepatic *INPP4B* expression in people with T2D and advanced hepatosteatosis, and a highly significant negative correlation between the expression of *INPP4B* and *PPARG* in human livers (Figure 3-6 f – g, and Figure 3-8 j).

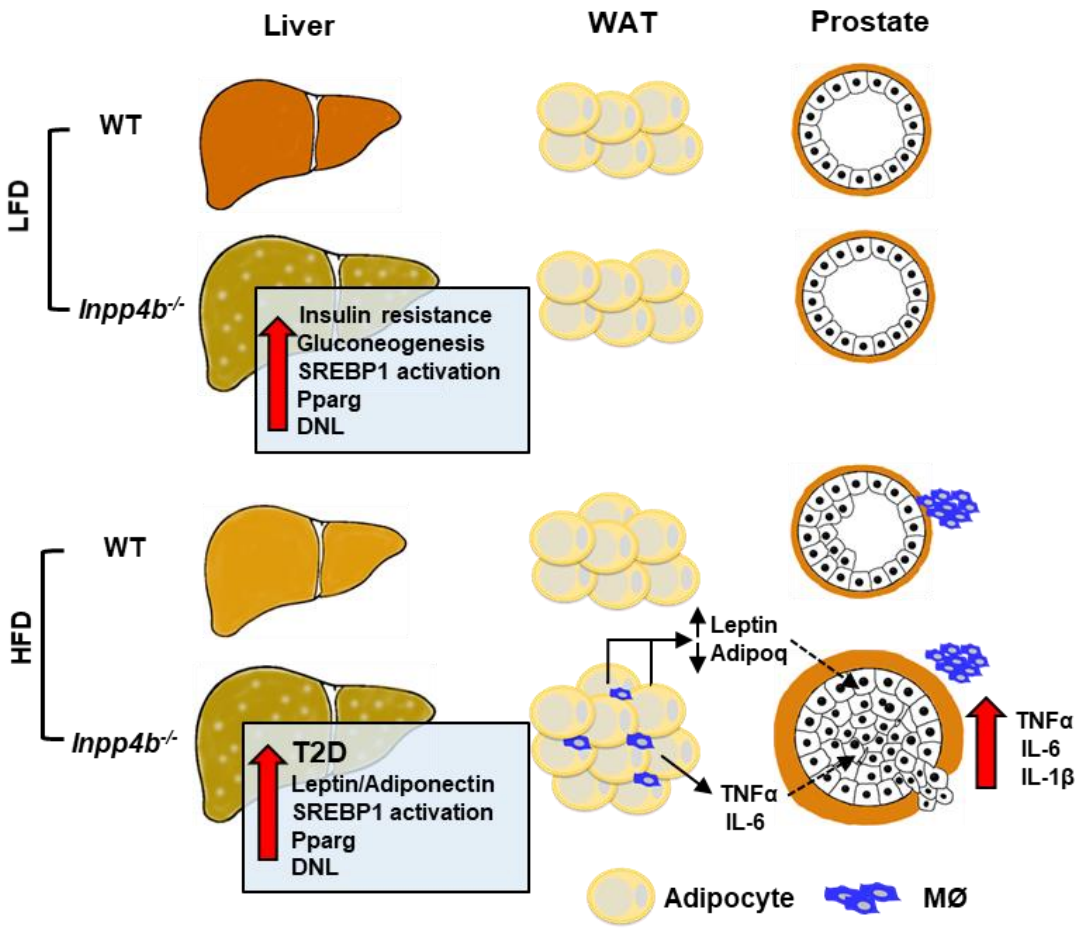

Figure 3-13**.** Physiological functions of INPP4B in liver, WAT, and prostate. The loss of INPP4B activates SREBP1, stimulates hepatic expression of *Pparg*, causing liver steatosis, insulin resistance, *de novo* lipogenesis (DNL), and an increased rate of gluconeogenesis. When consuming a HFD, the *Inpp4b*$^{-/-}$ males developed type 2 diabetes, inflammation and macrophage (MØ) infiltration of WAT, DNL and an increased Leptin/Adiponectin ratio, all of which were shown to stimulate the development of PIN. Consumption of an HFD promoted macrophage infiltration in prostates of both WT and *Inpp4b*$^{-/-}$ mice; however, increased production of proinflammatory cytokines was only evident in dorsolateral lobes of prostates of *Inpp4b*$^{-/-}$ mice.

Metabolic dysfunction and adipose inflammation in HFD *Inpp4b*$^{-/-}$ males affected the prostate gland development as is often observed in men with this condition. HFD *Inpp4b*$^{-/-}$ males were significantly more susceptible to obesity-induced neoplastic transformation of the prostate than the WT males (Figure 3-10 a – b). Circulating leptin, pro-inflammatory cytokines and locally activated immune cells likely contribute to the inflammatory environment of the prostate (218-220). Similar to our HFD *Inpp4b*$^{-/-}$ mouse model, IL6 is elevated in the serum of patients with metastatic PCa (221) and IL1β levels are increased in both the tumors and serum of prostate cancer patients and correlates with disease severity (222).

In summary, we discovered a novel function of INPP4B. We showed that INPP4B is an essential regulator of metabolic health. It protects the liver from steatosis, mediates insulin sensitivity and links obesity with neoplastic changes in the prostate epithelium. As shown in Figure 3-13, *Inpp4b* deficient animals developed hyperglycemia on normal chow and T2D on HFD by decreasing insulin sensitivity. Loss of INPP4B induced activation of hepatic SREBP1 leading to an increased expression of *Pparg* and other genes involved in lipogenesis. This ultimately caused NAFLD. Similar to men, the loss of INPP4B in HFD fed mice also promoted obesity-induced WAT inflammation and prostate neoplasia. In both mice and men, decline in hepatic INPP4B expression correlates with increasing levels of NAFLD. Thus, *Inpp4b*$^{-/-}$ males faithfully reproduce complex metabolic syndrome in men and INPP4B signaling cascade should be considered for therapeutic intervention in this wide-spread disease.

3.5. Materials and Methods

Animal studies

Inpp4b$^{-/-}$ mice were described previously (28, 54). WT and *Inpp4b*$^{-/-}$ males were fed with either LFD (LabDiet 5V75, St. Louis, MO) or HFD (TestDiet 58R3, St. Louis, MO). The HFD consisted of 59.4% fat, 25.7% carbohydrate, and 14.9% protein (total 22.8 kJ/g), whereas the regular chow contained 12.9% fat, 63.8% carbohydrate, and 23.2% protein (total 13.6 kJ/g). LFD groups were continuously maintained on LFD. For HFD cohorts, dams were fed the designated diet for 1 month prior to mating, during pregnancy, and 3 weeks' lactation. Male pups were maintained on the HFD until euthanasia. Mouse body weights were measured once a week. All LFD WT, LFD *Inpp4b*$^{-/-}$, HFD WT, and HFD *Inpp4b*$^{-/-}$ mice were euthanized and dissected at 12 weeks and their tissues where collected for analysis. All protocols were approved by Florida International University Institutional Animal Care and Use Committee.

Hemodynamic Measurements

Eleven–week-old HFD, WT, and *Inpp4b*$^{-/-}$ mice were anesthetized with 2% isoflurane in 100% oxygen. Each mouse was placed on a heating platform with the temperature around 38-40° C. A tail cuff connected to the pressurizing tubing was placed at the base of the mouse tail and attached to the CODA monitor (Kent Scientific, Torrington, CT). The heart rate, systolic blood pressure, diastolic blood pressure, and mean blood pressure where recorded using a non-invasive blood pressure system.

Gene expression analysis

RNA was isolated from tissues using Tri Reagent (Molecular Research Center, Cincinnati, OH) and reverse transcribed using a Verso cDNA synthesis Kit (Thermo Fisher Scientific).

The quantitative real time PCR was performed using primers and probes listed in Table 7 using a Roche 480 LightCycler (Roche). For gene expression analysis, samples were from LFD WT (N = 12), LFD *Inpp4b*$^{-/-}$ (N = 11), HFD WT (N = 9) and HFD *Inpp4b*$^{-/-}$ (N = 11) mice.

Table 7. Primers and corresponding probes used in CHAPTER 3.

Mouse gene primers and corresponding probe sets			
Gene	Forward primers	reverse primers	Probe
Ar	ccagtcccaattgtgtcaaa	tccctggtactgtccaaacg	58
Inpp4b	acagcaccagaaagtctgagc	ctttctgacatctgctcacgga	89
Apof	tctcaatggccggactgtat	aggatgagtcggaggctatg	17
Nkx3.1	cgactgaacccgagtctgat	aatcacctgagtgtgagagaagg	5
Msmb	cgtggtgttcatgtgacaaaa	ctcaaaggcctagtagcgttg	62
Pten	aggcacaagaggccctagat	ctgactgggaattgtgactcc	60
Probasin	tcatcctcctgctcacactg	gctaagtaaattgtttgccaagg	47
Pparg	ctctcagctgttcgccaag	cacgtgctctgtgacgatct	50
Adgre1	tgtcctccttgcctggac	gagacttctgagctgacactgc	29
Cd68	tccactgttggccctcac	ccccttggaccttggacta	10
Fasn	ttgctgaggacttcccaaac	gcgtcgatgctgtagactgt	17
Hk2	tgccaagcgtctccataag	aggaagcggacatcacaatc	75
Lep	cccaaaatgtgctgcagatag	ccagcagatggaggaggtc	80
Adipoq	ccatctggaggtgggagac	ctgcatagagtccattgtggtc	1
Il6	gctaccaaactggatataatcagga	ccaggtagctatggtactccagaa	6
Tnf	ttgtcttaataacgctgatttggt	gggagcagaggttcagtgat	64
Il1b	caggcaggcagtatcactca	tgtcctcatcctggaaggtc	76
Cck	cccagccatagaataagtgacc	attcgtagtcctcggcactg	42
Pcsk1	tccaaagttggaggcataaga	gaactagcctcaatggcatca	42
Gys1	ctgtcctgttcggcttcct	ccacatacggcttctcttcg	72
Furin	atgaatgacaacaggcatgg	cgggcattgtaagctacacc	74
Mafa	ctccagagccaggtggag	gtacaggtcccgctccttg	10
Tgfb1	tggagcaacatgtggaactc	cttggtaaccggctgctg	72
Col1a1	cctggacctcagggtattgctggacaac	aaggtccttctggatcaagtggt	72
Acta2	accacccacccagagtg	gctatgtgtgaagaggaagac	20
Insr	tctttcttcaggaagctacatctg	tgtccaaggcataaaaagaatagtt	91
Cd36	tggccttacttgggattgg	ggatttgcaagcacaatatgaa	9
Cyp2b13	gctgaggatggagaaggaga	tccagcaaagaagagagagagc	9
Cyp2b9	ggagaagtcaaaccacaacaca	gcaaagaagagagagagcacaga	9
Hao2	gaggcctccattggttcc	ccatctgcttgttgatgtcc	71

Igfbp3	gcagcctaagcacctacctc	tcctcctcggactcactgat	1
Mogat1	ttcaatgggagtagccttgc	gcattatgccaaagtagtgctg	6
Ppara	*ggcttctttcggcgaactat*	*cttgcagctccgatcacac*	41
Srebf1	ggttttgaacgacatcgaaga	cgggaagtcactgtcttggt	78
Vldlr	atggcatccgagactgtgtt	gcactgattgacgtttttgc	21

Glucose tolerance test (GTT) and Pyruvate tolerance test (PTT)

The glucose tolerance tests were performed on 11-week-old males as previously described (223). Briefly, after 6 hours of fasting, mice ($n \geq 8$) were weighed and given 2 g/kg of glucose (Sigma) through a gavage needle (18G, 5.08cm; Cadence Science, Cranston, RI). A drop of blood was sampled from each mouse at 0, 15, 30, 60, 90, and 120 minutes after oral gavage and the glucose concentration was determined immediately using the ACCU-CHEK Nano SmartView glucometer (Roche Diagnostics, Indianapolis, IN). For pyruvate tolerance testing, mice were fasted overnight, followed by intraperitoneal injection of pyruvate (1.5 g/kg, Sigma-Aldrich, ST. Louis, MO). The blood glucose levels were measured as above.

ELISA and adipokine array

Blood insulin levels were determined using the Ultra Sensitive Mouse Insulin ELISA Kit (Crystal Chem, Elk Grove Village, IL); the manufacturer's instructions were followed. Briefly, 5 µl of blood serum from LFD WT (N = 23), LFD *Inpp4b*$^{-/-}$ (N = 20), HFD WT (N = 9), and HFD *Inpp4b*$^{-/-}$ (N = 9) mice were used for the test. The insulin concentrations were measured using CLARIOstar plate reader (BMG Labtech, Cary, NC). A Mouse IL6 ELISA kit (Sigma-Aldrich) was used to determine the IL6 level in LFD WT (N = 6), LFD *Inpp4b*$^{-/-}$ (N = 10), HFD WT (N = 5), and HFD *Inpp4b*$^{-/-}$ (N = 5) mouse dorsolateral prostates. Adipokines and proinflammatory cytokines were detected in WAT protein

extracts using the Proteome Profiler Mouse Adipokine Array Kit (R&D Systems, Minneapolis, MN). Five samples from mice in each group were pooled and used for analysis. The signal was captured using an ImageQuant LAS 500 imager (GE Healthcare, Chicago, Illinois).

Morphometric quantification of steatosis

The steatosis was evaluated by measuring the surface of the unstained areas per field using 40X magnification. Five mice were selected from each group and 10 different areas from each mouse were counted using ImageJ software (NIH).

Oil red O staining

Fresh liver tissue was placed in OCT medium and snapped frozen in liquid nitrogen. Liver samples were cut at 12 μm sections and attached to glass slides. Oil red O was dissolved in hot propylene glycol and filtered through Whatman #2 filter paper. Slides were fixed in 4% PFA, rinsed in distilled water and in propylene glycol, stained in oil red O, and counterstained with hematoxylin. All images were acquired using an AxioCam MRc5 camera (Zeiss, Thornwood, NY).

Determination of triglycerides in mouse liver

The total triglycerides in liver were measured in LFD WT (N = 8), LFD *Inpp4b*$^{-/-}$ (N = 8), HFD WT (N = 6) and HFD *Inpp4b*$^{-/-}$ (N = 4) mice using a Triglyceride Colorimetric Assay Kit (Cayman Chemical, Ann Arbor, MI). The assay was performed according to the manufacturer's instruction. The total amount of triglyceride in liver were calculated.

RNA sequencing and data analysis

RNA was purified as described above from HFD WT (N=4) and HFD *Inpp4b*$^{-/-}$ (N = 4) and submitted to Novogene for RNA sequencing. The libraries were generated using the

NEBNext® Ultra™ RNA Library Prep Kit and used for Illumina 150-bp paired-end sequencing. Quality control assessment was done using Illumina RNA-seq pipeline to estimate genomic coverage, percent alignment and nucleotide quality. Raw reads were mapped to the reference mouse genome (the most recent build GRCm38) using HISAT2 (224) and STAR (225) software. For the differential analysis of known genes, the reads for each gene aligned by HISAT2 were counted using HTSeq software (226). Alignment by STAR was run with the option "quantMode TranscriptomeSAM" that allowed counting of reads aligned to each gene. Raw counts from HTSeq and STAR were imported into Bioconductor/R package DESeq2 (227), normalized and tested for differential gene expression. This analysis was done separately for the files produced by each aligner. In each analysis we selected genes that were expressed differentially based on the criteria of False Discovery Rate (FDR) less than 10% and Fold Change more than 1.3 to either direction. Data has been uploaded to NCBI's Sequence Read Archive (SRA) database with accession number GSE134466. Genes that showed differential expression after analysis of the files from both aligners have been selected for further analysis.

Pathway analysis and Gene Ontology (GO) analysis

Biological processes and pathways affected by INPP4B knockout in mouse liver, we performed using Gene Set Enrichment Analysis (GSEA, http://www.broad.mit.edu/gsea/index.html) and David bioinformatics functional annotation analysis with differentially expressed genes obtained from the RNA-seq analysis. The gene sets for KEGG pathways (c2 KEGG curated) and GO analysis (c5 curated) were acquired from Molecular Signatures Database (http://software.broadinstitute.org/gsea/msigdb/index.jsp). All pathways and Go biological

functions that are significantly affected by INPP4B were listed in Appendix. The normalized enrichment score (NES) with FDR less than 25% or p value less than 0.05 were considered significant (170).

Immunohistochemistry

The preparation of tissue sections for H&E and immunohistochemical staining were done as previously described (54). Briefly, 5 µM sections were deparaffinized and antigen retrieval was done by heating slides at 99° C for 15 minutes in 10 mM citrate buffer, pH=6. Sections were blocked in 1% H_2O_2 in water and 5% BSA in PBS. Primary antibodies were diluted in PBS at 1:6000 for α-SMA (#ab5694, AbCam, Cambridge, MA), 1:60,000 for insulin (#ab181547, AbCam), and 1:200 in Ki67 (#RB-1510-P1, Thermo Fisher). Antibodies were incubated overnight at 4° C or an hour at room temperature. Sections were washed and incubated with biotinylated anti-rabbit secondary antibody for 18 minutes, followed by incubation with streptavidin conjugated peroxidase for 30 minutes using the Vectastain ABC Kit (Vector Laboratories, Burlingame, CA). The staining was developed using the ImmPACT DAB Peroxidase Substrate Kit (Vector Labs, Burlingame, CA) and the slides were counterstained with hematoxylin.

Western blotting

Mouse tissues were homogenized with a glass grinder in ice-cold RIPA buffer with protease and phosphatase inhibitors. Cleared lysates were diluted to 4 µg/µl and 15-30 µg of protein was resolved on a 7.5% - 10% SDS-PAGE. The sources and dilutions of antibodies are listed in Table 8. The signal was captured using an ImageQuant LAS 500 imager and analyzed by ImageQuant TL software (GE Healthcare).

Table 8. Antibodies used in CHAPTER 3.

Antibody	cat #	concentration	RRID
phospho-Akt S473	Cell signaling #4051	1:1000	AB_331158
Total Akt	Cell signaling #4691	1:1000	AB_915783
phospho-PKCζ T410	Cell signaling #2060	1:1000	AB_561487
phospho-PKCβII S660	Cell signaling #9371	1:1000	AB_2168219
FAS	Cell signaling #3180	1:1000	AB_2100796
HK2	Cell signaling #2867	1:1000	AB_2232946
β-Tubulin	Millipore #05-661	1:5000	AB_309885
PTEN	Cell signaling #9188	1:1000	AB_2253290
AR	Millipore #06-680	1:1000	AB_310214
PPARγ	Cell signaling #2443	1:1000	AB_823598
Ki67	Thermo Fisher RB-1510-P1	1:200	AB_60160
SREBP1	Novus NB 600-582	1:1000	AB_531394
CD68	Abcam ab125212	1:800	AB_10975465
PR	Homemade	1:1500	N/A

Statistics

All data are presented as mean ± SEM. Two-way ANOVA was performed by Prism 7.0. P-values less than 0.05 were considered statistically significant.

CHAPTER 4: INPP4B IS ESSENTIAL FOR MAMMARY GLAND BRANCHING AND PROTECTS FROM NAFLD

4.1. Introduction

The hormones estrogen and progesterone are produced by the ovaries and regulates the development and physiology of the mammary gland (228). The corresponding ligand-dependent transcription factors, estrogen receptor-alpha (ERα) and progesterone receptor (PR) are expressed in approximately 30% of luminal cells within the mammary gland (229). Currently, more than 70% of breast cancers express ERα and their growth is ERα – dependent (82). ERα functions as a ligand-activated transcription factor that regulates a variety of genes that govern cell proliferation and survival in cancerous and non-cancerous breast epithelial cells (83). Therefore, endocrine therapies that suppress the tumor-proliferating effects of estrogen via interactions with ERα are a standard-of-care therapy. However, many patients develop resistance that leads to lethal metastatic disease. Many factors promote the development of aggressive breast cancer, including growth factors and kinase signaling pathways such as PI3K/AKT and p44/42 MAPK that phosphorylate and activate ERα independently of ligand (84-86).

Accumulating evidence demonstrates that overweight or obese individuals have an increased risk of developing postmenopausal breast cancer (230-233). Post-menopausal breast cancer patients frequently experience weight gain and worsened survival rates (234, 235). Similarly, the depletion of estrogens via an ovariectomy in female rodents leads to weight gain and metabolic disorders, including adipose dysfunction and changes in glucose metabolism (76, 236, 237). Many patients with metabolic disorders develop hepatic insulin resistance and non-alcoholic fatty liver disease (NAFLD) characterized by increased

triglyceride accumulation in the liver. Metabolic activity is regulated by multiple signaling pathways, main among them are INSR/AKT and the PKC signaling pathways. The insulin-stimulated uptake of glucose activates the AKT pathway, whereas circulating lipids activate PLC/PKC pathways, which in turn stimulate hepatic lipid synthesis (PKCζ and ι/λ) (238, 239).

Inositol polyphosphate 4-phosphatase type II (INPP4B) is a tumor suppressor and a dual-specificity phosphatase that dephosphorylates both lipid and phosphoprotein substrates, similar to the tumor suppressor PTEN (32). Several groups have shown that INPP4B functions as a tumor suppressor in various cancers including breast, ovary, thyroid, and prostate malignancies by inhibiting AKT signaling (29, 31, 134). We have previously shown that INPP4B also suppresses the PKC pathway (54, 134). In this dissertation research, our group has demonstrated that Inpp4b deficiency in male mice leads to the development of steatotic liver. In mice fed a high-fat diet (HFD), the presence of INPP4B protects male mice from weight gain, insulin resistance, and type 2 diabetes.

In this study, we investigated the role of INPP4B in normal female physiology and development and its role in the development of mammary gland cancers. Our data suggests that INPP4B regulates ERα transcriptional activity using a different mechanism than PTEN. Unlike PTEN, INPP4B knockdown significantly reduced the level of PR to below the threshold required for lobuloalveolar development in the mammary gland (240). Consistently, *Inpp4b* loss nearly abolished lateral branching in the mouse mammary gland at the age of 12 weeks. These results are consistent with observations made in the PR knockout mouse model. When fed an HFD, female *Inpp4b*$^{-/-}$ mice gained approximately 50% more weight than their wild type counterparts. *Inpp4b* loss led to an increase in white

adipose tissue weight and the development of hyperglycemia. Moreover, the HFD *Inpp4b*$^{-/-}$ female mice developed steatotic livers and exhibited the early stages of fibrotic disease. Further analysis of HFD fed *Inpp4b*$^{-/-}$ females revealed hyperplasia in the mammary end buds and an expansion of extracellular matrix (ECM) which plays an important role in both mammary gland development and tumorigenesis.

4.2. Results

4.2.1. INPP4B is positively correlated with ESR1 in human breast cancer.

INPP4B is expressed in ERα-and Her2-positive breast cancers but it is lost in nearly all triple-negative breast cancers (46, 99). We compared the correlation between the expression of INPP4B and the ERα encoding gene, *ESR1*, in 1100 tumor samples from women with invasive breast carcinoma. The expression of *INPP4B* was positively correlated with *ESR1* expression and retained a high Pearson's rank correlation coefficient (Figure 4-1 a, r = 0.6718). When ESR1 expression levels in individuals with altered INPP4B expression were exported, ESR1 was highly expressed when INPP4B expression was also high (Figure 4-1 b). The protein expression of INPP4B and ERα were acquired from 892 tumor samples using RPPA and the data were exported from cBioportal (https://www.cbioportal.org/). The INPP4B protein levels were positively correlated with ERα protein levels in human breast tumors (Figure 4-1 c). The expression of PTEN, another dual-specificity phosphatase, displayed a significantly weaker correlation with ESR1 (Figure 4-1 d, r = 0.2739). The ESR1 levels were not significantly affected by the alteration

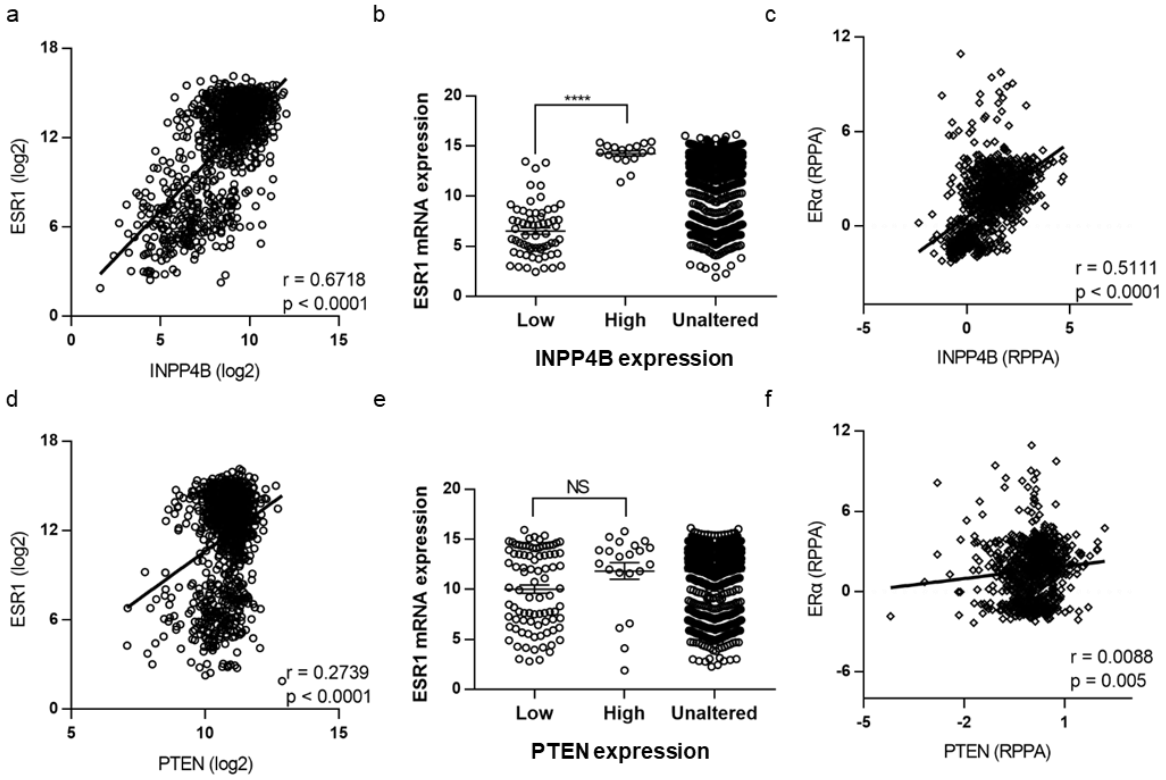

Figure 4-1**.** A positive correlation between INPP4B and ERα in human breast tissue samples. (a) Correlation between INPP4B expression and ESR1 expression in 1100 breast adenocarcinoma samples (TCGA, Provisional). (b) The corresponding mRNA level of ESR1 in samples expressing low or high levels of INPP4B. Samples were considered altered if their INPP4B expression levels were higher or lower than two standard deviations of the mean of all samples. (c) Correlation between INPP4B protein level and ERα protein level in 892 breast cancer samples (TCGA, Provisional). (d) Correlation between PTEN mRNA level and ESR1 mRNA level in samples described in (a). (e) The corresponding mRNA level of PTEN and ESR1 in samples expressing low or high PTEN levels. (f) Correlation between protein level of PTEN and ERα in samples described in (c).

of PTEN expression (Figure 4-1 e) and only a very weak correlation between PTEN and ERα protein levels was observed in breast cancer samples (Figure 4-1 f).

4.2.2. INPP4B and PTEN depletion both modulate ERα transcriptional activity.

To compare the regulation of ERα protein expression and transcriptional activity by INPP4B and PTEN, we performed an Affymetrix microarray using MCF7 cells that expresses functional ERα, INPP4B, and PTEN. We used specific siRNAs to knockdown INPP4B or PTEN and then exposed them to 1 nM E2 to activate ERα transcriptional activity. Depletion of INPP4B nor PTEN had an effect on ESR1 expression (Figure 4-2 a-c). Using Gene Set Enrichment Analysis (GSEA), we investigated whether ERα transcriptional activity was affected by the loss of either INPP4B or PTEN. An ERα signature with a total of 467 ERα regulated genes in the MCF7 cell line was generated from GSE8597. The GSEA indicated that a subset of ERα target genes was significantly enriched among INPP4B regulated genes (Normalized Enrichment Score (NES)=2.32, p value<0.001), and to a lesser extent among PTEN regulated genes (NES=1.76, p value<0.01) (Figure 4-2 d-f), suggesting that both tumor suppressors modulate ERα transcriptional output.

A comparison of the differentially regulated genes (DEG) affected by INPP4B or PTEN knockdown revealed common and specific regulation of genes by INPP4B and PTEN (Figure 4-3 a). We selected DEGs from the INPP4B knockdown samples and compared the expression of these genes to that in PTEN knockdown samples. As seen in Figure 4-2 f, many genes were affected by the loss of INPP4B but were unaltered by the PTEN knockdown. The list of genes that were preferentially up- or down-regulated by INPP4B or PTEN were exported and can be found in Figure 4-3 b-c. Using GSEA, we analyzed the

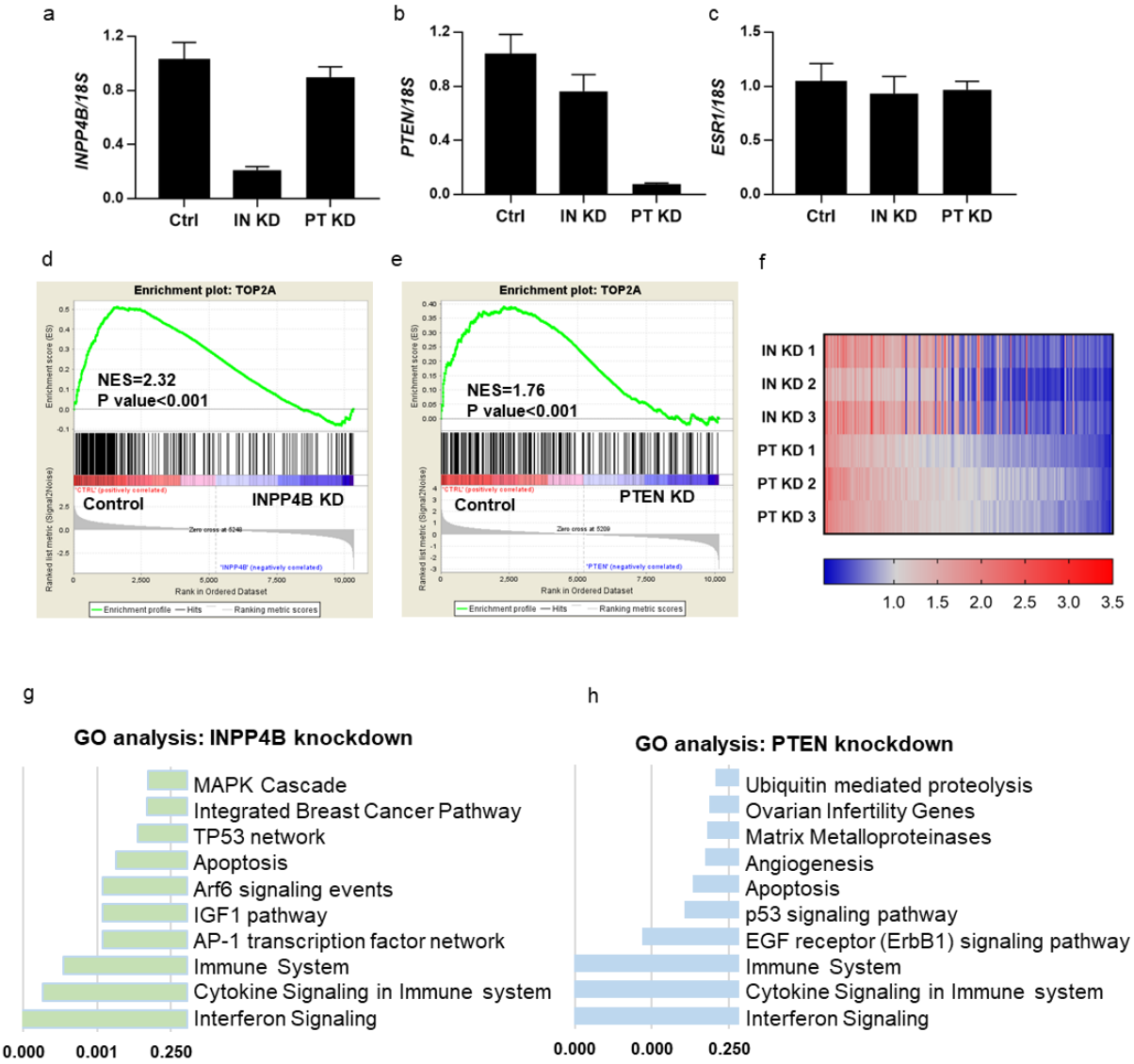

Figure 4-2. Both INPP4B and PTEN affect ERα transcriptional activity. (a-c) INPP4B and PTEN were knocked down using specific INPP4B siRNA (IN KD) and PTEN siRNA (PT KD) in MCF7 cells for 48 hours. The expression level of *INPP4B* (a), *PTEN* (b), and *ESR1* (c) were determined by RT-qPCR using 18S as a control. (d-e) GSEA of INPP4B (d) and PTEN (e) affected genes using ERα regulated gene as signature (GSE8597). (f) Forty-eight hours after INPP4B or PTEN knockdown, we treated MCF7 cells with 1 nM vehicle or E2 for 12 hours. RNA was extracted and used in the gene expression array. Comparison of the expression levels for differentially expressed genes (DEG) from INPP4B knockdown samples and PTEN knockdown samples. (g-h) KEGG functional enrichment analyses were done using GSEA. KEGG pathways were significantly enriched by differentially expressed gene caused by INPP4B knockdown (g) or PTEN knockdown (h). P-value was calculated and presented in logarithmic scale.

DEG in INPP4B or PTEN knockdown samples and applied the signatures from the Kyoto Encyclopedia of Genes and Genomes (KEGG) pathway database. As seen from Figure 4-2 g-h, INPP4B and PTEN depletion both affected immune system and p53 signaling pathways. However, different from PTEN, INPP4B affected genes were also involved in the IGF pathway, apoptosis and the MAPK cascade suggesting a divergent pattern of gene regulation by INPP4B and PTEN in MCF7 cells (Figure 4-2 g-h).

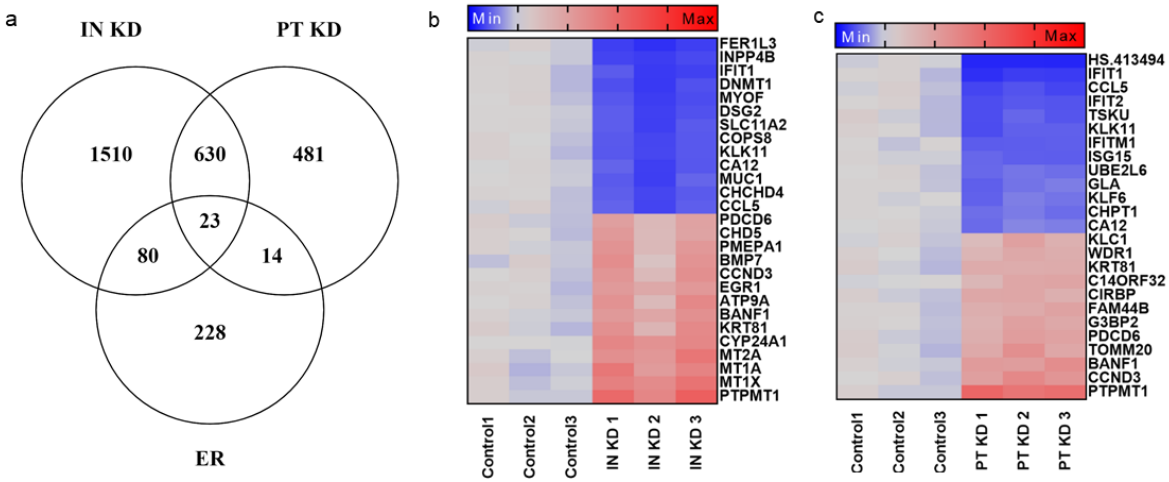

Figure 4-3**.** Comparison between INPP4B and PTEN affected genes. (a) Venn diagram of differentially expressed genes after INPP4B knockdown, PTEN knockdown and genes regulated by ERα. (b-c) Heat map of the most up-/down-regulated genes after INPP4B knockdown (b) or PTEN knockdown (c) in MCF7 cells.

4.2.3. Differential expression of INPP4B and PTEN regulated genes in breast cancer cells.

The representative genes that were preferentially affected by INPP4B or PTEN knockdown were selected based on the microarray data and changes in their expression levels were validated in MCF7 cells. We found that transcripts for PTPMT1 and CHD5 were upregulated and HERC5 transcripts were downregulated in a similar fashion by both INPP4B and PTEN knockdown (Figure 4-4 a). INPP4B knockdown specifically upregulated transcription of MT2A, while PTEN loss specifically upregulated CALU, a potential marker of breast cancer progression (241) that was induced in murine Her2 overexpressing breast tumors (242). The downregulation of MYOF was significantly stronger when INPP4B was knocked down compared to PTEN knockdown (Figure 4-4 b). We next investigated whether INPP4B and PTEN differentially modulate ERα-dependent gene expression. We selected representative estradiol (E2) induced genes and compared their expression levels following INPP4B or PTEN knockdown. As seen in Figure 4-4 c-i, all selected genes were significantly induced by E2. Depletion of either INPP4B or PTEN increased ERα-induced transcription of early growth response 3 (EGR3) (Figure 4-4 c). The ERα-induced SGK3, PGR, and UGT2B17 genes required both INPP4B and PTEN for their optimal expression (Figure 4-4 d-f). Even though both INPP4B and PTEN stimulated expression of MSMB, only the loss of PTEN essentially abolished MSMB expression (Figure 4-4 g). Conversely, two ERα-dependent genes, CYP24A1 and RAPGEFL, were regulated specifically by INPP4B in MCF7 cells (Figure 4-4 h-i).

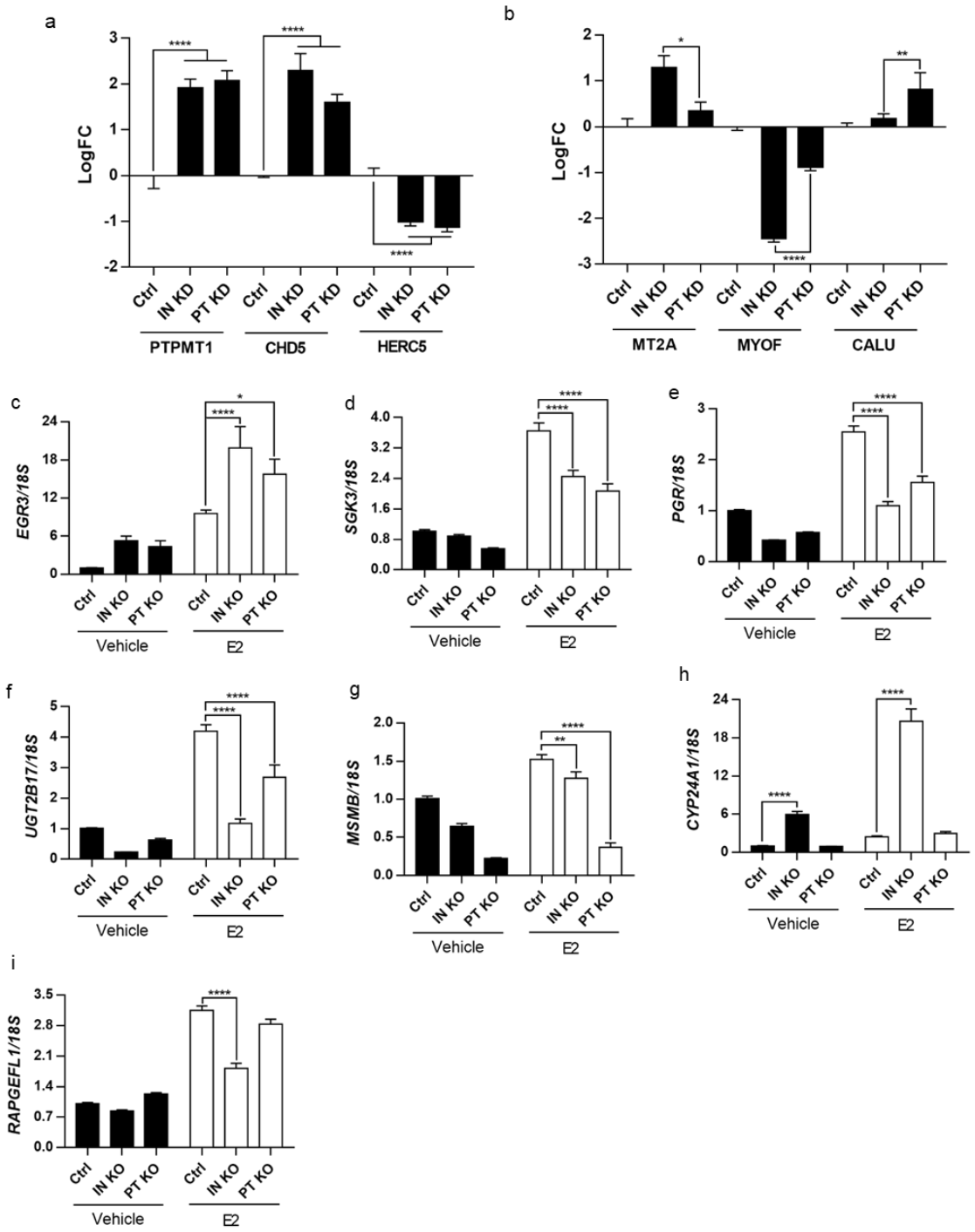

Figure 4-4**.** Differential gene expression patterns for INPP4B and PTEN. (a-b) RNAs from Figure 2 (a-c) were analyzed for *PTPMT1*, *CHD5*, *HERC5*, *MT2A*, *MYOF*, and *CALU* expression by RT-qPCR using 18S as control. (c-i) MCF7 cells were transfected with INPP4B or PTEN siRNA for 48 hours and treated with E2 for another 24 hours before harvest. Gene expression of *EGR3* (c), *SGK3* (d), *PGR* (e), *UGT2B17* (f), *MSMB* (g), *CYP24A1* (h), and *RAPGEFL1* (i) as analyzed by RT-qPCR.

4.2.4. INPP4B is required for optimal expression of progesterone receptor (PR)

PR is required for mammary gland morphogenesis and is a biomarker for breast cancer progression (243). INPP4B is required for both basal and E2 dependent expression of PGR, the PR encoding gene (Figure 4-4 e). Consistently, forty-eight hours after INPP4B knockdown, protein levels of both PR isoforms, PRA and PRB, were significantly reduced in the independently derived MCF7 and T47D cell lines (Figure 4-5 a-c). In tumors from 529 women with invasive carcinoma of the breast, we observed a positive and highly significant correlation between INPP4B and PGR on both RNA and protein levels (TCGA Provisional) (Figure 4-5 d-f).

4.2.5. INPP4B is essential for ductal branching in the mouse mammary gland

Using a previously described *Inpp4b* knockout (*Inpp4b*$^{-/-}$) mouse model (28, 54), we investigated the role of INPP4B in non-malignant mouse mammary gland. The level of estrogen fluctuates during the estrous cycle and stimulates the turnover of ERα and PR (244). The murine estrous cycle includes four stages, proestrus, estrus, metestrus, and diestrus (245). The diestrus stage has a relatively high level of both PR and ERα, when compared to other stages (244). We chose this stage to study the role of INPP4B in mouse mammary gland development. Both estrogen and progesterone signaling are required for the development of the mammary gland. During puberty ER signaling stimulates the expansion of the duct into the mammary gland fat pad (246), while epithelial PR is required for ductal branching in adulthood (228). Therefore, we examined the mammary gland from WT or *Inpp4b*$^{-/-}$ female mice at 11 weeks old. *Inpp4b*$^{-/-}$ females expressed similar levels of *Esr1* mRNA compared to WT controls, however a reduction in *Pgr* mRNA occurred in the mammary gland of *Inpp4b*$^{-/-}$ females (Figure 4-6 a-b).

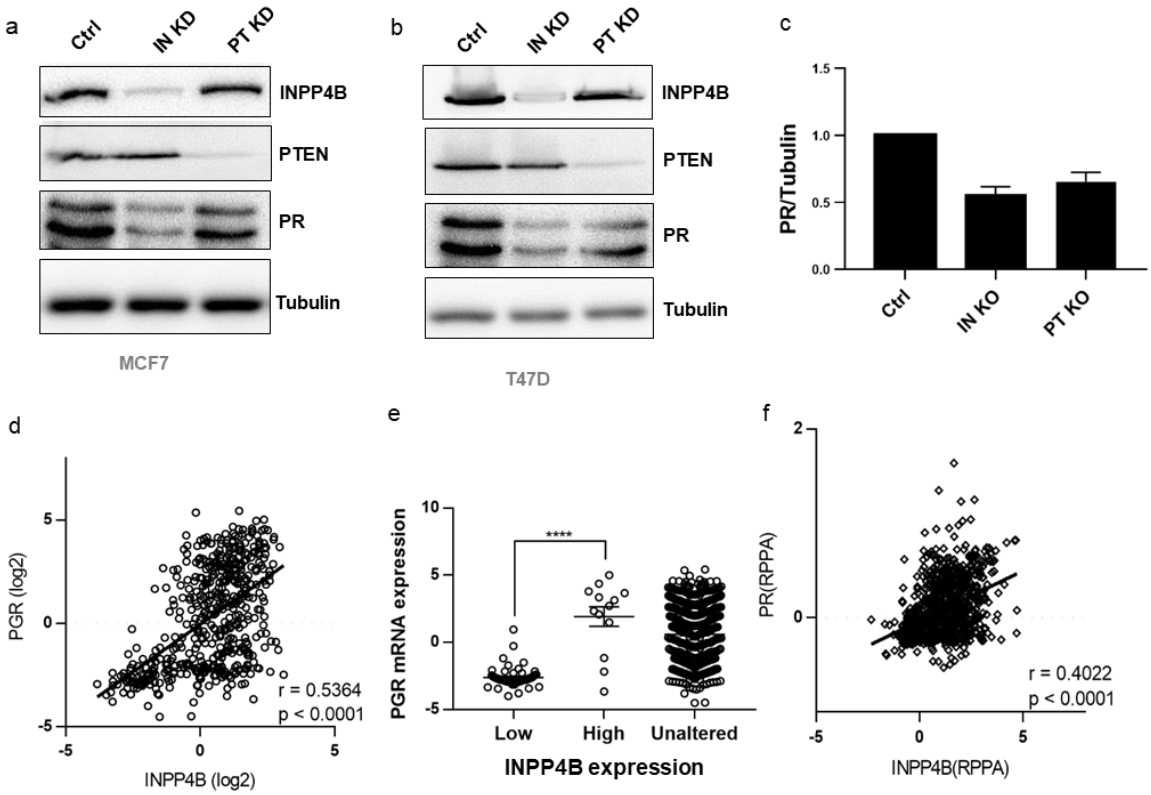

Figure 4-5**.** INPP4B is required for optimal induction of PR. (a-b) INPP4B and PTEN were knocked down using INPP4B or PTEN specific siRNAs in MCF7 or T47D cells in media supplemented with 10% FBS for 48 hours. The protein levels of INPP4B, PTEN, PR, and tubulin were compared by Western blotting in MCF7 cells (a) and T47D cells (b). (c) Quantification of PR level in MCF7 cell from four independent experiments. (d-f) Gene expression data was exported from the same source as Figure 1. (d) Correlation between INPP4B and PGR expression in breast adenocarcinoma samples. (e) The mRNA level of PR in samples expressing low or high INPP4B levels. (f) Correlation between INPP4B protein level and PR protein level in 892 breast cancer samples.

Using whole mounts, we assessed the ductal branching in WT and *Inpp4b*$^{-/-}$ females. At 11 weeks old, the mammary glands of WT female mice were fully arborized while the mammary glands from *Inpp4b*$^{-/-}$ females displayed significantly reduced side branching (Figure 4-6 c). The expression of amphiregulin, an ERα and PR regulated gene required for mammary gland development (247, 248), was strikingly reduced in the mammary tissue of knockout females (Figure 4-6 d).

4.2.6. INPP4B loss caused weight gain and hyperglycemia in mice fed with an HFD

We and others have previously shown that INPP4B suppresses the AKT and PKC pathways in multiple cell lines (46, 54). We confirmed that INPP4B knockdown activated AKT and PKC signaling in MCF7 cells (Figure 4-7 a-c). In the female mouse model, we showed *Inpp4b* knockout activated PKC pathway in mouse mammary glands (Figure 4-7 d). Both the AKT and PKC signaling pathways are conduits for insulin signaling and are associated with metabolic disorders. Therefore, we investigated the role of INPP4B in the diet-induced model of obesity.

The *Inpp4b*$^{-/-}$ female mice fed HFD had a 50% increase in body weight compared to the age-matched HFD WT mice (Figure 4-8 a). The weights of the visceral white adipose tissue (WAT) and #4 mammary gland in HFD *Inpp4b*$^{-/-}$ female mice were significantly increased when compared to the other three groups (Figure 4-8 b-c), suggesting that weight gain was due to increased adiposity. Diet-induced obesity is frequently accompanied by insulin resistance that disrupts glucose homeostasis (249). As seen from Figure 4-8 d, *Inpp4b*$^{-/-}$ female mice had significantly increased fasting circulating glucose levels compared to WT mice, especially when fed HFD. The non-fasting blood glucose was also elevated in HFD *Inpp4b*$^{-/-}$ females (Figure 4-8 e). Consistently, the glucose tolerance test confirmed that

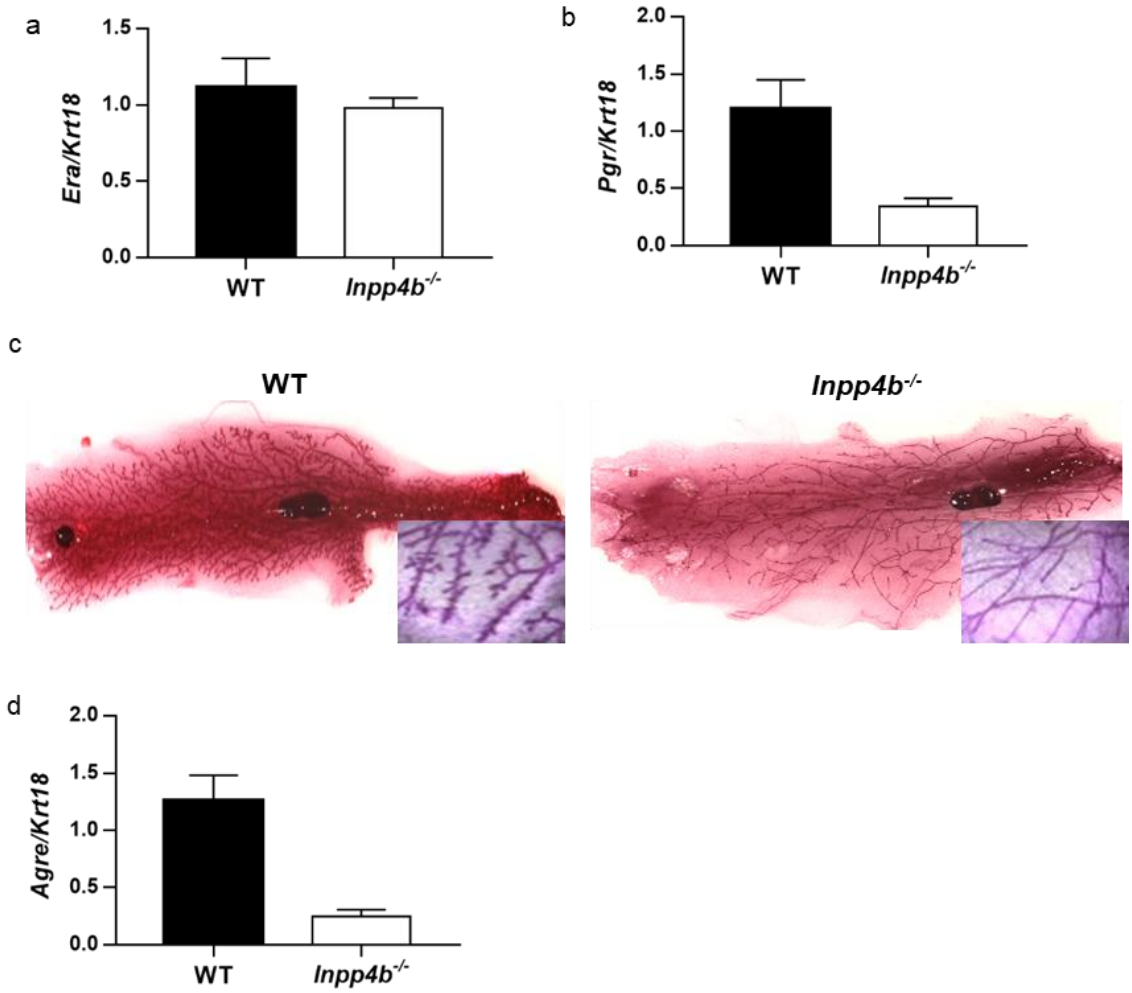

Figure 4-6. INPP4B is required for mouse mammary gland side branching. (a-b) Mammary glands were dissected from WT or *Inpp4b*$^{-/-}$ female mice at an age of 14 weeks. RNA was extracted, reversed transcribed, and analyzed for *Esr1* and *Pgr* expression by RT-qPCR using *Krt18* as control. (c) Whole mount of #4 mammary gland from WT and *Inpp4b*$^{-/-}$ female mice. (d) RNA from (a-b) were analyzed for *Agre* expression by RT-qPCR using *Krt18* as control.

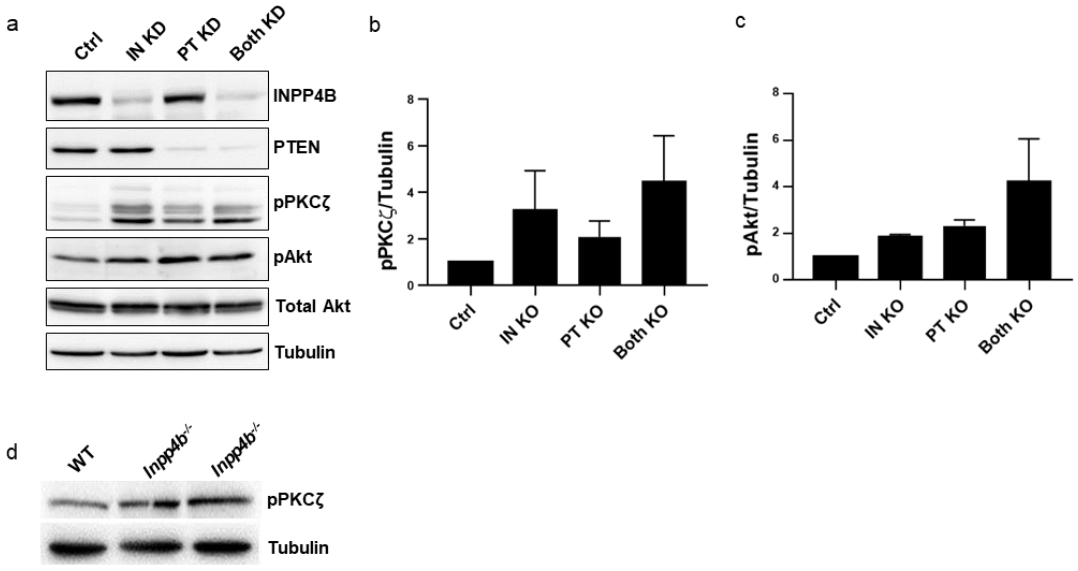

Figure 4-7. Loss of INPP4B activates AKT and PKC pathways. (a) MCF7 cells were transfected with INPP4B siRNA, PTEN siRNA, and both INPP4B and PTEN siRNA. Proteins were isolated and analyzed for INPP4B, PTEN, pPKCζ, pAKT, total AKT, and Tubulin by Western blotting. (b-c) Quantification of pPKCζ (b) and pAKT (c) from (a). (d) Mammary glands were dissected from WT and Inpp4b-/- female mice. Proteins were extracted and analyzed for pPKCζ and Tubulin by Western blotting.

HFD *Inpp4b*$^{-/-}$ mice had significant increases in blood glucose levels and increased glucose clearance times compared to controls, indicating that *Inpp4b* loss induces hyperglycemia in obese female mice (Figure 4-8 f). Circulating insulin was determined within groups of 5 mice each. As seen in Figure 4-8 g, HFD *Inpp4b*$^{-/-}$ mice exhibited a trend toward higher insulin levels compared to all other groups however it did not reach statistical significance ($p = 0.0805$). Consistent with the role of INPP4B during insulin signaling seen in the mouse model, gene expression analysis of the livers from nondiabetic (N=8) and Type 2 diabetic (N=6) women (GSE15653) revealed that INPP4B expression was significantly decreased in the livers of diabetic patients (Figure 4-8 h).

4.2.7. Inpp4b loss leads to NAFLD in female mice fed HFD

The emergence of hyperglycemia is an indicator of liver dysfunction, a key organ that regulates glycemic control. The liver weights of HFD *Inpp4b*$^{-/-}$ female mice were significantly increased compared to the control mice (Figure 4-9 a). The histological examination of H&E stained liver sections revealed that HFD *Inpp4b*$^{-/-}$ female mice developed severe steatosis (Figure 4-9 b-c). The morphometric quantification of unstained liver section areas, which identifies lipid droplets, indicated a significant increase of lipid droplets in the livers of *Inpp4b*$^{-/-}$ female mice. Extensive macrovesicular steatosis was observed in the hepatic lobes of HFD *Inpp4b*$^{-/-}$ female mice; microvesicular steatosis was observed in knockout mice fed with LFD; and no steatosis was detected in WT females (Figure 4-9 c). Consistently, Oil Red O staining confirmed the accumulation of fat within the livers of HFD knockout mice compared to WT on the same diet (Figure 4-9 d). Sirius red staining indicated an accumulation and expansion of collagen in the livers of HFD *Inpp4b*$^{-/-}$ female mice, which is a defining characteristic of liver fibrosis (Figure 4-9 e).

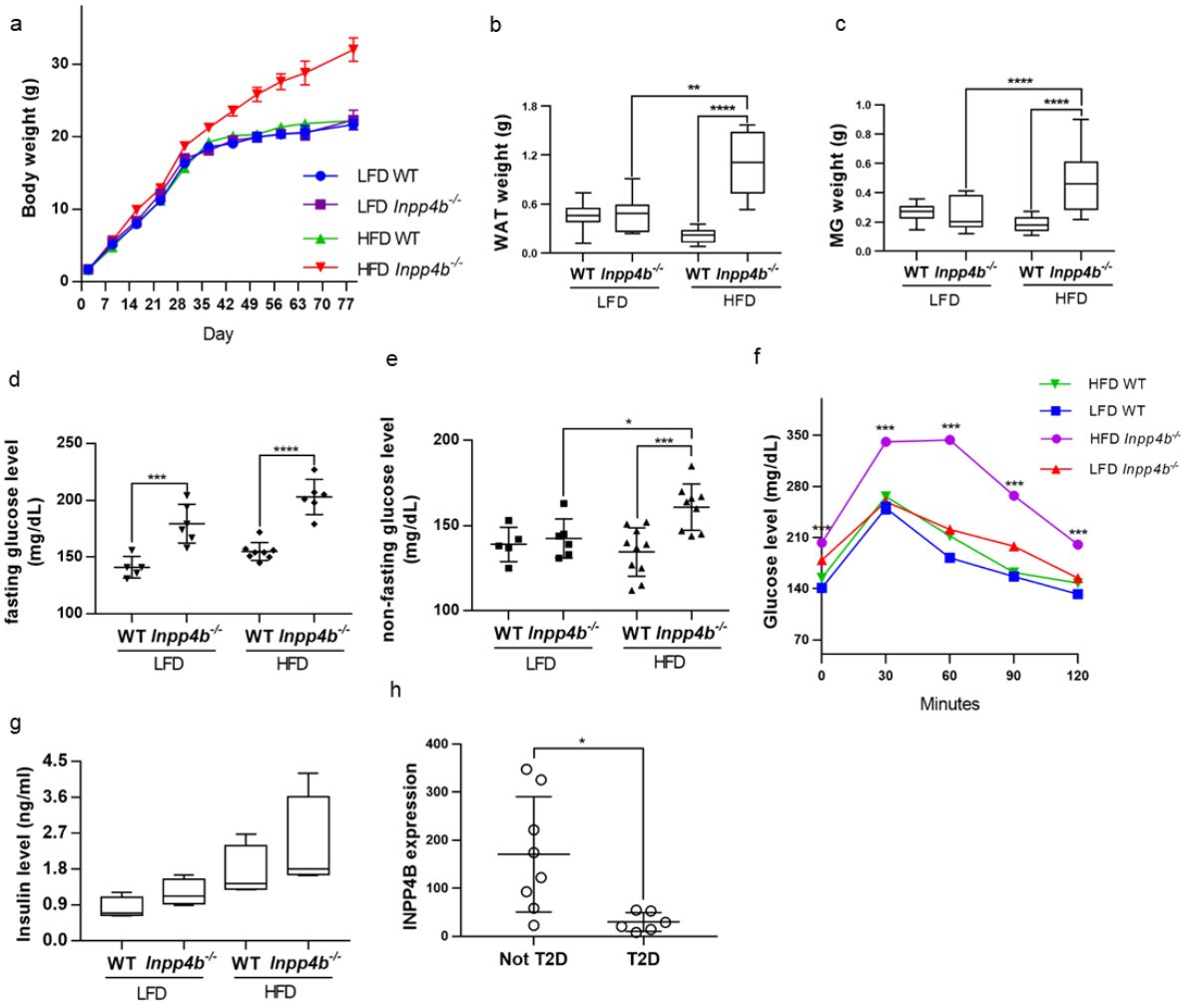

Figure 4-8. Loss of INPP4B caused weight gain and hyperglycemia in mice fed an HFD. (a) Bodyweight of LFD WT (N=5), LFD Inpp4b-/- (N=7), HFD WT (N=16), and HFD Inpp4b-/- (N=10) female mice were recorded every week till week 11. (b-c) Weights of visceral white adipose tissue (WAT) and #4 mammary gland were compared in indicated groups at 16-17 weeks of age. (d-e) Blood glucose level was measured after 6 hours fasting (d) or without fasting (e) in LFD WT, LFD Inpp4b-/-, HFD WT, and HFD Inpp4b-/- female mice. At least 5 mice were included in each group. (f) Oral glucose test of LFD WT (N=6), LFD Inpp4b-/- (N=6), HFD WT (N=11), and HFD Inpp4b-/- (N=9) female mice. Mice were weighed and treated with 2 g/kg of glucose and blood glucose was measured at different time points as indicated. (g) Blood insulin was measured using a mouse insulin ELISA kit for the indicated groups (5 mice per group). (h) Comparison of INPP4B expression in livers of subjects with or without type 2 diabetes. Data were exported from GSE15653.

4.2.8. Inpp4b loss caused hyperplasia in mammary gland and expansion in the extracellular matrix (ECM)

Since INPP4B is a tumor suppressor in breast cancer, we examined whether *Inpp4b* deficiency affects the mouse mammary gland morphology. H&E staining of the mammary glands from WT and knockout females on HFD showed abnormal duct and alveolar structures (Figure 4-10). We next used histological markers to distinguish the functional layers of the mammary duct and examined the origin of the abnormal duct structures. The luminal cells were identified by CK8 expression, myoepithelial cells were identified by alpha smooth muscle actin (αSMA) expression, and the basal membrane was stained with trichrome blue to visualize collagen fibers. As seen in Figure 8a, loss of INPP4B resulted in end bud hyperplasia for mice fed either diet. In HFD groups, *Inpp4b* knockout females had enlarged adipocytes compared to their WT. The myoepithelial layer remained similar in all groups, however expansion of the epithelial layer occurred in the mammary glands of *Inpp4b*$^{-/-}$ female mice fed either diet. Interestingly, *Inpp4b* loss resulted in the expansion of the ECM surrounding both the end buds and ducts (Figure 4-11 a). Fibroblasts participate in the formation of the ECM surrounding ducts by producing and secreting ECM molecules including collagen (250). Using Trichrome staining, we showed that loss of INPP4B promoted the accumulation of collagen surrounding the ducts in *Inpp4b*$^{-/-}$ females (Figure 4-11 b).

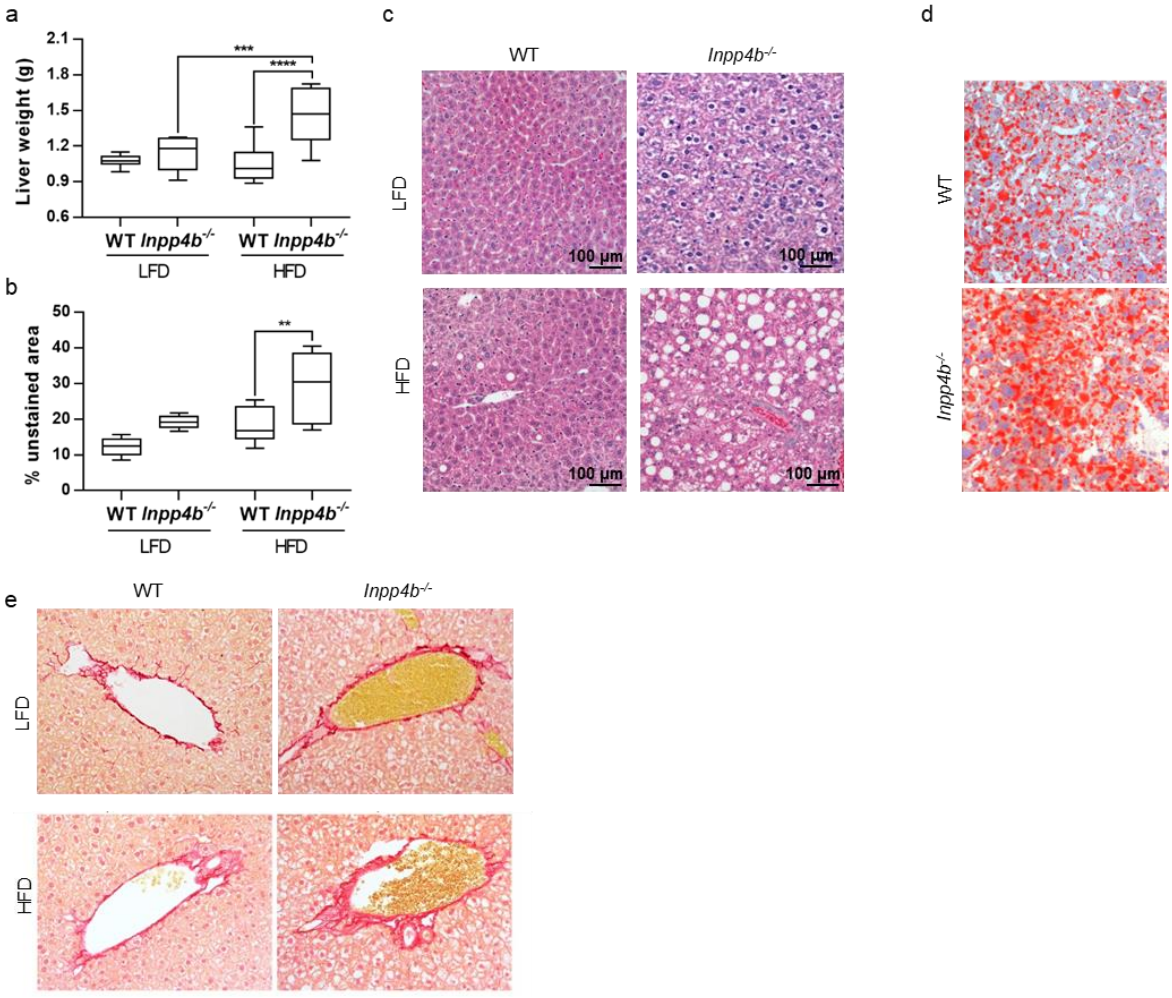

Figure 4-9. *Inpp4b* depletion leads to NAFLD with fibrosis. (a) Liver weights of LFD WT (N=10), LFD *Inpp4b*$^{-/-}$ (N=7), HFD WT (N=11), and HFD *Inpp4b*$^{-/-}$ (N=9) female mice. (b) Morphometric quantification of the unstained area from H&E staining in LFD WT (N=9), LFD *Inpp4b*$^{-/-}$ (N=5), HFD WT (N=11), and HFD *Inpp4b*$^{-/-}$ (N=6) female mice. (c) H&E staining of liver sections from designated groups. (d) Oil Red O staining of frozen liver sections in HFD WT, and HFD *Inpp4b*$^{-/-}$ female mice. (e) Sirius Red staining of liver sections from designated groups.

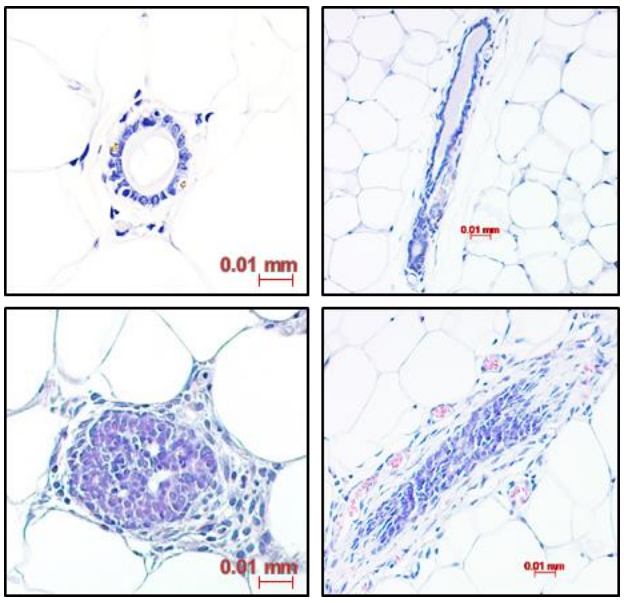

Figure 4-10. INPP4B loss induced hyperplasia in end buds and duct of mouse mammary gland. Representative image of H&E staining of mammary glands from HFD WT, and HFD *Inpp4b*$^{-/-}$ males.

4.3. Discussion

INPP4B has a well-documented tumor suppressor function in prostate and breast cancers (29, 31, 46, 47). The downstream targets of INPP4B include the INSR/PI3K/Akt, PLC/PKC, and steroid receptor pathways. Multiple groups, including our own, have shown that INPP4B can suppress Akt signaling in malignant and nonmalignant epithelial cells and mouse tissues. Additionally, we have shown that INPP4B also suppress PKC signaling in multiple cell lines and mouse model (53, 54). Finally, our group has been the first to show regulation of AR, ERα, and PR activity by INPP4B (54).

The early stages of breast cancer are ERα positive and estrogen dependent. We have previously reported that INPP4B regulates AR activity in prostate cancer. Interestingly, INPP4B is expressed in ERα^{+} breast cancers but was found histologically negative in triple-

negative breast cancers, the most aggressive subtype (46, 99), which suggests a correlation between INPP4B and ERα in breast cancer progression. Analysis of breast cancer transcriptomes and proteomes showed that INPP4B positively correlates with ERα on both the mRNA and protein levels in breast cancer patients (Figure 4-1) suggesting a functional crosstalk exists between INPP4B and ERα signaling. In MCF7 cells, INPP4B knockdown did not affect ERα expression, however it did regulate ERα transcriptional activity (Figure 4-2 a, c-d). INPP4B knockdown reduced the E2-mediated induction of *SGK3*, *PGR*, *UGT2B17*, *MSMB,* and *RAPGEFL1* (Figure 4-4 d-i). On the other hand, INPP4B reduced the expression of *EGR3* and *CYP24A1*, which are upregulated in rapidly proliferating cells (Figure 4-4 c and h). A comparative gene hybridization analysis that measures copy number in breast cancer identified *CYP24A1* as a potential oncogene (251). We compared the gene expression patterns after INPP4B and PTEN knockdown. A subset of genes was altered with both INPP4B and PTEN knockdown. However, we demonstrated that a subset of genes, including *CYP24A1* and *RAPGEFL1,* were preferentially regulated by INPP4B (Figure 4-2 f and Figure 4-4 h-i).

In this report, we show that loss of INPP4B leads to a reduction in PR RNA and protein levels in both breast cancer cells and the normal mouse mammary gland (Figure 4-5 and Figure 4-6). PR, a direct ERα target gene, is required for ductal branching and alveologenesis in the mammary gland (228). PGR is expressed as two protein isoforms, PRA and PRB (252). The PRA isoform predominately functions in uterine development (253) and PRB functions in the mammary gland (254). PRB is sufficient to stimulate the ductal branching (243, 254). In Figure 4-5, we showed that INPP4B was required for the

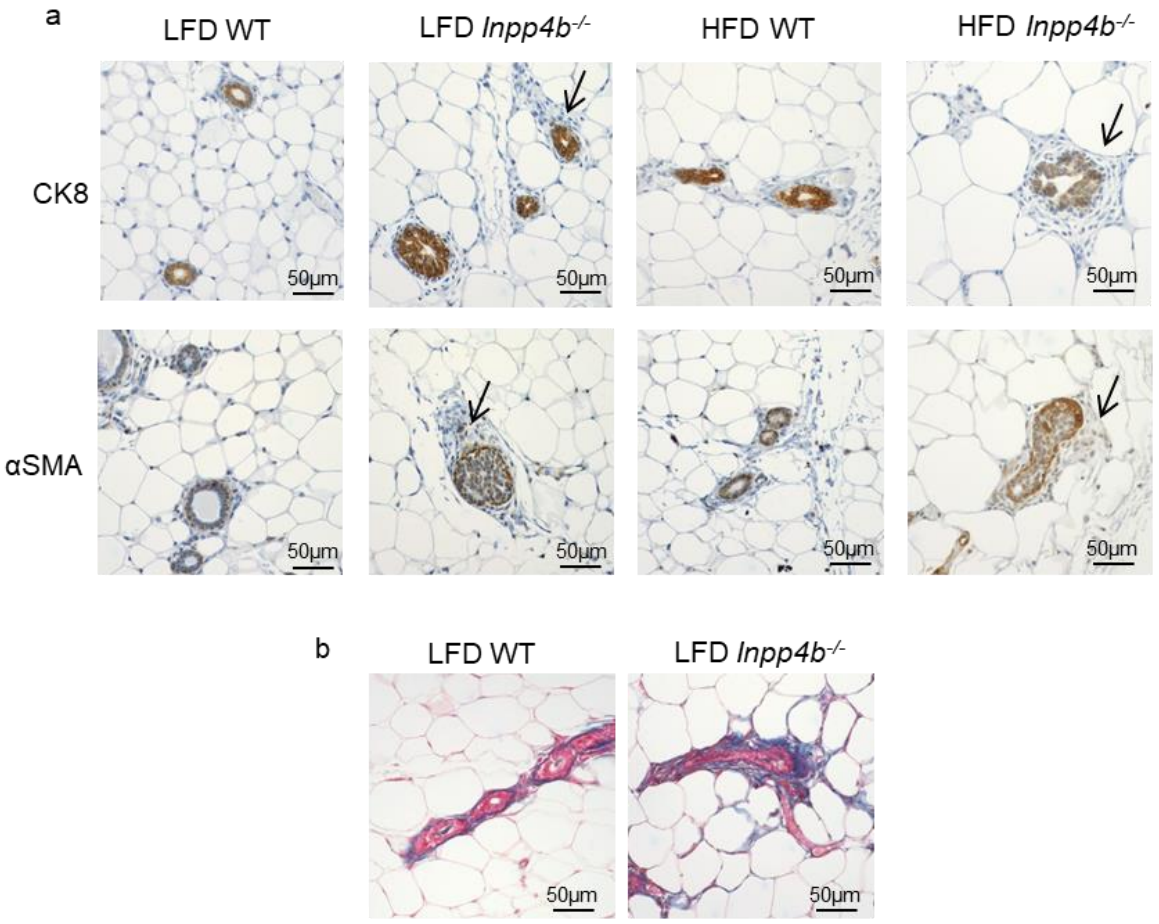

Figure 4-11. Loss of INPP4B causes hyperplasia in the mammary gland and expansion of ECM. (a) Mammary glands from 16 weeks old LFD WT, LFD *Inpp4b*$^{-/-}$, HFD WT, and HFD *Inpp4b*$^{-/-}$ female mice were sectioned, stained for CK8 or αSMA, and counterstained with hematoxylin. Examples of TEB that stained positive for CK8 and αSMA were presented. (b) Trichrome staining of mammary gland sections from LFD WT and LFD *Inpp4b*$^{-/-}$ mice.

optimal expression of both PR isoforms in breast cancer cell lines, suggesting that *Inpp4b* loss may affect mammary gland development similar to PR knockout models (243). Indeed, loss of INPP4B led to a deficiency in the ductal side branching of healthy mouse mammary glands (Figure 4-6). In the normal mammary gland, approximately 70% of epithelial cells are $ER\alpha^-$ and PR^- and require stimulation from adjacent $ER\alpha^+$ and PR^+ cells to proliferate through paracrine signaling (255). ER- and PR- mediate the transcription and secretion of amphiregulin, WNT4, and RANKL, which in turn, stimulate the proliferation of $ER\alpha^-$ and PR^- mammary epithelial cells (255). Wnt4, RANKL, and the EGFR ligand AREG, are PR target genes that have also been implicated in the regulation of ductal branching (133, 256, 257). Amphiregulin is also an ERα target gene and its expression was significantly reduced within the mouse mammary gland of *Inpp4b* knockout animals in (Figure 4-6 d).

Multiple groups, including ours, have shown that INPP4B inhibits the AKT pathway. PI3K/Akt signaling is activated in all advanced breast and prostate cancers concomitantly with the loss of INPP4b and PTEN (29, 46, 132). We have shown INPP4B mediated suppression of the PKC pathway in human prostate cancer cell lines and in the mouse prostate (53, 54). However, nothing was previously known about the INPP4B regulation of AKT and PKC signaling in physiologically normal organs.

The insulin receptor and fatty acid mediated signaling pathways lead to the phosphorylation of AKT and PKC in the liver, muscle and adipose tissues, which affects both glucose and lipid metabolism (258-260). The AKT and PKC pathways are associated with metabolic disorders in obese or diabetic individuals. In this report, we show that AKT and PKC pathways are activated by INPP4B knockdown in MCF7 cells, and in the

mammary glands of *Inpp4b*$^{-/-}$ female mice. (Figure 4-7 a-d). Moreover, AKT and PKC phosphorylation was increased in the livers of the *Inpp4b*$^{-/-}$ mice, suggesting a role for INPP4B in the insulin response. To determine the role of INPP4B in metabolic health, we designed 4 experimental groups: LFD WT, HFD WT, LFD *Inpp4b*$^{-/-}$, and HFD *Inpp4b*$^{-/-}$ females. The HFD, which contained 60% fat, did not increase the weight of the WT females when compared to the LFD group. Remarkably, the *Inpp4b*$^{-/-}$ females were 50% heavier compared to the HFD WT females. Correspondingly, the visceral fat weight in the knockout group was increased on average by 400% compared to that of HFD WT females (Figure 4-8 b-c). The increased visceral adiposity in humans frequently causes metabolic dysfunction which is characterized by insulin resistance, dyslipidemia, and inflammation (261). In our previous report, we showed that HFD *Inpp4b*$^{-/-}$ male mice developed type 2 diabetes. Despite extreme weight gains, HFD *Inpp4b*$^{-/-}$ female mice only developed hyperglycemia. Estrogen signaling in females has been shown to protect against insulin resistance and glucose intolerance in the HFD treated mice, which may contribute to the gender differences within the metabolic phenotype of *Inpp4b*$^{-/-}$ mice (236). Approximately 70% of obese and 30% of lean individuals are metabolically unhealthy (175). Hepatic accumulation of fat is the best marker of metabolic disease (184). The increased prevalence of obesity and metabolic disorders in the US also increases the risk of developing NAFLD (262). Indeed, HFD fed *Inpp4b*$^{-/-}$ females developed severe NAFLD and liver fibrosis (Figure 4-9).

Diet-induced obesity increases the risk of developing breast cancer in premenopausal women (263, 264). Here we showed that *Inpp4b*$^{-/-}$ female mice developed hyperplasia in the end buds by 17 weeks old (Figure 4-10 and Figure 4-11). In addition, the deletion of

Inpp4b in female mice expanded the ECM of mammary tissue (Figure 4-11). The ECM is composed of macromolecules including collagen, fibronectin and polysaccharides (265). Using Trichome staining, we showed the accumulation of collagen surrounding the ducts (Figure 4-11 b). Obesity increases differentiation of active fibroblasts leading to the ECM remodeling which promotes breast cancer progression (266).

In this study, we systematically investigated the role of INPP4B in breast cancer models and normal mouse physiology. In breast cancer cells, we showed INPP4B modulates ERα transcriptional activity and stimulates PR expression. We show that while INPP4B and PTEN have similar enzymatic activities, they are functionally distinct. In healthy mouse mammary glands, INPP4B stimulates ductal side branching, due in part to its ability to regulate ERα and PR activity, and it regulates the stromal sheath surrounding ducts and alveoli. Adipose and hepatic INPP4B expression protected HFD-fed female mice from developing hyperglycemia, NAFLD, and liver fibrosis.

4.4. Materials and methods

Cell culture

The human breast adenocarcinoma cell line MCF7 and T47D were purchased from ATCC (Manassas, VA). MCF7 cells were maintained in DMEM media (Thermo Fisher Scientific, Waltham, MA) supplemented with 10% fetal bovine serum (FBS). T47D cells were maintained in RPMI 1640 (Thermo Fisher Scientific, Waltham, MA) supplemented with 10% FBS and 0.2 units/ml bovine insulin (Sigma, ST. Louis, MO). FBS and charcoal stripped serum (CSS) were purchased from Sigma-Aldrich (St. Louis, MO). Estradiol (E2) were purchased from Sigma.

siRNA transfections

INPP4B and PTEN were knocked down by customer-designed INPP4B and PTEN siRNAs (267) using non-coding siRNA as control (Thermo Fisher Scientific). Briefly, 20-40 nM siRNAs were diluted in OPTI-MEM medium and transfected using Lipofectamine RNAiMAX Reagent (Thermo Fisher Scientific) as recommended by the manufacturer.

Microarray and Gene Set Enrichment Analysis (GSEA)

MCF7 cells were transfected with 80 pmol control or INPP4B specific siRNAs as described in the previous section. After transfection, cells were maintained in complete medium. At the end of day 2, cells were treated with 100 nM of E2 for another 24 hours before harvest. Total RNA was extracted, quantified, evaluated for quality, and analyzed using the Illumina Human HT-12v4 expression Beadchip platform as described previously (268). To investigate the correlation between INPP4B and ERα transcriptional activity, Gene Set Enrichment Analysis was performed as previously described (267, 269). ERα signature was generated from GSE8597 which includes 466 genes significantly changed ($p<0.05$) after 24 hours of E2 treatment.

Gene expression analysis

RNA was prepared from breast cancer cells or mouse tissues using Tri Reagent (Molecular Research Center, Cincinnati, OH). The RNA concentration was determined by NanoVue Plus (GE Healthcare BioSciences, Piscataway, NJ). The real-time quantitative reverse transcription (qRT-PCR) was performed using Verso cDNA synthesis Kit (Thermo Fisher Scientific) and a Roche 480 LightCycler (Roche, Basel, Switzerland). The corresponding primers and probes were designed from Universal Probe Library and were listed in Table 9.

Table 9. Primers and corresponding probes used in CHAPTER 4.

Human gene primers and corresponding probe sets			
Gene	Forward primers	reverse primers	probe
ESR1	ttactgaccaacctggcaga	atcatggagggtcaaatcca	24
INPP4B	tgtctgatgctgacgctaaga	ccacaaaccaatccagcaa	41
PTEN	ggggaagtaaggaccagagac	tccagatgattctttaacaggtagc	48
PGR	gggtgagactcttcatctatcca	tgcatctgttaccagccagt	2
PTPMT1	cgaggttcctgtgcaactct	tgtggatgtatgaccggatct	75
CHD5	ctccctaggcctgtttgtgt	agactcagaaacgccttcca	2
HERC5	ggctctcacagtgccctact	atgaccaagttgcccatgtt	66
MT2A	ctagccgcctcttcagctc	gcaggtgcaggagtcacc	68
MYOF	tggtggggaagtggaagtaa	tcaggtaacaaggtccaaacg	2
CALU	gaggcccctccattactagc	tccctggatagaagagaattgg	33
EGR3	cgcaagcgtgtgtgtttaag	ggggaagagtttggggtaaa	26
SGK3	ctgactattctatagtgaatgccagtg	ggtgcataagagaaaccaacg	16
UGT2B17	tgtcagaagaaagtgccaaca	gccatcaaatctccatagaacc	61
MSMB	ggagtcctgcttatcacaatga	acgaaggtggcaaagatcac	2
CYP24A1	tcatcatggccatcaaaaca	gcagctcgactggagtgac	88
RAPEGFL1	ccctctgcaagcagaacc	gttgtccagccccatgac	62

Mouse gene primers and corresponding probe sets			
Gene	Forward primers	reverse primers	probe
Esr1	gctcctaacttgctcctggac	cagcaacatgtcaaagatctcc	97
Pgr	tgcacctgatctaatcctaaatga	ggtaaggcacagcgagtagaa	72
Agre	aagaaaacgggactgtgcat	ggcttggcaatgattcaact	73

Western blotting

The protein extraction from cultured cells (134) and mouse tissue (267) was previously described. Cleared lysates were diluted to 4 µg/µl and 15-80 µg of protein was resolved on a 7.5% - 12.5% SDS-PAGE. The protein was transferred using nitrocellulose or PVDF membrane (0.2 µm) and the membrane was blocked using 5% BSA or non-fat milk. The blot was incubated with primary antibodies against INPP4B, PTEN, PR, pAKT S473, total AKT, pPKCζ T410, and β-tubulin. The sources and dilutions of antibodies are listed in

Table 10. The signal was captured using a Gel Logic 2000 imaging system or ImageQuant LAS 500 imager and analyzed by Carestream Molecular Imaging software (Carestream, Rochester, NY) or ImageQuant TL software (GE Healthcare).

Table 10. Antibodies used in CHAPTER 4.

Antibody	cat #	concentration	RRID
phospho-Akt S473	Cell signaling #4051	1:1000	AB_331158
Total Akt	Cell signaling #4691	1:1000	AB_915783
phospho-PKCζ T410	Cell signaling #2060	1:1000	AB_561487
phospho-PKCβII S660	Cell signaling #9371	1:1000	AB_2168219
INPP4B	Cell signaling #8450	1:1000	AB_10859372
PTEN	Cell signaling #9188	1:1000	AB_2253290
β-Tubulin	Millipore #05-661	1:5000	AB_309885
PR	Santa Cruz sc-810	1:600	AB_628172

Animal studies

Inpp4b$^{-/-}$ mice and high-fat diet treated *Inpp4b*$^{-/-}$ mice were described previously and in Chapter 2 (28, 54). WT and *Inpp4b*$^{-/-}$ females were fed with either LFD (LabDiet 5V75, St. Louis, MO) or HFD (TestDiet 58R3, St. Louis, MO) for 12-13 weeks after wean. Mouse body weights were recorded once a week. All LFD WT, LFD *Inpp4b*$^{-/-}$, HFD WT, and HFD *Inpp4b*$^{-/-}$ female mice were euthanized and dissected at 13 weeks, weighed and their tissues were collected for gene expression, protein, and histological analysis. All protocols were approved by the Florida International University Institutional Animal Care and Use Committee.

Whole mount

Mouse #4 mammary gland fat pad were flattened onto a pre-cleaned glass slide and fixed in ethanol/acetic acid (3:1) solution overnight at room temperature. Fixed tissues were washed in 70% ethanol and distilled water. The staining solution was made by 0.2%

Carmine red (Sigma) and 0.5% aluminum potassium sulfate (Fisher) in distilled water. The slides were stained with Carmine Alum solution overnight, dehydrolyzed in graded ethanol, cleared in xylene, and stored in toluene (Sigma).

Glucose tolerance test

The glucose tolerance test were performed on 14-week-old females as exact previously described (54). Briefly, after overnight fasting, the mice were weight and gived 2 g/kg of glucose by oral gavage. The blood glucose was tested at before administration, 30, 60, 90, and 120 min after administration using glucose meter.

Histological analysis

The tissue sectioning, H&E staining, and immunoblotting were described previously (267). Briefly, 4.5 μM sections were deparaffinized in xylene, hydrolyzed in gradient ethanol and stained with hematoxylin and eosin. The level of hepatosteatosis was measured by counting the surface of unstained areas per field in liver sections using ImageJ as described in Chapter 2. For immunoblotting, the antigen was retrieved by heating in 10 mM sodium citrate buffer. Sections were blocked then incubated with primary antibodies CK8 (#ab53280, Abcam, Cambridge, MA) and α-SMA (#ab5694) overnight at 4 °C. ABC kit (Vector Laboratories, Burlingame, CA) and Peroxidase substrate kit (Vector Laboratories) were used to visualize the staining as suggested by instruction.

Sirius Red Staining

Sections were processed in xylene and gradient ethanol. Slides were stained in 0.4% Sirius Red staining reagent (Lucerna-Chem, Switzerland), soak in 0.5% acidic acid, and processed in distilled water, ethanol and xylenes before mounting.

Oil Red O staining

Fresh liver tissue was placed in OCT medium and snapped frozen in liquid nitrogen. Liver samples were cut at 12 μm sections and attached to glass slides. Oil red O was dissolved in hot propylene glycol and filtered through Whatman #2 filter paper. Slides were fixed in 4% PFA, rinsed in distilled water and in propylene glycol, stained in oil red O, and counterstained with hematoxylin. All images were acquired using an AxioCam MRc5 camera (Zeiss, Thornwood, NY).

Trichrome Staining

After deparaffinization and hydration, slides were fixed in Bouin's solution (Sigma, #HY10-1) at 56 °C for 20min. Slides were stained in sequence of Weigert's Iron Hematoxylin (Sigma, #HT1079), Biebrich Scarlet-Acid Fucshin (Sigma, #HT15-1), Phosphotungstic/Phosphomolybdic acid solution, Aniline Blue solution (Sigma, #15-4), 1% acetic acid. After washing, the slides were dehydrated and cleared in xylenes before mounting.

Statistics

Student t-tests were used to test for inequality of means from two independent samples. Two-way ANOVA was performed for experiments related to the HFD-treated experiment by Prism 7.0. P-values less than 0.05 were considered statistically significant. Values are present as mean ± SEM. All cell culture-based experiments were repeated at least three times and biological triplicated were used for each point. In the mouse-based analysis, samples from at least 8 mice were used unless stated otherwise.

CHAPTER 5: SUMMARY AND FUTURE DIRECTIONS

INPP4B is a tumor suppressor in breast, prostate, and other cancers (29, 31, 46, 155), which acts as a dual-specificity phosphatase similar to another tumor suppressor PTEN. While INPP4B is highly expressed in various tissues in both human and mouse ice and humans (Figure 1-5), very little is known about its physiological function. In my dissertation research, I investigated the function of INPP4B in modulation of tumor-promoting androgen and estrogen signaling, as well as in metabolic health.

In the first experimental part of the dissertation (Chapter Two), I demonstrated that INPP4B regulates AR transcriptional activity in part through AKT and PKC pathways. INPP4B-dependent regulation of the proteome in androgen-dependent prostate cancer cell line LNCaP was investigated using reverse phase protein arrays (RPPA). INPP4B knockdown significantly elevated the phosphorylation levels of oncogenic kinases including SRC, MAPK, and AKT, while the protein level of tumor suppressor RB1 was significantly reduced. Both overexpression and downregulation of the epigenetic regulator Enhancer of zeste homologue 2 (EZH2) have been described in aggressive cancer (270-273). In LNCaP cells, EZH2 levels significantly decreased following INPP4B knockdown. INPP4B was also required for the optimal expression of EZH2 in androgen independently derived prostate cancer cell line, VCaP, as well as in mouse ventral prostate. In our previous study, we showed that one-year-old mice develop hyperplasia without the observation of neoplastic transformation (267) suggesting the downregulation of EZH2 might play a compensatory role in mouse prostate of *Inpp4b*$^{-/-}$ males in preventing the development of the prostate cancer. Currently, specific EZH2 inhibitors like GSK126 have been used in

clinical trials for CRPC patients (274, 275). In future studies, we will investigate whether EZH2 reciprocally regulates INPP4B signaling.

In Chapter 3, I showed loss of INPP4B induced high levels of inflammatory cytokines (*Il6*, *Tnf*, and *Il1b*) and adipokines (Leptin/Adiponectin), which are risk factors for prostate cancer (213). Levels of these cytokines are further elevated by diet-induced obesity in *Inpp4b*$^{-/-}$ male mice leading to the development of high grade prostatic intraepithelial neoplasia. In addition to systemic and local inflammation in knockout males, I found that INPP4B is a major regulator of metabolic health in both lean and obese mouse model. Specifically, I showed that INPP4B protects against liver steatosis. Using RNA-sequencing and pathway analysis, I demonstrated that *Inpp4b* knockout activates lipid transfer, synthesis, and storage pathways leading to the accumulation of lipids in mouse livers, insulin resistance, and ultimately to the development of type 2 diabetes (T2D). Under the diabetic condition, the insulin signaling activates AKT pathways which promotes the proteolysis of SREBP1. SREBP1 further activates PPARγ expression, and together these transcription factors stimulate expression of a subset of genes that are involved in lipid uptake and synthesis. This process eventually leads to hepatic lipid accumulation. Interestingly, the pathway analysis also showed that *Inpp4b* knockout regulates the metabolism of histidine, arginine, and proline. Histidine metabolism was recently found to increase the tumor cell resistance to a chemotherapeutic drug, methotrexate (276). Arginine and proline metabolisms are tightly associated with neurodegenerative diseases such as Parkinson's disease (277).

In Chapter 4, I demonstrated that INPP4B regulates ERα transcriptome. INPP4B knockdown reduces the level of a subset of ERα direct target genes, including PR, and

inhibits mammary gland side branching. Previous studies have shown INPP4B is lost in most of the triple-negative breast cancers (TNBC) and might be the best prognostic marker for TNBC with the odds ratio of 108 (46, 99). However, the role of INPP4B in HER2 positive breast cancers is unknown. HER2 is a human homolog of the murine ERBB2, whose overexpression in mouse induces mammary gland tumors similar to human HER2 positive tumors. Using MMTV-Erbb2 overexpressing mice, I tested whether the loss of INPP4B accelerates cancer progression. I mated the *Inpp4b*$^{-/-}$ mice with MMTV-Erbb2 transgenic mice to generate the MMTV-Erbb2;*Inpp4b*$^{-/-}$ female mice. Both MMTV-Erbb2 and MMTV-Erbb2;*Inpp4b*$^{-/-}$ female mice were subjected to either a low-fat diet or a high-fat diet (HFD). We noticed that the loss of INPP4B increased tumor incidence and worsened the survival of mice regardless of the diets. Remarkably, the diet was irrelevant to control females. Only in MMTV-Erbb2;*Inpp4b*$^{-/-}$ female mice, HFD accelerated tumor progression. In future studies, we will continue to investigate the molecular mechanism behind this phenomenon.

We are the first to investigate the INPP4B role in metabolism. We discovered that metabolic regulation by INPP4B is sexually dimorphic. In obese males, *Inpp4b*$^{-/-}$ mice have significantly elevated blood glucose, insulin resistance, and gluconeogenesis, which is consistent with T2D. In females, a combination of *Inpp4b* knockout and HFD cause hyperglycemia but do not impair insulin sensitivity. HFD *Inpp4b*$^{-/-}$ female mice develop a more severe nonalcoholic fatty liver disease (NAFLD) with liver fibrosis compared to obese male mice. In future studies, we will perform RNA sequencing to explore gender differences in metabolic health between male and female *Inpp4b*$^{-/-}$ mice.

The liver is not only crucial for glucose homeostasis and lipid metabolism, it also plays an essential role in drug detoxification. This liver function is also sexually dimorphic. Female and male individuals have a different expression pattern of cytochrome p450s (CYPs), key enzymes that are involved in drug and xenobiotic metabolism. Interestingly, analysis of the RNA sequencing results from livers of WT and *Inpp4b*$^{-/-}$ male mice indicated that the genes upregulated in liver of *Inpp4b*$^{-/-}$ males, such as *Cyp2b9* and *Cyp2b13*, are originally highly expressed in WT females (207). The loss of INPP4B causes a female-like expression pattern of CYPs in the male liver, suggesting that INPP4B might be a key regulator of sexual dimorphism of drug metabolism. In the follow-up studies, we will explore physiological consequences of the feminization of the *Inpp4b*$^{-/-}$ male livers. We will compare the RNA sequencing data and xenobiotic metabolism between male and female livers of WT and *Inpp4b*$^{-/-}$ mice. This will provide more evidence to evaluate whether *Inpp4b* regulates sexual dimorphism in the liver.

In summary, my dissertation research has demonstrated that INPP4B is a tumor suppressor that regulates steroid hormone signaling in prostate and breast cancer cells. Importantly for normal physiology, INPP4B protects against metabolic disorders and obesity.

I experimentally demonstrated that INPP4B regulates steroid receptor transcriptional activity in prostate and breast cancers. I revealed that INPP4B might be a regulator of lipid storage and gender-specific xenobiotic metabolism in obese mice. When feed with HFD, both *Inpp4b*$^{-/-}$ male and female mice developed hyperglycemia but only male have insulin resistance and progressed to T2D. In obese models, loss of INPP4B caused metabolic changes eventually lead to development of fatty liver disease which progresses to liver

fibrosis. Thus, I elucidated tumor-suppressive actions of INPP4B and determined that INPP4B is a major determinant of metabolic health.

REFERENCES

1. Billcliff PG, Lowe M. Inositol lipid phosphatases in membrane trafficking and human disease. Biochem J. 2014;461(2):159-75.

2. Liu Y, Bankaitis VA. Phosphoinositide phosphatases in cell biology and disease. Prog Lipid Res. 2010;49(3):201-17.

3. McCrea HJ, De Camilli P. Mutations in phosphoinositide metabolizing enzymes and human disease. Physiology (Bethesda). 2009;24:8-16.

4. Di Paolo G, De Camilli P. Phosphoinositides in cell regulation and membrane dynamics. Nature. 2006;443(7112):651-7.

5. Balla T. Phosphoinositides: tiny lipids with giant impact on cell regulation. Physiol Rev. 2013;93(3):1019-137.

6. Hakim S, Bertucci MC, Conduit SE, Vuong DL, Mitchell CA. Inositol polyphosphate phosphatases in human disease. Curr Top Microbiol Immunol. 2012;362:247-314.

7. Myers MP, Pass I, Batty IH, Van der Kaay J, Stolarov JP, Hemmings BA, et al. The lipid phosphatase activity of PTEN is critical for its tumor supressor function. Proc Natl Acad Sci U S A. 1998;95(23):13513-8.

8. Worby CA, Dixon JE. Pten. Annu Rev Biochem. 2014;83:641-69.

9. Hlobilkova A, Knillova J, Bartek J, Lukas J, Kolar Z. The mechanism of action of the tumour suppressor gene PTEN. Biomed Pap Med Fac Univ Palacky Olomouc Czech Repub. 2003;147(1):19-25.

10. Steck PA, Pershouse MA, Jasser SA, Yung WK, Lin H, Ligon AH, et al. Identification of a candidate tumour suppressor gene, MMAC1, at chromosome 10q23.3 that is mutated in multiple advanced cancers. Nat Genet. 1997;15(4):356-62.

11. Cairns P, Evron E, Okami K, Halachmi N, Esteller M, Herman JG, et al. Point mutation and homozygous deletion of PTEN/MMAC1 in primary bladder cancers. Oncogene. 1998;16(24):3215-8.

12. Kohno T, Takahashi M, Manda R, Yokota J. Inactivation of the PTEN/MMAC1/TEP1 gene in human lung cancers. Genes Chromosomes Cancer. 1998;22(2):152-6.

13. Tashiro H, Blazes MS, Wu R, Cho KR, Bose S, Wang SI, et al. Mutations in PTEN are frequent in endometrial carcinoma but rare in other common gynecological malignancies. Cancer Res. 1997;57(18):3935-40.

14. Liaw D, Marsh DJ, Li J, Dahia PL, Wang SI, Zheng Z, et al. Germline mutations of the PTEN gene in Cowden disease, an inherited breast and thyroid cancer syndrome. Nat Genet. 1997;16(1):64-7.

15. Di Cristofano A, Pesce B, Cordon-Cardo C, Pandolfi PP. Pten is essential for embryonic development and tumour suppression. Nat Genet. 1998;19(4):348-55.

16. Shen-Li H, Koujak S, Szablocs M, Parsons R. Reduction of Pten dose leads to neoplastic development in multiple organs of Pten (shRNA) mice. Cancer Biol Ther. 2010;10(11):1194-200.

17. Podsypanina K, Ellenson LH, Nemes A, Gu J, Tamura M, Yamada KM, et al. Mutation of Pten/Mmac1 in mice causes neoplasia in multiple organ systems. Proc Natl Acad Sci U S A. 1999;96(4):1563-8.

18. Shi Y, Wang J, Chandarlapaty S, Cross J, Thompson C, Rosen N, et al. PTEN is a protein tyrosine phosphatase for IRS1. Nat Struct Mol Biol. 2014;21(6):522-7.

19. Lee JO, Yang H, Georgescu MM, Di Cristofano A, Maehama T, Shi Y, et al. Crystal structure of the PTEN tumor suppressor: implications for its phosphoinositide phosphatase activity and membrane association. Cell. 1999;99(3):323-34.

20. Kim YJ, Jahan N, Bahk YY. Biochemistry and structure of phosphoinositide phosphatases. BMB Rep. 2013;46(1):1-8.

21. Rizo J, Sudhof TC. C2-domains, structure and function of a universal Ca2+-binding domain. J Biol Chem. 1998;273(26):15879-82.

22. Norris FA, Auethavekiat V, Majerus PW. The Isolation and Characterization of cDNA Encoding Human and Rat Brain Inositol Polyphosphate 4-Phosphatase. The Journal of Biological Chemistry. 1995;270(27):6.

23. Norris FA, Atkins RC, Majerus PW. The cDNA Cloning and Characterization of Inositol Polyphosphate 4-Phosphatase Type II. The Journal of Biological Chemistry. 1997;272(38):6.

24. Croft A, Guo ST, Sherwin S, Farrelly M, Yan XG, Zhang XD, et al. Functional identification of a novel transcript variant of INPP4B in human colon and breast cancer cells. Biochem Biophys Res Commun. 2017;485(1):47-53.

25. Ferron M, Vacher J. Characterization of the murine Inpp4b gene and identification of a novel isoform. Gene. 2006;376(1):152-61.

26. Agoulnik IU, Hodgson MC, Bowden WA, Ittmann MM. INPP4B: the New Kid on the PI3K Block. Oncotarget. 2011;2(4):8.

27. Mehrotra B, Myszka DG, Prestwich GD. Binding kinetics and ligand specificity for the interactions of the C2B domain of synaptogmin II with inositol polyphosphates and phosphoinositides. Biochemistry. 2000;39(32):9679-86.

28. Ferron M, Boudiffa M, Arsenault M, Rached M, Pata M, Giroux S, et al. Inositol polyphosphate 4-phosphatase B as a regulator of bone mass in mice and humans. Cell Metab. 2011;14(4):466-77.

29. Gewinner C, Wang ZC, Richardson A, Teruya-Feldstein J, Etemadmoghadam D, Bowtell D, et al. Evidence that inositol polyphosphate 4-phosphatase type II is a tumor suppressor that inhibits PI3K signaling. Cancer Cell. 2009;16(2):115-25.

30. Yue F, Cheng Y, Breschi A, Vierstra J, Wu W, Ryba T, et al. A comparative encyclopedia of DNA elements in the mouse genome. Nature. 2014;515(7527):355-64.

31. Kofuji S, Kimura H, Nakanishi H, Nanjo H, Takasuga S, Liu H, et al. INPP4B Is a PtdIns(3,4,5)P3 Phosphatase That Can Act as a Tumor Suppressor. Cancer Discov. 2015;5(7):730-9.

32. Lopez SM, Hodgson MC, Packianathan C, Bingol-Ozakpinar O, Uras F, Rosen BP, et al. Determinants of the tumor suppressor INPP4B protein and lipid phosphatase activities. Biochem Biophys Res Commun. 2013;440(2):277-82.

33. Guo ST, Chi MN, Yang RH, Guo XY, Zan LK, Wang CY, et al. INPP4B is an oncogenic regulator in human colon cancer. Oncogene. 2016;35(23):3049-61.

34. Balk SP. Androgen receptor as a target in androgen-independent prostate cancer. Urology. 2002;60(3 Suppl 1):132-8; discussion 8-9.

35. Yeh S, Tsai M-Y, Xu Q, Mu X-M, Lardy H, Huang K-E, et al. Generation and characterization of androgen receptor knockout (ARKO) mice: An in vivo model for the study of androgen functions in selective tissues. PNAS, Proceedings of the National Academy of Sciences. 2002;99(21):6.

36. Bellacosa A, Testa JR, Staal SP, Tsichlis PN. A retroviral oncogene, akt, encoding a serine-threonine kinase containing an SH2-like region. Science. 1991;254(5029):274-7.

37. Franke TF, Yang SI, Chan TO, Datta K, Kazlauskas A, Morrison DK, et al. The protein kinase encoded by the Akt proto-oncogene is a target of the PDGF-activated phosphatidylinositol 3-kinase. Cell. 1995;81(5):727-36.

38. Frech M, Andjelkovic M, Ingley E, Reddy KK, Falck JR, Hemmings BA. High affinity binding of inositol phosphates and phosphoinositides to the pleckstrin homology domain of RAC/protein kinase B and their influence on kinase activity. J Biol Chem. 1997;272(13):8474-81.

39. Rudge SA, Wakelam MJ. Phosphatidylinositolphosphate phosphatase activities and cancer. J Lipid Res. 2016;57(2):176-92.

40. Hers I, Vincent EE, Tavare JM. Akt signalling in health and disease. Cell Signal. 2011;23(10):1515-27.

41. Manning BD, Cantley LC. AKT/PKB signaling: navigating downstream. Cell. 2007;129(7):1261-74.

42. Yuan ZQ, Sun M, Feldman RI, Wang G, Ma X, Jiang C, et al. Frequent activation of AKT2 and induction of apoptosis by inhibition of phosphoinositide-3-OH kinase/Akt pathway in human ovarian cancer. Oncogene. 2000;19(19):2324-30.

43. Sun M, Paciga JE, Feldman RI, Yuan Z, Coppola D, Lu YY, et al. Phosphatidylinositol-3-OH Kinase (PI3K)/AKT2, activated in breast cancer, regulates and is induced by estrogen receptor alpha (ERalpha) via interaction between ERalpha and PI3K. Cancer Res. 2001;61(16):5985-91.

44. Sun M, Wang G, Paciga JE, Feldman RI, Yuan ZQ, Ma XL, et al. AKT1/PKBalpha kinase is frequently elevated in human cancers and its constitutive activation is required for oncogenic transformation in NIH3T3 cells. Am J Pathol. 2001;159(2):431-7.

45. Balsara BR, Pei J, Mitsuuchi Y, Page R, Klein-Szanto A, Wang H, et al. Frequent activation of AKT in non-small cell lung carcinomas and preneoplastic bronchial lesions. Carcinogenesis. 2004;25(11):2053-9.

46. Fedele CG, Ooms LM, Ho M, Vieusseux J, O'Toole SA, Millar EK, et al. Inositol polyphosphate 4-phosphatase II regulates PI3K/Akt signaling and is lost in human basal-like breast cancers. Proc Natl Acad Sci U S A. 2010;107(51):22231-6.

47. Hodgson MC, Shao L-j, Frolov A, Li R, Peterson LE, Ayala G, et al. Decreased Expression and Androgen Regulation of the Tumor Suppressor Gene INPP4B in Prostate Cancer. Cancer Research. 2011;71(2):11.

48. Newton AC. Diacylglycerol's affair with protein kinase C turns 25. Trends Pharmacol Sci. 2004;25(4):175-7.

49. Newton AC. Regulation of the ABC kinases by phosphorylation: protein kinase C as a paradigm. Biochem J. 2003;370(Pt 2):361-71.

50. Creba JA, Downes CP, Hawkins PT, Brewster G, Michell RH, Kirk CJ. Rapid breakdown of phosphatidylinositol 4-phosphate and phosphatidylinositol 4,5-bisphosphate in rat hepatocytes stimulated by vasopressin and other Ca2+-mobilizing hormones. Biochem J. 1983;212(3):733-47.

51. Nishizuka Y. The protein kinase C family and lipid mediators for transmembrane signaling and cell regulation. Alcohol Clin Exp Res. 2001;25(5 Suppl ISBRA):3S-7S.

52. Cornford P, Evans J, Dodson A, Parsons K, Woolfenden A, Neoptolemos J, et al. Protein kinase C isoenzyme patterns characteristically modulated in early prostate cancer. Am J Pathol. 1999;154(1):137-44.

53. Hodgson MC, Deryugina EI, Suarez E, Lopez SM, Lin D, Xue H, et al. INPP4B suppresses prostate cancer cell invasion. Cell Commun Signal. 2014;12:61.

54. Zhang M, Suarez E, Vasquez JL, Nathanson L, Peterson LE, Rajapakshe K, et al. Inositol polyphosphate 4-phosphatase type II regulation of androgen receptor activity. Oncogene. 2018.

55. Wen Y, Hu MC, Makino K, Spohn B, Bartholomeusz G, Yan DH, et al. HER-2/neu promotes androgen-independent survival and growth of prostate cancer cells through the Akt pathway. Cancer Res. 2000;60(24):6841-5.

56. Lin HK, Hu YC, Yang L, Altuwaijri S, Chen YT, Kang HY, et al. Suppression versus induction of androgen receptor functions by the phosphatidylinositol 3-kinase/Akt pathway in prostate cancer LNCaP cells with different passage numbers. J Biol Chem. 2003;278(51):50902-7.

57. Lin HK, Yeh S, Kang HY, Chang C. Akt suppresses androgen-induced apoptosis by phosphorylating and inhibiting androgen receptor. Proc Natl Acad Sci U S A. 2001;98(13):7200-5.

58. Taneja SS, Ha S, Swenson NK, Huang HY, Lee P, Melamed J, et al. Cell-specific regulation of androgen receptor phosphorylation in vivo. J Biol Chem. 2005;280(49):40916-24.

59. Siegel RL, Miller KD, Jemal A. Cancer statistics, 2016. CA Cancer J Clin. 2016;66(1):7-30.

60. Society AC. Cancer facts and figures 2018. American Cancer Society. 2018:9-23.

61. Sharifi N, Gulley JL, Dahut WL. Androgen deprivation therapy for prostate cancer. JAMA. 2005;294(2):238-44.

62. Jenster G. The role of the androgen receptor in the development and progression of prostate cancer. Semin Oncol. 1999;26(4):407-21.

63. Yuan X, Cai C, Chen S, Chen S, Yu Z, Balk SP. Androgen receptor functions in castration-resistant prostate cancer and mechanisms of resistance to new agents targeting the androgen axis. Oncogene. 2014;33(22):2815-25.

64. Lowrance WT, Murad MH, Oh WK, Jarrard DF, Resnick MJ, Cookson MS. Castration-Resistant Prostate Cancer: AUA Guideline Amendment 2018. J Urol. 2018;200(6):1264-72.

65. Gillessen S, Attard G, Beer TM, Beltran H, Bossi A, Bristow R, et al. Management of Patients with Advanced Prostate Cancer: The Report of the Advanced Prostate Cancer Consensus Conference APCCC 2017. Eur Urol. 2018;73(2):178-211.

66. Watson PA, Arora VK, Sawyers CL. Emerging mechanisms of resistance to androgen receptor inhibitors in prostate cancer. Nat Rev Cancer. 2015;15(12):701-11.

67. Tan MH, Li J, Xu HE, Melcher K, Yong EL. Androgen receptor: structure, role in prostate cancer and drug discovery. Acta Pharmacol Sin. 2015;36(1):3-23.

68. Lonergan PE, Tindall DJ. Androgen receptor signaling in prostate cancer development and progression. J Carcinog. 2011;10:20.

69. Buchanan G, Irvine RA, Coetzee GA, Tilley WD. Contribution of the androgen receptor to prostate cancer predisposition and progression. Cancer Metastasis Rev. 2001;20(3-4):207-23.

70. Steinkamp MP, O'Mahony OA, Brogley M, Rehman H, Lapensee EW, Dhanasekaran S, et al. Treatment-dependent androgen receptor mutations in prostate cancer exploit multiple mechanisms to evade therapy. Cancer Res. 2009;69(10):4434-42.

71. Ware KE, Garcia-Blanco MA, Armstrong AJ, Dehm SM. Biologic and clinical significance of androgen receptor variants in castration resistant prostate cancer. Endocr Relat Cancer. 2014;21(4):T87-T103.

72. Arora VK, Schenkein E, Murali R, Subudhi SK, Wongvipat J, Balbas MD, et al. Glucocorticoid receptor confers resistance to antiandrogens by bypassing androgen receptor blockade. Cell. 2013;155(6):1309-22.

73. Sahu B, Laakso M, Pihlajamaa P, Ovaska K, Sinielnikov I, Hautaniemi S, et al. FoxA1 specifies unique androgen and glucocorticoid receptor binding events in prostate cancer cells. Cancer Res. 2013;73(5):1570-80.

74. Heemers HV, Tindall DJ. Androgen receptor (AR) coregulators: a diversity of functions converging on and regulating the AR transcriptional complex. Endocr Rev. 2007;28(7):778-808.

75. Zhu ML, Kyprianou N. Androgen receptor and growth factor signaling cross-talk in prostate cancer cells. Endocr Relat Cancer. 2008;15(4):841-9.

76. Heine PA, Taylor JA, Iwamoto GA, Lubahn DB, Cooke PS. Increased adipose tissue in male and female estrogen receptor-alpha knockout mice. Proc Natl Acad Sci U S A. 2000;97(23):12729-34.

77. Chen H, Li H, Chen Q. INPP4B overexpression suppresses migration, invasion and angiogenesis of human prostate cancer cells. Clin Exp Pharmacol Physiol. 2017;44(6):700-8.

78. Goldhirsch A, Wood WC, Coates AS, Gelber RD, Thurlimann B, Senn HJ, et al. Strategies for subtypes--dealing with the diversity of breast cancer: highlights of the St. Gallen International Expert Consensus on the Primary Therapy of Early Breast Cancer 2011. Ann Oncol. 2011;22(8):1736-47.

79. Hamilton KJ, Hewitt SC, Arao Y, Korach KS. Estrogen Hormone Biology. Curr Top Dev Biol. 2017;125:109-46.

80. Mehta RG, Hawthorne M, Mehta RR, Torres KE, Peng X, McCormick DL, et al. Differential roles of ERalpha and ERbeta in normal and neoplastic development in the mouse mammary gland. PLoS One. 2014;9(11):e113175.

81. Warner M, Huang B, Gustafsson JA. Estrogen Receptor beta as a Pharmaceutical Target. Trends Pharmacol Sci. 2017;38(1):92-9.

82. Cancer Genome Atlas N. Comprehensive molecular portraits of human breast tumours. Nature. 2012;490(7418):61-70.

83. Frasor J, Danes JM, Komm B, Chang KC, Lyttle CR, Katzenellenbogen BS. Profiling of estrogen up- and down-regulated gene expression in human breast cancer cells: insights into gene networks and pathways underlying estrogenic control of proliferation and cell phenotype. Endocrinology. 2003;144(10):4562-74.

84. Bunone G, Briand PA, Miksicek RJ, Picard D. Activation of the unliganded estrogen receptor by EGF involves the MAP kinase pathway and direct phosphorylation. EMBO J. 1996;15(9):2174-83.

85. Campbell RA, Bhat-Nakshatri P, Patel NM, Constantinidou D, Ali S, Nakshatri H. Phosphatidylinositol 3-kinase/AKT-mediated activation of estrogen receptor alpha: a new model for anti-estrogen resistance. J Biol Chem. 2001;276(13):9817-24.

86. Kato S, Endoh H, Masuhiro Y, Kitamoto T, Uchiyama S, Sasaki H, et al. Activation of the estrogen receptor through phosphorylation by mitogen-activated protein kinase. Science. 1995;270(5241):1491-4.

87. Mohammed H, Russell IA, Stark R, Rueda OM, Hickey TE, Tarulli GA, et al. Progesterone receptor modulates ERalpha action in breast cancer. Nature. 2015;523(7560):313-7.

88. Kabos P, Finlay-Schultz J, Li C, Kline E, Finlayson C, Wisell J, et al. Patient-derived luminal breast cancer xenografts retain hormone receptor heterogeneity and help define unique estrogen-dependent gene signatures. Breast Cancer Res Treat. 2012;135(2):415-32.

89. Thomas C, Gustafsson JA. Progesterone receptor-estrogen receptor crosstalk: a novel insight. Trends Endocrinol Metab. 2015;26(9):453-4.

90. Citri A, Yarden Y. EGF-ERBB signalling: towards the systems level. Nat Rev Mol Cell Biol. 2006;7(7):505-16.

91. Schiff R, Massarweh SA, Shou J, Bharwani L, Mohsin SK, Osborne CK. Cross-talk between estrogen receptor and growth factor pathways as a molecular target for overcoming endocrine resistance. Clin Cancer Res. 2004;10(1 Pt 2):331S-6S.

92. Wolff AC, Hammond ME, Hicks DG, Dowsett M, McShane LM, Allison KH, et al. Recommendations for human epidermal growth factor receptor 2 testing in breast

cancer: American Society of Clinical Oncology/College of American Pathologists clinical practice guideline update. J Clin Oncol. 2013;31(31):3997-4013.

93. Loibl S, Gianni L. HER2-positive breast cancer. Lancet. 2017;389(10087):2415-29.

94. Wieduwilt MJ, Moasser MM. The epidermal growth factor receptor family: biology driving targeted therapeutics. Cell Mol Life Sci. 2008;65(10):1566-84.

95. Loibl S, Darb-Esfahani S, Huober J, Klimowicz A, Furlanetto J, Lederer B, et al. Integrated Analysis of PTEN and p4EBP1 Protein Expression as Predictors for pCR in HER2-Positive Breast Cancer. Clin Cancer Res. 2016;22(11):2675-83.

96. Rimawi MF, Schiff R, Osborne CK. Targeting HER2 for the treatment of breast cancer. Annu Rev Med. 2015;66:111-28.

97. Denkert C, Liedtke C, Tutt A, von Minckwitz G. Molecular alterations in triple-negative breast cancer-the road to new treatment strategies. Lancet. 2017;389(10087):2430-42.

98. Bianchini G, Balko JM, Mayer IA, Sanders ME, Gianni L. Triple-negative breast cancer: challenges and opportunities of a heterogeneous disease. Nat Rev Clin Oncol. 2016;13(11):674-90.

99. Won JR, Gao D, Chow C, Cheng J, Lau SY, Ellis MJ, et al. A survey of immunohistochemical biomarkers for basal-like breast cancer against a gene expression profile gold standard. Mod Pathol. 2013;26(11):1438-50.

100. Vasudevan KM, Barbie DA, Davies MA, Rabinovsky R, McNear CJ, Kim JJ, et al. AKT-independent signaling downstream of oncogenic PIK3CA mutations in human cancer. Cancer Cell. 2009;16(1):21-32.

101. Gasser JA, Inuzuka H, Lau AW, Wei W, Beroukhim R, Toker A. SGK3 mediates INPP4B-dependent PI3K signaling in breast cancer. Mol Cell. 2014;56(4):595-607.

102. Hales CM, Carroll MD, Fryar CD, Ogden CL. Prevalence of Obesity Among Adults and Youth: United States, 2015-2016. NCHS Data Brief. 2017(288):1-8.

103. Osborn O, Olefsky JM. The cellular and signaling networks linking the immune system and metabolism in disease. Nat Med. 2012;18(3):363-74.

104. Akinyemiju T, Moore JX, Judd S, Lakoski S, Goodman M, Safford MM, et al. Metabolic dysregulation and cancer mortality in a national cohort of blacks and whites. BMC Cancer. 2017;17(1):856.

105. Petersen MC, Shulman GI. Mechanisms of Insulin Action and Insulin Resistance. Physiol Rev. 2018;98(4):2133-223.

106. Samuel VT, Shulman GI. Nonalcoholic Fatty Liver Disease as a Nexus of Metabolic and Hepatic Diseases. Cell Metab. 2018;27(1):22-41.

107. Menke A, Casagrande S, Geiss L, Cowie CC. Prevalence of and Trends in Diabetes Among Adults in the United States, 1988-2012. JAMA. 2015;314(10):1021-9.

108. Haeusler RA, McGraw TE, Accili D. Biochemical and cellular properties of insulin receptor signalling. Nat Rev Mol Cell Biol. 2018;19(1):31-44.

109. Boucher J, Kleinridders A, Kahn CR. Insulin receptor signaling in normal and insulin-resistant states. Cold Spring Harb Perspect Biol. 2014;6(1).

110. Choi SM, Tucker DF, Gross DN, Easton RM, DiPilato LM, Dean AS, et al. Insulin regulates adipocyte lipolysis via an Akt-independent signaling pathway. Mol Cell Biol. 2010;30(21):5009-20.

111. Perry RJ, Camporez JG, Kursawe R, Titchenell PM, Zhang D, Perry CJ, et al. Hepatic acetyl CoA links adipose tissue inflammation to hepatic insulin resistance and type 2 diabetes. Cell. 2015;160(4):745-58.

112. Titchenell PM, Quinn WJ, Lu M, Chu Q, Lu W, Li C, et al. Direct Hepatocyte Insulin Signaling Is Required for Lipogenesis but Is Dispensable for the Suppression of Glucose Production. Cell Metab. 2016;23(6):1154-66.

113. Samuel VT, Shulman GI. Mechanisms for insulin resistance: common threads and missing links. Cell. 2012;148(5):852-71.

114. Nakae J, Barr V, Accili D. Differential regulation of gene expression by insulin and IGF-1 receptors correlates with phosphorylation of a single amino acid residue in the forkhead transcription factor FKHR. EMBO J. 2000;19(5):989-96.

115. Gross DN, van den Heuvel AP, Birnbaum MJ. The role of FoxO in the regulation of metabolism. Oncogene. 2008;27(16):2320-36.

116. Eberle D, Hegarty B, Bossard P, Ferre P, Foufelle F. SREBP transcription factors: master regulators of lipid homeostasis. Biochimie. 2004;86(11):839-48.

117. Li S, Brown MS, Goldstein JL. Bifurcation of insulin signaling pathway in rat liver: mTORC1 required for stimulation of lipogenesis, but not inhibition of gluconeogenesis. Proc Natl Acad Sci U S A. 2010;107(8):3441-6.

118. Jelenik T, Kaul K, Sequaris G, Flogel U, Phielix E, Kotzka J, et al. Mechanisms of Insulin Resistance in Primary and Secondary Nonalcoholic Fatty Liver. Diabetes. 2017;66(8):2241-53.

119. Brown MS, Goldstein JL. Selective versus total insulin resistance: a pathogenic paradox. Cell Metab. 2008;7(2):95-6.

120. Czech MP. Insulin action and resistance in obesity and type 2 diabetes. Nat Med. 2017;23(7):804-14.

121. Avignon A, Yamada K, Zhou X, Spencer B, Cardona O, Saba-Siddique S, et al. Chronic activation of protein kinase C in soleus muscles and other tissues of insulin-resistant type II diabetic Goto-Kakizaki (GK), obese/aged, and obese/Zucker rats. A mechanism for inhibiting glycogen synthesis. Diabetes. 1996;45(10):1396-404.

122. Considine RV, Nyce MR, Allen LE, Morales LM, Triester S, Serrano J, et al. Protein kinase C is increased in the liver of humans and rats with non-insulin-dependent diabetes mellitus: an alteration not due to hyperglycemia. J Clin Invest. 1995;95(6):2938-44.

123. Jornayvaz FR, Shulman GI. Diacylglycerol activation of protein kinase Cepsilon and hepatic insulin resistance. Cell Metab. 2012;15(5):574-84.

124. Bezy O, Tran TT, Pihlajamaki J, Suzuki R, Emanuelli B, Winnay J, et al. PKCdelta regulates hepatic insulin sensitivity and hepatosteatosis in mice and humans. J Clin Invest. 2011;121(6):2504-17.

125. Frangioudakis G, Burchfield JG, Narasimhan S, Cooney GJ, Leitges M, Biden TJ, et al. Diverse roles for protein kinase C delta and protein kinase C epsilon in the generation of high-fat-diet-induced glucose intolerance in mice: regulation of lipogenesis by protein kinase C delta. Diabetologia. 2009;52(12):2616-20.

126. Li Y, Soos TJ, Li X, Wu J, Degennaro M, Sun X, et al. Protein kinase C Theta inhibits insulin signaling by phosphorylating IRS1 at Ser(1101). J Biol Chem. 2004;279(44):45304-7.

127. Agoulnik IU, Hodgson MC, Bowden WA, Ittmann MM. INPP4B: the new kid on the PI3K block. Oncotarget. 2011;2(4):321-8.

128. Norris FA, Atkins RC, Majerus PW. The cDNA cloning and characterization of inositol polyphosphate 4-phosphatase type II. Evidence for conserved alternative splicing in the 4-phosphatase family. J Biol Chem. 1997;272(38):23859-64.

129. Westbrook TF, Martin ES, Schlabach MR, Leng Y, Liang AC, Feng B, et al. A genetic screen for candidate tumor suppressors identifies REST. Cell. 2005;121(6):837-48.

130. Barnache S, Le Scolan E, Kosmider O, Denis N, Moreau-Gachelin F. Phosphatidylinositol 4-phosphatase type II is an erythropoietin-responsive gene. Oncogene. 2006;25(9):1420-3.

131. Hsu I, Yeh CR, Slavin S, Miyamoto H, Netto GJ, Tsai YC, et al. Estrogen receptor alpha prevents bladder cancer via INPP4B inhibited akt pathway in vitro and in vivo. Oncotarget. 2014;5(17):7917-35.

132. Taylor BS, Schultz N, Hieronymus H, Gopalan A, Xiao Y, Carver BS, et al. Integrative genomic profiling of human prostate cancer. Cancer Cell. 2010;18(1):11-22.

133. Beleut M, Rajaram RD, Caikovski M, Ayyanan A, Germano D, Choi Y, et al. Two distinct mechanisms underlie progesterone-induced proliferation in the mammary gland. Proc Natl Acad Sci U S A. 2010;107(7):2989-94.

134. Hodgson MC, Shao LJ, Frolov A, Li R, Peterson LE, Ayala G, et al. Decreased expression and androgen regulation of the tumor suppressor gene INPP4B in prostate cancer. Cancer Res. 2011;71(2):572-82.

135. Li Chew C, Lunardi A, Gulluni F, Ruan DT, Chen M, Salmena L, et al. In Vivo Role of INPP4B in Tumor and Metastasis Suppression through Regulation of PI3K-AKT Signaling at Endosomes. Cancer Discov. 2015;5(7):740-51.

136. Hodgson MC, Deryugina EI, Suarez E, Lopez SM, Lin D, Xue H, et al. INPP4B suppresses prostate cancer cell invasion. Cell Commun Signal. 2014;12(1):61.

137. Chen M, Nowak DG, Trotman LC. Molecular pathways: PI3K pathway phosphatases as biomarkers for cancer prognosis and therapy. Clin Cancer Res. 2014;20(12):3057-63.

138. Newton AC. Regulation of the ABC kinases by phosphorylation : protein kinase C as a paradigm. Biochemical Journal. 2003;370(8):11.

139. Creba JA, Downes CP, Hawkins PT, Brewster G, Michell RH, Kirk CJ. Rapid breakdown of phosphatidylinositol 4-phosphate and phosphatidylinositol 4,5-bisphosphate in rat hepatocytes stimulated by vasopressin and other Ca2+-mobilizing hormones. Biochemical Journal. 1983;212(3):15.

140. Cornford P, Evans J, Dodson A, Parsons K, Woolfenden A, Neoptolemos J, et al. Protein Kinase C Isoenzyme Patterns Characteristically Modulated in Early Prostate Cancer. The American Journal of Pathology. 1999;154(1):137-44.

141. Konopatskaya O, Poole AW. Protein kinase Calpha: disease regulator and therapeutic target. Trends Pharmacol Sci. 2010;31(1):8-14.

142. Kim KM, Kang DW, Moon WS, Park JB, Park CK, Sohn JH, et al. PKCtheta expression in gastrointestinal stromal tumor. Mod Pathol. 2006;19(11):1480-6.

143. Carver BS, Chapinski C, Wongvipat J, Hieronymus H, Chen Y, Chandarlapaty S, et al. Reciprocal feedback regulation of PI3K and androgen receptor signaling in PTEN-deficient prostate cancer. Cancer Cell. 2011;19(5):575-86.

144. Ponguta LA, Gregory CW, French FS, Wilson EM. Site-specific androgen receptor serine phosphorylation linked to epidermal growth factor-dependent growth of castration-recurrent prostate cancer. J Biol Chem. 2008;283(30):20989-1001.

145. Benavides F, Blando J, Perez CJ, Garg R, Conti CJ, DiGiovanni J, et al. Transgenic overexpression of PKCepsilon in the mouse prostate induces preneoplastic lesions. Cell Cycle. 2011;10(2):268-77.

146. Hafeez BB, Zhong W, Weichert J, Dreckschmidt NE, Jamal MS, Verma AK. Genetic ablation of PKC epsilon inhibits prostate cancer development and metastasis in transgenic mouse model of prostate adenocarcinoma. Cancer Res. 2011;71(6):2318-27.

147. Saporita AJ, Zhang Q, Navai N, Dincer Z, Hahn J, Cai X, et al. Identification and characterization of a ligand-regulated nuclear export signal in androgen receptor. J Biol Chem. 2003;278(43):41998-2005.

148. Lopez SM, Agoulnik AI, Zhang M, Peterson LE, Suarez E, Gandarillas GA, et al. Nuclear Receptor Corepressor 1 expression and output declines with prostate cancer progression. Clin Cancer Res. 2016.

149. Guo Z, Yang X, Sun F, Jiang R, Linn DE, Chen H, et al. A novel androgen receptor splice variant is up-regulated during prostate cancer progression and promotes androgen depletion-resistant growth. Cancer Res. 2009;69(6):2305-13.

150. Hu R, Lu C, Mostaghel EA, Yegnasubramanian S, Gurel M, Tannahill C, et al. Distinct transcriptional programs mediated by the ligand-dependent full-length androgen receptor and its splice variants in castration-resistant prostate cancer. Cancer Res. 2012;72(14):3457-62.

151. Krause WC, Shafi AA, Nakka M, Weigel NL. Androgen receptor and its splice variant, AR-V7, differentially regulate FOXA1 sensitive genes in LNCaP prostate cancer cells. Int J Biochem Cell Biol. 2014;54:49-59.

152. Benesh EC, Humphrey PA, Wang Q, Moley KH. Maternal high-fat diet induces hyperproliferation and alters Pten/Akt signaling in prostates of offspring. Sci Rep. 2013;3:3466.

153. Shankar E, Vykhovanets EV, Vykhovanets OV, Maclennan GT, Singh R, Bhaskaran N, et al. High-fat diet activates pro-inflammatory response in the prostate through association of Stat-3 and NF-kappaB. Prostate. 2012;72(3):233-43.

154. Wang XD, Wang BE, Soriano R, Zha J, Zhang Z, Modrusan Z, et al. Expression profiling of the mouse prostate after castration and hormone replacement: implication of H-cadherin in prostate tumorigenesis. Differentiation. 2007;75(3):219-34.

155. Hodgson MC, Bowden WA, Agoulnik IU. Androgen receptor footprint on the way to prostate cancer progression. World J Urol. 2012;30(3):279-85.

156. Mulholland DJ, Tran LM, Li Y, Cai H, Morim A, Wang S, et al. Cell autonomous role of PTEN in regulating castration-resistant prostate cancer growth. Cancer Cell. 2011;19(6):792-804.

157. Chen Y, Chi P, Rockowitz S, Iaquinta PJ, Shamu T, Shukla S, et al. ETS factors reprogram the androgen receptor cistrome and prime prostate tumorigenesis in response to PTEN loss. Nat Med. 2013;19(8):1023-9.

158. Agoulnik IU, Vaid A, Bingman WE, 3rd, Erdeme H, Frolov A, Smith CL, et al. Role of SRC-1 in the promotion of prostate cancer cell growth and tumor progression. Cancer Res. 2005;65(17):7959-67.

159. Sun S, Sprenger CC, Vessella RL, Haugk K, Soriano K, Mostaghel EA, et al. Castration resistance in human prostate cancer is conferred by a frequently occurring androgen receptor splice variant. J Clin Invest. 2010;120(8):2715-30.

160. Shafi AA, Putluri V, Arnold JM, Tsouko E, Maity S, Roberts JM, et al. Differential regulation of metabolic pathways by androgen receptor (AR) and its constitutively active splice variant, AR-V7, in prostate cancer cells. Oncotarget. 2015;6(31):31997-2012.

161. Jenster G, Trapman J, Brinkmann AO. Nuclear import of the human androgen receptor. Biochem J. 1993;293 (Pt 3):761-8.

162. Kooijman EE, King KE, Gangoda M, Gericke A. Ionization properties of phosphatidylinositol polyphosphates in mixed model membranes. Biochemistry. 2009;48(40):9360-71.

163. Kim J, Choi YL, Vallentin A, Hunrichs BS, Hellerstein MK, Peehl DM, et al. Centrosomal PKCbetaII and pericentrin are critical for human prostate cancer growth and angiogenesis. Cancer Res. 2008;68(16):6831-9.

164. Patek S, Willder J, Heng J, Taylor B, Horgan P, Leung H, et al. Androgen receptor phosphorylation status at serine 578 predicts poor outcome in prostate cancer patients. Oncotarget. 2017;8(3):4875-87.

165. Gavrielides MV, Gonzalez-Guerrico AM, Riobo NA, Kazanietz MG. Androgens regulate protein kinase Cdelta transcription and modulate its apoptotic function in prostate cancer cells. Cancer Res. 2006;66(24):11792-801.

166. Henttu P, Vihko aP. The Protein Kinase C Activator, Phorbol Ester, Elicits Disparate Functional Responses in Androgen-Sensitive and Androgen-Independent Human Prostatic Cancer Cells Biochemical and Biophysical Research Communications. 1998;224(1):5.

167. Wu D, Foreman TL, Gregory CW, McJilton MA, Wescott GG, Ford OH, et al. Protein Kinase Cε Has the Potential to Advance the Recurrence of Human Prostate Cancer. Cancer Research. 2002;62(8):7.

168. Mahajan K, Coppola D, Challa S, Fang B, Chen YA, Zhu W, et al. Ack1 mediated AKT/PKB tyrosine 176 phosphorylation regulates its activation. PLoS One. 2010;5(3):e9646.

169. Warde P, Mason M, Ding K, Kirkbride P, Brundage M, Cowan R, et al. Combined androgen deprivation therapy and radiation therapy for locally advanced prostate cancer: a randomised, phase 3 trial. Lancet. 2011;378(9809):2104-11.

170. Subramanian A, Tamayo P, Mootha VK, Mukherjee S, Ebert BL, Gillette MA, et al. Gene set enrichment analysis: a knowledge-based approach for interpreting genome-wide expression profiles. Proc Natl Acad Sci U S A. 2005;102(43):15545-50.

171. Hieronymus H, Lamb J, Ross KN, Peng XP, Clement C, Rodina A, et al. Gene expression signature-based chemical genomic prediction identifies a novel class of HSP90 pathway modulators. Cancer Cell. 2006;10(4):321-30.

172. Nelson PS, Clegg N, Arnold H, Ferguson C, Bonham M, White J, et al. The program of androgen-responsive genes in neoplastic prostate epithelium. Proceedings of the National Academy of Sciences of the United States of America. 2002;99(18):11890-5.

173. Cancer Genome Atlas Research N. The Molecular Taxonomy of Primary Prostate Cancer. Cell. 2015;163(4):1011-25.

174. Collaborators GBDD. Health effects of dietary risks in 195 countries, 1990-2017: a systematic analysis for the Global Burden of Disease Study 2017. Lancet. 2019;393(10184):1958-72.

175. Wildman RP, Muntner P, Reynolds K, McGinn AP, Rajpathak S, Wylie-Rosett J, et al. The obese without cardiometabolic risk factor clustering and the normal weight with cardiometabolic risk factor clustering: prevalence and correlates of 2 phenotypes among the US population (NHANES 1999-2004). Arch Intern Med. 2008;168(15):1617-24.

176. Quail DF, Dannenberg AJ. The obese adipose tissue microenvironment in cancer development and progression. Nat Rev Endocrinol. 2018.

177. Rohrmann S, Smit E, Giovannucci E, Platz EA. Association between markers of the metabolic syndrome and lower urinary tract symptoms in the Third National Health and Nutrition Examination Survey (NHANES III). Int J Obes (Lond). 2005;29(3):310-6.

178. Cao Y, Ma J. Body mass index, prostate cancer-specific mortality, and biochemical recurrence: a systematic review and meta-analysis. Cancer Prev Res (Phila). 2011;4(4):486-501.

179. Liss MA, Al-Bayati O, Gelfond J, Goros M, Ullevig S, DiGiovanni J, et al. Higher baseline dietary fat and fatty acid intake is associated with increased risk of incident prostate cancer in the SABOR study. Prostate Cancer Prostatic Dis. 2018.

180. Fabbrini E, Magkos F, Mohammed BS, Pietka T, Abumrad NA, Patterson BW, et al. Intrahepatic fat, not visceral fat, is linked with metabolic complications of obesity. Proc Natl Acad Sci U S A. 2009;106(36):15430-5.

181. Feldman A, Eder SK, Felder TK, Kedenko L, Paulweber B, Stadlmayr A, et al. Clinical and Metabolic Characterization of Lean Caucasian Subjects With Non-alcoholic Fatty Liver. Am J Gastroenterol. 2017;112(1):102-10.

182. Samuel VT, Shulman GI. The pathogenesis of insulin resistance: integrating signaling pathways and substrate flux. J Clin Invest. 2016;126(1):12-22.

183. Kumashiro N, Erion DM, Zhang D, Kahn M, Beddow SA, Chu X, et al. Cellular mechanism of insulin resistance in nonalcoholic fatty liver disease. Proc Natl Acad Sci U S A. 2011;108(39):16381-5.

184. Perry RJ, Samuel VT, Petersen KF, Shulman GI. The role of hepatic lipids in hepatic insulin resistance and type 2 diabetes. Nature. 2014;510(7503):84-91.

185. Vegiopoulos A, Rohm M, Herzig S. Adipose tissue: between the extremes. EMBO J. 2017;36(14):1999-2017.

186. Jiang F, Li S, Pan L, Jia C. Association of the G1057D polymorphism in insulin receptor substrate 2 gene with type 2 diabetes mellitus: a meta-analysis. J Diabetes Complications. 2015;29(5):731-6.

187. Ristow M, Muller-Wieland D, Pfeiffer A, Krone W, Kahn CR. Obesity associated with a mutation in a genetic regulator of adipocyte differentiation. N Engl J Med. 1998;339(14):953-9.

188. Vasseur F, Meyre D, Froguel P. Adiponectin, type 2 diabetes and the metabolic syndrome: lessons from human genetic studies. Expert Rev Mol Med. 2006;8(27):1-12.

189. Yang MM, Wang J, Fan JJ, Ng TK, Sun DJ, Guo X, et al. Variations in the Obesity Gene "LEPR" Contribute to Risk of Type 2 Diabetes Mellitus: Evidence from a Meta-Analysis. J Diabetes Res. 2016;2016:5412084.

190. Stern JH, Rutkowski JM, Scherer PE. Adiponectin, Leptin, and Fatty Acids in the Maintenance of Metabolic Homeostasis through Adipose Tissue Crosstalk. Cell Metab. 2016;23(5):770-84.

191. Fasshauer M, Bluher M. Adipokines in health and disease. Trends Pharmacol Sci. 2015;36(7):461-70.

192. Gupta RK. Adipocytes. Curr Biol. 2014;24(20):R988-93.

193. Fantuzzi G. Adipose tissue, adipokines, and inflammation. J Allergy Clin Immunol. 2005;115(5):911-9; quiz 20.

194. Sartipy P, Loskutoff DJ. Monocyte chemoattractant protein 1 in obesity and insulin resistance. Proc Natl Acad Sci U S A. 2003;100(12):7265-70.

195. Amano SU, Cohen JL, Vangala P, Tencerova M, Nicoloro SM, Yawe JC, et al. Local proliferation of macrophages contributes to obesity-associated adipose tissue inflammation. Cell Metab. 2014;19(1):162-71.

196. Mu JL, Naggert JK, Svenson KL, Collin GB, Kim JH, McFarland C, et al. Quantitative trait loci analysis for the differences in susceptibility to atherosclerosis and diabetes between inbred mouse strains C57BL/6J and C57BLKS/J. J Lipid Res. 1999;40(7):1328-35.

197. Scherer PE. Adipose tissue: from lipid storage compartment to endocrine organ. Diabetes. 2006;55(6):1537-45.

198. Kim JY, van de Wall E, Laplante M, Azzara A, Trujillo ME, Hofmann SM, et al. Obesity-associated improvements in metabolic profile through expansion of adipose tissue. J Clin Invest. 2007;117(9):2621-37.

199. Clee SM, Attie AD. The genetic landscape of type 2 diabetes in mice. Endocr Rev. 2007;28(1):48-83.

200. Pihlajamaki J, Boes T, Kim EY, Dearie F, Kim BW, Schroeder J, et al. Thyroid hormone-related regulation of gene expression in human fatty liver. J Clin Endocrinol Metab. 2009;94(9):3521-9.

201. Rehfeld JF. Cholecystokinin-From Local Gut Hormone to Ubiquitous Messenger. Front Endocrinol (Lausanne). 2017;8:47.

202. Liang W, Menke AL, Driessen A, Koek GH, Lindeman JH, Stoop R, et al. Establishment of a general NAFLD scoring system for rodent models and comparison to human liver pathology. PLoS One. 2014;9(12):e115922.

203. Tang W, Yang L, Yang T, Liu M, Zhou Y, Lin J, et al. INPP4B inhibits cell proliferation, invasion and chemoresistance in human hepatocellular carcinoma. Onco Targets Ther. 2019;12:3491-507.

204. Suppli MP, Rigbolt KTG, Veidal SS, Heeboll S, Eriksen PL, Demant M, et al. Hepatic transcriptome signatures in patients with varying degrees of nonalcoholic fatty liver disease compared with healthy normal-weight individuals. Am J Physiol Gastrointest Liver Physiol. 2019;316(4):G462-G72.

205. Evans RM, Barish GD, Wang YX. PPARs and the complex journey to obesity. Nat Med. 2004;10(4):355-61.

206. Vamecq J, Latruffe N. Medical significance of peroxisome proliferator-activated receptors. Lancet. 1999;354(9173):141-8.

207. Chikada H, Ida K, Ando E, Inagaki Y, Sakamoto A, Kamiya A. Establishment and analysis of a mouse model that regulates sex-related differences in liver drug metabolism. Lab Invest. 2018;98(11):1500-11.

208. Greenawalt DM, Dobrin R, Chudin E, Hatoum IJ, Suver C, Beaulaurier J, et al. A survey of the genetics of stomach, liver, and adipose gene expression from a morbidly obese cohort. Genome Res. 2011;21(7):1008-16.

209. Kim JB, Spiegelman BM. ADD1/SREBP1 promotes adipocyte differentiation and gene expression linked to fatty acid metabolism. Genes Dev. 1996;10(9):1096-107.

210. Horton JD, Goldstein JL, Brown MS. SREBPs: activators of the complete program of cholesterol and fatty acid synthesis in the liver. J Clin Invest. 2002;109(9):1125-31.

211. Shimano H, Sato R. SREBP-regulated lipid metabolism: convergent physiology - divergent pathophysiology. Nat Rev Endocrinol. 2017;13(12):710-30.

212. Sajan MP, Standaert ML, Nimal S, Varanasi U, Pastoor T, Mastorides S, et al. The critical role of atypical protein kinase C in activating hepatic SREBP-1c and NFkappaB in obesity. J Lipid Res. 2009;50(6):1133-45.

213. Gucalp A, Iyengar NM, Zhou XK, Giri DD, Falcone DJ, Wang H, et al. Periprostatic adipose inflammation is associated with high-grade prostate cancer. Prostate Cancer Prostatic Dis. 2017;20(4):418-23.

214. Rhee H, Vela I, Chung E. Metabolic Syndrome and Prostate Cancer: a Review of Complex Interplay Amongst Various Endocrine Factors in the Pathophysiology and Progression of Prostate Cancer. Horm Cancer. 2016;7(2):75-83.

215. Nelson WG, De Marzo AM, Isaacs WB. Prostate cancer. N Engl J Med. 2003;349(4):366-81.

216. De Marzo AM, Platz EA, Sutcliffe S, Xu J, Gronberg H, Drake CG, et al. Inflammation in prostate carcinogenesis. Nat Rev Cancer. 2007;7(4):256-69.

217. Shappell SB, Thomas GV, Roberts RL, Herbert R, Ittmann MM, Rubin MA, et al. Prostate pathology of genetically engineered mice: definitions and classification. The consensus report from the Bar Harbor meeting of the Mouse Models of Human Cancer Consortium Prostate Pathology Committee. Cancer Res. 2004;64(6):2270-305.

218. Dib LH, Ortega MT, Fleming SD, Chapes SK, Melgarejo T. Bone marrow leptin signaling mediates obesity-associated adipose tissue inflammation in male mice. Endocrinology. 2014;155(1):40-6.

219. Sfanos KS, De Marzo AM. Prostate cancer and inflammation: the evidence. Histopathology. 2012;60(1):199-215.

220. Zhu P, Baek SH, Bourk EM, Ohgi KA, Garcia-Bassets I, Sanjo H, et al. Macrophage/cancer cell interactions mediate hormone resistance by a nuclear receptor derepression pathway. Cell. 2006;124(3):615-29.

221. Nguyen DP, Li J, Tewari AK. Inflammation and prostate cancer: the role of interleukin 6 (IL-6). BJU Int. 2014;113(6):986-92.

222. Liu Q, Russell MR, Shahriari K, Jernigan DL, Lioni MI, Garcia FU, et al. Interleukin-1beta promotes skeletal colonization and progression of metastatic prostate cancer cells with neuroendocrine features. Cancer Res. 2013;73(11):3297-305.

223. Andrikopoulos S, Blair AR, Deluca N, Fam BC, Proietto J. Evaluating the glucose tolerance test in mice. Am J Physiol Endocrinol Metab. 2008;295(6):E1323-32.

224. Kim D, Langmead B, Salzberg SL. HISAT: a fast spliced aligner with low memory requirements. Nat Methods. 2015;12(4):357-60.

225. Dobin A, Gingeras TR. Mapping RNA-seq Reads with STAR. Curr Protoc Bioinformatics. 2015;51:11 4 1-9.

226. Anders S, Pyl PT, Huber W. HTSeq--a Python framework to work with high-throughput sequencing data. Bioinformatics. 2015;31(2):166-9.

227. Love MI, Huber W, Anders S. Moderated estimation of fold change and dispersion for RNA-seq data with DESeq2. Genome Biol. 2014;15(12):550.

228. Brisken C, O'Malley B. Hormone action in the mammary gland. Cold Spring Harb Perspect Biol. 2010;2(12):a003178.

229. Clarke RB, Howell A, Potten CS, Anderson E. Dissociation between steroid receptor expression and cell proliferation in the human breast. Cancer Res. 1997;57(22):4987-91.

230. Suzuki R, Orsini N, Saji S, Key TJ, Wolk A. Body weight and incidence of breast cancer defined by estrogen and progesterone receptor status--a meta-analysis. Int J Cancer. 2009;124(3):698-712.

231. Bhaskaran K, Douglas I, Forbes H, dos-Santos-Silva I, Leon DA, Smeeth L. Body-mass index and risk of 22 specific cancers: a population-based cohort study of 5.24 million UK adults. Lancet. 2014;384(9945):755-65.

232. Chan DS, Vieira AR, Aune D, Bandera EV, Greenwood DC, McTiernan A, et al. Body mass index and survival in women with breast cancer-systematic literature review and meta-analysis of 82 follow-up studies. Ann Oncol. 2014;25(10):1901-14.

233. Emaus A, Veierod MB, Tretli S, Finstad SE, Selmer R, Furberg AS, et al. Metabolic profile, physical activity, and mortality in breast cancer patients. Breast Cancer Res Treat. 2010;121(3):651-60.

234. Picon-Ruiz M, Morata-Tarifa C, Valle-Goffin JJ, Friedman ER, Slingerland JM. Obesity and adverse breast cancer risk and outcome: Mechanistic insights and strategies for intervention. CA Cancer J Clin. 2017;67(5):378-97.

235. Arce-Salinas C, Aguilar-Ponce JL, Villarreal-Garza C, Lara-Medina FU, Olvera-Caraza D, Alvarado Miranda A, et al. Overweight and obesity as poor prognostic factors in locally advanced breast cancer patients. Breast Cancer Res Treat. 2014;146(1):183-8.

236. Riant E, Waget A, Cogo H, Arnal JF, Burcelin R, Gourdy P. Estrogens protect against high-fat diet-induced insulin resistance and glucose intolerance in mice. Endocrinology. 2009;150(5):2109-17.

237. Wallen WJ, Belanger MP, Wittnich C. Sex hormones and the selective estrogen receptor modulator tamoxifen modulate weekly body weights and food intakes in adolescent and adult rats. J Nutr. 2001;131(9):2351-7.

238. Cho H, Mu J, Kim JK, Thorvaldsen JL, Chu Q, Crenshaw EB, 3rd, et al. Insulin resistance and a diabetes mellitus-like syndrome in mice lacking the protein kinase Akt2 (PKB beta). Science. 2001;292(5522):1728-31.

239. Taniguchi CM, Kondo T, Sajan M, Luo J, Bronson R, Asano T, et al. Divergent regulation of hepatic glucose and lipid metabolism by phosphoinositide 3-kinase via Akt and PKClambda/zeta. Cell Metab. 2006;3(5):343-53.

240. Macias H, Hinck L. Mammary gland development. Wiley Interdiscip Rev Dev Biol. 2012;1(4):533-57.

241. Lai TC, Chou HC, Chen YW, Lee TR, Chan HT, Shen HH, et al. Secretomic and proteomic analysis of potential breast cancer markers by two-dimensional differential gel electrophoresis. J Proteome Res. 2010;9(3):1302-22.

242. Menon R, Roy A, Mukherjee S, Belkin S, Zhang Y, Omenn GS. Functional implications of structural predictions for alternative splice proteins expressed in Her2/neu-induced breast cancers. J Proteome Res. 2011;10(12):5503-11.

243. Conneely OM, Jericevic BM, Lydon JP. Progesterone receptors in mammary gland development and tumorigenesis. J Mammary Gland Biol Neoplasia. 2003;8(2):205-14.

244. Silberstein GB, Van Horn K, Hrabeta-Robinson E, Compton J. Estrogen-triggered delays in mammary gland gene expression during the estrous cycle: evidence for a novel timing system. J Endocrinol. 2006;190(2):225-39.

245. McLean AC, Valenzuela N, Fai S, Bennett SA. Performing vaginal lavage, crystal violet staining, and vaginal cytological evaluation for mouse estrous cycle staging identification. J Vis Exp. 2012(67):e4389.

246. Mallepell S, Krust A, Chambon P, Brisken C. Paracrine signaling through the epithelial estrogen receptor alpha is required for proliferation and morphogenesis in the mammary gland. Proc Natl Acad Sci U S A. 2006;103(7):2196-201.

247. Obr AE, Grimm SL, Bishop KA, Pike JW, Lydon JP, Edwards DP. Progesterone receptor and Stat5 signaling cross talk through RANKL in mammary epithelial cells. Mol Endocrinol. 2013;27(11):1808-24.

248. Ciarloni L, Mallepell S, Brisken C. Amphiregulin is an essential mediator of estrogen receptor alpha function in mammary gland development. Proc Natl Acad Sci U S A. 2007;104(13):5455-60.

249. Kahn BB, Flier JS. Obesity and insulin resistance. J Clin Invest. 2000;106(4):473-81.

250. Luhr I, Friedl A, Overath T, Tholey A, Kunze T, Hilpert F, et al. Mammary fibroblasts regulate morphogenesis of normal and tumorigenic breast epithelial cells by mechanical and paracrine signals. Cancer Lett. 2012;325(2):175-88.

251. Albertson DG, Ylstra B, Segraves R, Collins C, Dairkee SH, Kowbel D, et al. Quantitative mapping of amplicon structure by array CGH identifies CYP24 as a candidate oncogene. Nat Genet. 2000;25(2):144-6.

252. Gronemeyer H. Transcription activation by estrogen and progesterone receptors. Annu Rev Genet. 1991;25:89-123.

253. Mulac-Jericevic B, Mullinax RA, DeMayo FJ, Lydon JP, Conneely OM. Subgroup of reproductive functions of progesterone mediated by progesterone receptor-B isoform. Science. 2000;289(5485):1751-4.

254. Mulac-Jericevic B, Lydon JP, DeMayo FJ, Conneely OM. Defective mammary gland morphogenesis in mice lacking the progesterone receptor B isoform. Proc Natl Acad Sci U S A. 2003;100(17):9744-9.

255. Carroll JS, Hickey TE, Tarulli GA, Williams M, Tilley WD. Deciphering the divergent roles of progestogens in breast cancer. Nat Rev Cancer. 2017;17(1):54-64.

256. Brisken C, Heineman A, Chavarria T, Elenbaas B, Tan J, Dey SK, et al. Essential function of Wnt-4 in mammary gland development downstream of progesterone signaling. Genes Dev. 2000;14(6):650-4.

257. Fernandez-Valdivia R, Mukherjee A, Ying Y, Li J, Paquet M, DeMayo FJ, et al. The RANKL signaling axis is sufficient to elicit ductal side-branching and alveologenesis in the mammary gland of the virgin mouse. Dev Biol. 2009;328(1):127-39.

258. Huang X, Liu G, Guo J, Su Z. The PI3K/AKT pathway in obesity and type 2 diabetes. Int J Biol Sci. 2018;14(11):1483-96.

259. Itani SI, Ruderman NB, Schmieder F, Boden G. Lipid-induced insulin resistance in human muscle is associated with changes in diacylglycerol, protein kinase C, and IkappaB-alpha. Diabetes. 2002;51(7):2005-11.

260. Wright LE, Brandon AE, Hoy AJ, Forsberg GB, Lelliott CJ, Reznick J, et al. Amelioration of lipid-induced insulin resistance in rat skeletal muscle by overexpression of Pgc-1beta involves reductions in long-chain acyl-CoA levels and oxidative stress. Diabetologia. 2011;54(6):1417-26.

261. Patel P, Abate N. Body fat distribution and insulin resistance. Nutrients. 2013;5(6):2019-27.

262. Bechmann LP, Hannivoort RA, Gerken G, Hotamisligil GS, Trauner M, Canbay A. The interaction of hepatic lipid and glucose metabolism in liver diseases. J Hepatol. 2012;56(4):952-64.

263. Cecchini RS, Costantino JP, Cauley JA, Cronin WM, Wickerham DL, Land SR, et al. Body mass index and the risk for developing invasive breast cancer among high-risk women in NSABP P-1 and STAR breast cancer prevention trials. Cancer Prev Res (Phila). 2012;5(4):583-92.

264. Anderson GL, Neuhouser ML. Obesity and the risk for premenopausal and postmenopausal breast cancer. Cancer Prev Res (Phila). 2012;5(4):515-21.

265. Ghajar CM, Bissell MJ. Extracellular matrix control of mammary gland morphogenesis and tumorigenesis: insights from imaging. Histochem Cell Biol. 2008;130(6):1105-18.

266. Seo BR, Bhardwaj P, Choi S, Gonzalez J, Andresen Eguiluz RC, Wang K, et al. Obesity-dependent changes in interstitial ECM mechanics promote breast tumorigenesis. Sci Transl Med. 2015;7(301):301ra130.

267. Zhang M, Suarez E, Vasquez JL, Nathanson L, Peterson LE, Rajapakshe K, et al. Inositol polyphosphate 4-phosphatase type II regulation of androgen receptor activity. Oncogene. 2019;38(7):1121-35.

268. Lopez SM, Agoulnik AI, Zhang M, Peterson LE, Suarez E, Gandarillas GA, et al. Nuclear Receptor Corepressor 1 Expression and Output Declines with Prostate Cancer Progression. Clin Cancer Res. 2016;22(15):3937-49.

269. Zhang M, Krause WC, Agoulnik IU. Techniques for Evaluation of AR Transcriptional Output and Recruitment to DNA. Methods Mol Biol. 2018;1786:219-36.

270. Varambally S, Dhanasekaran SM, Zhou M, Barrette TR, Kumar-Sinha C, Sanda MG, et al. The polycomb group protein EZH2 is involved in progression of prostate cancer. Nature. 2002;419(6907):624-9.

271. Bracken AP, Pasini D, Capra M, Prosperini E, Colli E, Helin K. EZH2 is downstream of the pRB-E2F pathway, essential for proliferation and amplified in cancer. EMBO J. 2003;22(20):5323-35.

272. De Raedt T, Beert E, Pasmant E, Luscan A, Brems H, Ortonne N, et al. PRC2 loss amplifies Ras-driven transcription and confers sensitivity to BRD4-based therapies. Nature. 2014;514(7521):247-51.

273. Lee W, Teckie S, Wiesner T, Ran L, Prieto Granada CN, Lin M, et al. PRC2 is recurrently inactivated through EED or SUZ12 loss in malignant peripheral nerve sheath tumors. Nat Genet. 2014;46(11):1227-32.

274. Saad F, Shore N, Zhang T, Sharma S, Cho HK, Jacobs IA. Emerging therapeutic targets for patients with advanced prostate cancer. Cancer Treat Rev. 2019;76:1-9.

275. Yamagishi M, Uchimaru K. Targeting EZH2 in cancer therapy. Curr Opin Oncol. 2017;29(5):375-81.

276. Kanarek N, Keys HR, Cantor JR, Lewis CA, Chan SH, Kunchok T, et al. Histidine catabolism is a major determinant of methotrexate sensitivity. Nature. 2018;559(7715):632-6.

277. Kori M, Aydin B, Unal S, Arga KY, Kazan D. Metabolic Biomarkers and Neurodegeneration: A Pathway Enrichment Analysis of Alzheimer's Disease, Parkinson's Disease, and Amyotrophic Lateral Sclerosis. OMICS. 2016;20(11):645-61.

APPENDIX

Buffers used in ChIP assay

SDS Lysis Buffer (100 ml)

10 ml 10% SDS

2 ml 0.5 M EDTA pH 8.1

5 ml 1 M Tris-HCl pH 8.1

Bring to 100 ml with water

ChIP Dilution Buffer (500 ml)

27.5 ml 10% Triton X-100

1.2 ml 0.5 M EDTA pH 8.1

8.4 ml 1 M Tris-HCl pH 8.1

16.7 ml 5 M NaCl

Bring to 500 ml with water

Low Salt Immune Complex Wash Buffer (500 ml)

5 ml 10% SDS

50 ml 10% Triton X-100

2 ml 0.5 M EDTA pH 8.1

10 ml 1 M Tris-HCl pH 8.1

15 ml 5 M NaCl

Bring to 500 ml with water

Elution Buffer (10 ml) is made fresh the day of use.

1 ml 10% SDS

1 ml 1 M $NaHCO_3$

8 ml water

TE Buffer (500 ml)

5 ml 1 M Tris pH 8.1

1 ml 0.5 M EDTA pH 8.1

Bring to 500 ml with water

High Salt Immune Complex Wash Buffer

Add 1.02 g NaCl to 50 ml of Low Salt Immune Complex Wash Buffer

KEGG pathways significantly affect by *Inpp4b* knockout

KEGG pathway analysis				
INPP4B KNOCKOUT compared to WT	ES	NES	NOM p-val	FDR q-val
KEGG_PARKINSONS_DISEASE	0.55	2.00	0.00	0.00
KEGG_HISTIDINE_METABOLISM	0.64	1.96	0.00	0.00
KEGG_FATTY_ACID_METABOLISM	0.59	1.92	0.00	0.00
KEGG_OXIDATIVE_PHOSPHORYLATION	0.53	1.92	0.00	0.00
KEGG_ALZHEIMERS_DISEASE	0.50	1.88	0.00	0.00
KEGG_TRYPTOPHAN_METABOLISM	0.58	1.84	0.00	0.00
KEGG_PROPANOATE_METABOLISM	0.58	1.84	0.00	0.00
KEGG_VALINE_LEUCINE_AND_ISOLEUCINE_DEGRADATION	0.55	1.83	0.00	0.00
KEGG_PEROXISOME	0.50	1.79	0.00	0.01
KEGG_GALACTOSE_METABOLISM	0.57	1.76	0.00	0.01
KEGG_BUTANOATE_METABOLISM	0.56	1.76	0.00	0.01
KEGG_PYRUVATE_METABOLISM	0.55	1.75	0.00	0.01
KEGG_BETA_ALANINE_METABOLISM	0.58	1.73	0.00	0.01
KEGG_HUNTINGTONS_DISEASE	0.46	1.71	0.00	0.01
KEGG_RETINOL_METABOLISM	0.54	1.70	0.00	0.01
KEGG_ETHER_LIPID_METABOLISM	0.59	1.69	0.01	0.01
KEGG_BIOSYNTHESIS_OF_UNSATURATED_FATTY_ACIDS	0.57	1.64	0.01	0.02
KEGG_ARGININE_AND_PROLINE_METABOLISM	0.49	1.63	0.00	0.03
KEGG_PENTOSE_PHOSPHATE_PATHWAY	0.54	1.60	0.01	0.03
KEGG_NITROGEN_METABOLISM	0.55	1.59	0.02	0.03
KEGG_LYSINE_DEGRADATION	0.48	1.58	0.00	0.04
KEGG_GLYCOLYSIS_GLUCONEOGENESIS	0.46	1.57	0.01	0.04
KEGG_CARDIAC_MUSCLE_CONTRACTION	0.46	1.56	0.00	0.04

KEGG_DRUG_METABOLISM_CYTOCHROME_P450	0.46	1.53	0.01	0.06
KEGG_PPAR_SIGNALING_PATHWAY	0.44	1.53	0.00	0.05
KEGG_PROXIMAL_TUBULE_BICARBONATE_RECLAMATION	0.53	1.52	0.03	0.06
KEGG_GLYCOSYLPHOSPHATIDYLINOSITOL_GPI_ANCHOR_BIOSYNTHESIS	0.48	1.51	0.02	0.07
KEGG_GLYCEROLIPID_METABOLISM	0.46	1.49	0.02	0.08
KEGG_GLYCEROPHOSPHOLIPID_METABOLISM	0.43	1.48	0.01	0.08

GO biological functions significantly affected by *Inpp4b* knockdown

GO enrichment analysis				
INPP4B KNOCKOUT compared to WT	NES	NOM p-val	FDR q-val	FWER p-val
GO_OXIDATIVE_PHOSPHORYLATION	2.26	0.00	0.00	0.00
GO_RESPIRATORY_CHAIN	2.19	0.00	0.00	0.00
GO_ELECTRON_TRANSPORT_CHAIN	2.17	0.00	0.00	0.00
GO_INNER_MITOCHONDRIAL_MEMBRANE_PROTEIN_COMPLEX	2.16	0.00	0.00	0.00
GO_NADH_DEHYDROGENASE_COMPLEX	2.11	0.00	0.00	0.00
GO_MITOCHONDRIAL_RESPIRATORY_CHAIN_COMPLEX_ASSEMBLY	2.10	0.00	0.00	0.01
GO_OXIDOREDUCTASE_ACTIVITY_ACTING_ON_NAD_P_H_QUINONE_OR_SIMILAR_COMPOUND_AS_ACCEPTOR	2.07	0.00	0.00	0.01
GO_MITOCHONDRIAL_RESPIRATORY_CHAIN_COMPLEX_I_BIOGENESIS	2.05	0.00	0.00	0.02
GO_MITOCHONDRIAL_PROTEIN_COMPLEX	2.05	0.00	0.00	0.02
GO_FATTY_ACID_BETA_OXIDATION	1.98	0.00	0.01	0.08
GO_OXIDOREDUCTASE_ACTIVITY_ACTING_ON_THE_CH_OH_GROUP_OF_DONORS_NAD_OR_NADP_AS_ACCEPTOR	1.96	0.00	0.01	0.11
GO_MITOCHONDRIAL_MEMBRANE_PART	1.94	0.00	0.01	0.13
GO_OXIDOREDUCTASE_ACTIVITY_ACTING_ON_CH_OH_GROUP_OF_DONORS	1.94	0.00	0.01	0.13
GO_MONOCARBOXYLIC_ACID_CATABOLIC_PROCESS	1.93	0.00	0.01	0.14
GO_LIPID_OXIDATION	1.93	0.00	0.01	0.16
GO_HYDRO_LYASE_ACTIVITY	1.92	0.00	0.01	0.19
GO_NUCLEOSIDE_TRIPHOSPHATE_METABOLIC_PROCESS	1.90	0.00	0.02	0.25
GO_OXIDOREDUCTASE_COMPLEX	1.84	0.00	0.04	0.54
GO_CARBON_OXYGEN_LYASE_ACTIVITY	1.83	0.00	0.04	0.55
GO_ELECTRON_CARRIER_ACTIVITY	1.83	0.00	0.05	0.60
GO_MITOCHONDRIAL_ATP_SYNTHESIS_COUPLED_PROTON_TRANSPORT	1.82	0.00	0.05	0.62
GO_OXIDOREDUCTASE_ACTIVITY_ACTING_ON_NAD_P_H	1.82	0.00	0.04	0.62

GO_CYTOCHROME_COMPLEX	1.82	0.00	0.04	0.64
GO_FATTY_ACID_CATABOLIC_PROCESS	1.82	0.00	0.04	0.64
GO_ORGANIC_ACID_CATABOLIC_PROCESS	1.80	0.00	0.05	0.72
GO_CELLULAR_RESPIRATION	1.80	0.00	0.05	0.73
GO_CHEMOATTRACTANT_ACTIVITY	1.77	0.00	0.08	0.88
GO_ORGANELLAR_SMALL_RIBOSOMAL_SUBUNIT	1.77	0.00	0.08	0.90
GO_ISOPRENOID_BINDING	1.75	0.00	0.09	0.94
GO_SMALL_MOLECULE_CATABOLIC_PROCESS	1.75	0.00	0.09	0.94
GO_ORGANELLE_INNER_MEMBRANE	1.74	0.00	0.10	0.96
GO_PHOSPHATIDYLCHOLINE_BINDING	1.73	0.00	0.11	0.98
GO_FATTY_ACYL_COA_BINDING	1.73	0.00	0.11	0.98
GO_THIOLESTER_HYDROLASE_ACTIVITY	1.72	0.00	0.11	0.99
GO_NUCLEOSIDE_MONOPHOSPHATE_METABOLIC_PROCESS	1.72	0.00	0.12	0.99
GO_PROTON_TRANSPORTING_ATP_SYNTHASE_COMPLEX	1.72	0.00	0.12	0.99
GO_CELLULAR_KETONE_METABOLIC_PROCESS	1.71	0.00	0.12	1.00
GO_REGULATION_OF_CATECHOLAMINE_SECRETION	1.71	0.00	0.12	1.00
GO_NONMOTILE_PRIMARY_CILIUM_ASSEMBLY	1.70	0.00	0.13	1.00
GO_PEROXISOME_ORGANIZATION	1.69	0.00	0.15	1.00
GO_RESPONSE_TO_HYDROPEROXIDE	1.68	0.00	0.15	1.00
GO_POSITIVE_CHEMOTAXIS	1.68	0.00	0.16	1.00
GO_MICROBODY_PART	1.68	0.00	0.16	1.00
GO_FATTY_ACID_BETA_OXIDATION_USING_ACYL_COA_DEHYDROGENASE	1.68	0.00	0.16	1.00
GO_OXIDOREDUCTASE_ACTIVITY_ACTING_ON_THE_CH_CH_GROUP_OF_DONORS	1.68	0.00	0.16	1.00
GO_MICROBODY_LUMEN	1.67	0.00	0.16	1.00
GO_NUCLEOSIDE_TRIPHOSPHATE_BIOSYNTHETIC_PROCESS	1.67	0.00	0.16	1.00

GO_ORGANELLAR_RIBOSOME	1.66	0.00	0.17	1.00
GO_HYDROGEN_TRANSPORT	1.66	0.00	0.17	1.00
GO_GLUTAMATE_METABOLIC_PROCESS	1.66	0.00	0.17	1.00
GO_MICROBODY	1.66	0.00	0.18	1.00
GO_VITAMIN_BINDING	1.65	0.00	0.18	1.00
GO_REGULATION_OF_STEROL_TRANSPORT	1.64	0.00	0.20	1.00
GO_PHOTORECEPTOR_CELL_MAINTENANCE	1.64	0.01	0.19	1.00
GO_COENZYME_BINDING	1.64	0.00	0.19	1.00
GO_NAD_BINDING	1.64	0.00	0.20	1.00
GO_BASE_EXCISION_REPAIR	1.64	0.00	0.20	1.00
GO_GLYCOSYL_COMPOUND_METABOLIC_PROCESS	1.64	0.00	0.20	1.00
GO_OXIDOREDUCTASE_ACTIVITY_ACTING_ON_A_HEME_GROUP_OF_DONORS	1.63	0.01	0.20	1.00
GO_ACYL_COA_DEHYDROGENASE_ACTIVITY	1.63	0.01	0.20	1.00
GO_HYDROGEN_ION_TRANSMEMBRANE_TRANSPORT	1.63	0.00	0.20	1.00
GO_ALDO_KETO_REDUCTASE_NADP_ACTIVITY	1.63	0.01	0.20	1.00
GO_CELLULAR_ALDEHYDE_METABOLIC_PROCESS	1.63	0.00	0.20	1.00
GO_MICROBODY_MEMBRANE	1.63	0.00	0.20	1.00
GO_ENERGY_DERIVATION_BY_OXIDATION_OF_ORGANIC_COMPOUNDS	1.63	0.00	0.20	1.00
GO_CELLULAR_LIPID_CATABOLIC_PROCESS	1.63	0.00	0.20	1.00
GO_POSITIVE_REGULATION_OF_CARBOHYDRATE_METABOLIC_PROCESS	1.62	0.00	0.20	1.00
GO_POSITIVE_REGULATION_OF_INSULIN_SECRETION	1.62	0.00	0.20	1.00
GO_FATTY_ACID_METABOLIC_PROCESS	1.62	0.00	0.20	1.00
GO_LIPID_CATABOLIC_PROCESS	1.62	0.00	0.20	1.00
GO_O_ACYLTRANSFERASE_ACTIVITY	1.61	0.00	0.22	1.00
GO_NUCLEOSIDE_SALVAGE	1.61	0.02	0.22	1.00

GO_ENERGY_COUPLED_PROTON_TRANSPORT_DOWN_ELECTROCHEMICAL_GRADIENT	1.60	0.01	0.23	1.00
GO_MONOSACCHARIDE_CATABOLIC_PROCESS	1.60	0.00	0.24	1.00
GO_SYNAPTIC_VESICLE_ENDOCYTOSIS	1.59	0.02	0.25	1.00
GO_GENERATION_OF_PRECURSOR_METABOLITES_AND_ENERGY	1.59	0.00	0.25	1.00
GO_ALPHA_AMINO_ACID_CATABOLIC_PROCESS	1.59	0.00	0.25	1.00
GO_PRIMARY_ALCOHOL_METABOLIC_PROCESS	1.59	0.01	0.25	1.00
GO_RIBONUCLEOSIDE_TRIPHOSPHATE_BIOSYNTHETIC_PROCESS	1.59	0.01	0.25	1.00
GO_POSITIVE_REGULATION_OF_ANION_TRANSPORT	1.59	0.01	0.24	1.00
GO_NEGATIVE_REGULATION_OF_ANTIGEN_RECEPTOR_MEDIATED_SIGNALING_PATHWAY	1.59	0.01	0.24	1.00

AR signature

TMEM97	CEP170P1	APOBEC3B	MPC1	HMGB2	OIP5
TOP2A	OPRK1	RANBP2	MRS2	DDX39A	PRKAG2
CKS1B	c11orf95	SKAP2	ZNF277	H2AFX	CDC20
bbx	UFL1	TOX3	il6st	GPR63	NREP
ERLIN2	CCNA2	PLCB4	CENPU	SP2	TMEM106B
SMARCD3	TAGLN2	AZGP1	DNAJB6	RDX	AURKB
ZFP36L1	RACGAP1	OPTN	WDFY3	SP3	DPYSL2
UGT2B15	WTH3DI	MIR4640	PPP1R2	ZBTB43	CTBS
AGA	HIST4H4	GINS2	NUMA1	DUSP10	ZSCAN31
LOC81691	GUF1	RLN2	ZWILCH	ATRX	UBE3A
SUPT7L	MIR3658	HTR2C	Hist1h4h	GTF3A	TK1
BUB1	TOR1AIP1	ZCCHC10	MYBL2	PKNOX2	NMU
RASA1	CITED2	NCAPD2	FUBP3	APC	GINS1
SRM	CDCA3	ppp1cb	PBX1	SSBP2	APPBP2
RFC5	FOXO3	NCOA2	ABCG1	RFC3	FKBP5
DAAM1	TRIP13	SUCLG2	IFRD1	MEX3C	DENND1B
FAM179B	PLK2	MFSD6	STX7	UGT2B28	GCC2
PRDX4	cep350	TUBB6	arfip1	PTPRK	ID3
TANK	DTL	ZNF529	MED13	Hist1h2bg	SH3BGRL
USP9Y	RAD51C	ITGB3BP	MCM2	MCTP1	PTTG3P
CHEK2	TMCO3	DZIP3	CAMK2N1	FEN1	APP
PCDH11X	GLT8D1	MCM6	NCAPG	PLPP1	FERMT2
TCFL5	ERBIN	FOXM1	LOC102724093	MAP1LC3B	RCAN2
FAM13B	MOAP1	PAIP1	LGALS8	FANCI	VPS45
KIF11	PATZ1	GAL	SLC7A11	HMMR	PFDN4
GGCT	PDE10A	MELK	GRAMD3	UBE2C	TNKS
PCYOX1	RNASE4	PTPRG	GGPS1	AURKA	GMNN
PNMA2	IL1RN	TIA1	KIF5C	FEM1B	RCOR3
TACC3	NEBL	PSPC1	RPA3	DHFR	TMOD3
COL6A2	TMPO	CEP68	GMCL1	RCBTB1	PJA2
SHTN1	UBE2S	DTYMK	ASF1B	KLK13	KIF15
AUTS2	SEMA6A	GALNT10	OCLN	CDCA8	ARHGAP5
TMEM38B	TRPS1	NPTN	ATAD2	DOPEY1	ABI1
RSBN1	KPNA2	FAM198B	GGH	SLC4A4	NAIP
RRM2	PEX10	FBXL4	EIF4E	PRRG1	APPL1
ATXN1	PCNA	TROAP	NAMPT	GPR137B	BRCA1
HS2ST1	KCNQ3	RAP1GDS1	NAB1	SORL1	KLK3
GTSE1	TULP4	FBXL5	VPS13B	NDC80	BBIP1
NET1	TMSB15A	ECT2	TGOLN2	ZBTB10	LMNB1

CDK1	WDR47	SPAG5	SMAD4	ROR1	MIA3
KIAA0101	ARID4B	TPX2	ABCC2	BZW2	CDC6
TRAPPC13	AZGP1	ALDH5A1	SAT1	KIF20A	MDK
SPAST	EIF4EBP1	RFC2	GNAI1	TNFRSF21	ATP5S
appl2	HJURP	ASPM	mthfd2	SH3YL1	
ABAT	ZNF184	PTTG1	OPLAH	CD24	
PRC1	CENPA	RAD51AP1	COBLL1	ESPL1	
ASAP2	TYMS	RTN1	PBK	CDC45	
DCTN1	NR2F2	PLA2G2A	BCHE	CENPF	
KDM6A	KLK2	RALGPS1	COBL	MCM7	
HMGCS2	CREBZF	SOCS2	DNMT1	MCM4	
CENPN	FAM64A	ABHD5	SLC38A6	POLA2	
SMAD2	KCNN2	SELENBP1	TMEM144	BUB1B	
ATP2B1	TTC3P1	ID1	MCM10	ALDH6A1	
ATP2C1	KIF4A	GTSE1	LIN7C	ARFGAP3	
EBP	TUSC3	PAK2	LPGAT1	MAN1A1	
ZNF652	NDC1	SMA4	KAT6B	KANK1	
FZD3	CSE1L	MANEA	NEK1	ZNF223	
DICER1	DLG1	GOLGA8A	CCDC91	TAF9B	
MCM5	TMED7-TICAM2	VPS54	SYNGR3	PARPBP	
SMC4	PPIF	GPSM2	NFAT5	MAN1A2	
CDC42EP3	ZNF83	MAST4	CREBBP	GPER1	
CDKN3	SCAPER	PTPN13	KTN1	SH3BP5	
PTPRR	PLK1	CCNB2	SEZ6L2	SLC30A4	
LAPTM4B	KCNQ2	NEK2	MAP4K3	AGR2	
FNBP1L	LTBP3	TCF12	NR3C2	MYRIP	
RNASEH2A	IDS	TUBA1A	LRIF1	CKS2	
BIRC5	CENPM	MICU2	FOXN3	WDYHV1	
JMJD1C	MCM3AP	SNRK	ROCK2	EPS8	
VEZF1	CSTF2T	NUSAP1	hist1h2am	SGPL1	
DLGAP5	REEP4	RALGAPA1	COL5A2	NPM1	
RRM1	PLEKHB1	SCYL2	ZWINT	MAD2L1	
ASPH	CHD1	APBB2	ARHGAP12	ZNF43	
SI	KLF9	GNAQ	MIR7110	MIR1292	
NR2C1	RIT1	STAG2	LAMP2	UGT2B17	
NACC2	CCNB1	TBC1D4	NAP1L3	ZNF226	

ERα signature

TOP2A	BTG2	CENPN	depdc1b	WDHD1	CDCA3
SLC29A1	PCP4	BUB1	CENPN	dsn1	TMPRSS2
CKS1B	CDCA5	NT5E	DSCAM	FGD3	LRIG1
ABHD2	CENPN	CDC7	STIL	PBK	NDC80
TIFA	DDIAS	TK1	SLIT2	CENPH	MASTL
RET	ABCA1	MKI67	DAB2	FANCD2	KIF2C
EPB41L5	CREBRF	ZGRF1	LMCD1	TNFRSF11B	DEPDC1
PPIF	LMBR1	TIMELESS	RBM24	CDKN3	MYO19
COL21A1	CTGF	LIMA1	CEP152	MCM10	TNFRSF21
GABBR2	ATAD2	PSD3	SPIN4	UPK1A	TP53INP1
C8orf44-SGK3	MCM5	SYTL4	RFC2	BRI3BP	SLF1
BRIP1	RERG	CENPU	NCAPG	FIGNL1	MCM10
SMC2	MCM10	C8orf46	KNTC1	AGR3	TRIB2
MIR1178	CDKN3	TYMS	L1CAM	S1PR3	ESPL1
UGT2B15	ESCO2	CREBRF	CCNB2	KLK11	CDC45
PHF19	NUSAP1	KIF4A	TNFRSF11B	NCAPG2	EGR3
CHEK1	CXCL12	TYMS	HELLS	RAB31	UBE2QL1
DHFR	FAM110B	PHF19	RAD54B	GAS2L3	MCM4
MCM8	DTL	KIF18B	NUSAP1	AHRR	POLA2
FKBP5	RNASEH2A	MME	BLM	SOX3	PGR
BUB1	RAB27B	PPIF	SHCBP1	GEN1	RERG
FHL1	MKI67	IL17RB	PGR	KIF23	FANCG
CENPJ	TGFB2	CENPM	MTFR2	HES1	TNS3
SKP2	BIRC5	HELLS	CCNG2	WDR76	BUB1B
RFC5	ARHGAP36	RET	PP14571	RRM1	POLD3
ZNF367	LOC100505984	PTGER4	CDH26	FEN1	CDKN2C
NEMP1	DLGAP5	PARPBP	POLQ	ZWINT	C1orf168
RAB31	FANCI	IGFBP3	CHAC2	MKI67	BLNK
NUAK1	PLAC1	E2F8	KIAA0101	ATAD2	CEP128
slc39a8	c4orf46	NUF2	APOD	FHL1	ABHD2
IQGAP3	RRM1	CDK6	DHFR	RAD18	NEMP1
CDKN2B	RASD1	SFXN2	CENPU	DEPDC1	ercc6l
NPAS3	KIF23	RAB27B	ZWILCH	THRIL	DRAM1
LMBR1	CDC25A	MND1	FANCA	RBL1	FHL1
ALDH1A3	CCNA2	GINS2	PSCA	FHL1	GINS3
TMEM140	RNF207	CYP1A1	TGFB2	TMPO	IGFBP3
UGT1A10	UGT1A10	CENPO	AREG	IGDCC3	MAD2L1
FABP5	TICRR	SPC25	XBP1	PSMC3IP	MAD2L1

DNA2	CHEK1	RLN2	MYBL2	ORC1	CYP26B1
ACACB	RACGAP1	DONSON	PGM2L1	DSCC1	CDYL2
HIST2H2BE	CENPQ	PSD3	NPY1R	AREG	LMO7
CHEK2	HIST4H4	TOP2A	KIAA1524	GINS3	GTSE1
IL1R1	BARD1	FOS	IL17RB	SNAI2	OIP5
STON1	ITGB8	CDK1	NTN4	E2F2	ABHD2
NEK2	DHFR	CDCA7	RGS22	RAD51	LMBR1
RNF144B	TRIP13	EXO1	HSPA2	ASPM	CDT1
LINC01016	TGFBI	HEY2	EPAS1	KIF14	MCM5
GREB1	HMMR	SKA3	LIG1	SCNN1A	FAM110B
HELLS	GINS4	UNG	CLIP4	CENPK	E2F7
IL17RB	POLQ	PKIB	NCAPG	RFC3	SPC24
c4orf46	BIRC5	ITGB3BP	MCM2	PRIM1	ccdc83
DUT	TTK	hcar3	ATAD2	brca2	JAK2
GRHL3	CCNA2	LOC100505984	SGO2	CHEK1	MCM7
CDC14B	DTL	POLA1	CDT1	CDK1	VRK1
LINC01016	FAM161A	CDH26	ATAD2	FEN1	AURKB
KIF11	BRCA1	MCM6	ASF1B	GABBR2	SGO2
POLE2	TTF2	FOXM1	DHRS3	ESPL1	TK1
TACC3	KLHL24	NASP	MKI67	RGCC	ANLN
RAD54L	FANCI	MELK	CENPL	FANCI	MYO1B
RRM2	TCF19	MCM4	GGH	CHAF1A	ANLN
KNL1	HELLS	DBF4	PCSK6	UBE2C	UBE2QL1
FAM72C	CEP55	ACAA2	TIPIN	FSTL4	GINS1
CENPU	FIGNL1	UBE2T	PRICKLE1	KLHL24	UHRF1
GTSE1	C1orf226	ECT2	MCM3	SGO1	FBXO5
ABHD2	TMPO	SPAG5	PRICKLE1	DHFR	CDC6
CDK1	PLK4	SKA1	PKIB	TMPO-AS1	DNAJC9
GABBR2	CDC25A	TPX2	UGT2B15	CCDC34	
KIAA0101	PCNA	RFC2	DEPTOR	PSD3	
FBXO5	slc39a8	ASPM	CDC6	MYBL1	
LDLRAD4	RAB31	c18orf54	HIST1H3E	CDCA8	
PRC1	RFC3	RAD51AP1	NEIL3	TGFB2	
HS3ST3A1	CENPI	MCM4	CSTA	SMC2	
TMPRSS3	TGFB2	LOC100505984	CCNE2	DEPDC1	
IMPA2	RMI1	C8orf44-SGK3	CENPW	GABBR2	
BRIP1	DUT	WDHD1	SALL4	RFC4	
CXCL12	brca2	HIST1H2BC	CCNE2	IGSF1	
EPB41L5	WDHD1	CENPI	KIF14	GLA	
PDK1	GMNN	KIF15	MGP	NCAPH	
MIR6756	PLK4	RRM2	BRCA1	CDCA2	
LIMA1	DUT	FANCA	LMNB1	ST3GAL1	

VITA

MANQI ZHANG

Miami, Florida

2010 - 2014	B.S., Pharmacy
	China Pharmaceutical University
	Nanjing, China
2014 - 2019	PhD. Biochemistry
	Florida International University
	Miami, FL
2014 - 2015	Teaching Assistant
	Florida International University
	Miami, FL
2015 - 2018	Research Assistant
	Florida International University
	Miami, FL
2018 – 2019	Dissertation Year Fellowship
	Florida International University
	Miami, FL

PUBLICATIONS AND PRESENTATIONS

Zhang M, Suarez E, Vasquez JL, Nathanson L, Peterson LE, Rajapakshe K, Basil P, Weigel NL, Coarfa C, Agoulnik IU. (2019) Inositol polyphosphate 4-phosphatase type II regulation of androgen receptor activity. *Oncogene*, 38(7):1121-1135. (IF: 6.634).

Zhang M, Krause WC, Agoulnik IU (2018) Techniques for evaluation of AR transcriptional output and recruitment to DNA. In: Culig Z (ed) Prostate cancer: methods and protocols. Methods in molecular biology, vol 1786. Springer, New York, pp 219–236

Lopez SM, Agoulnik AI, Zhang M, Peterson LE, Suarez E, Gandarillas GA, Frolov A, Li R, Rajapakshe K, Coarfa C, Ittmann MM, Weigel NL, Agoulnik IU. (2016) Nuclear Receptor Corepressor 1 expression and output declines with prostate cancer progression. *Clinical Cancer Research.* 22(15); 3937-49 (IF: 8.911).

Zhang, M, Rieger, JL, Weigel, NL, Nathanson, L, Agoulnik, IU. INPP4B Regulation of AR Transcriptional Activity and Cell Signaling in Prostate Cancer Cells and in Mouse Prostate. 99th Annual Meeting of the Endocrine Society (ENDO 2017), Orlando, FL, April 1st –April 4th.

Zhang M, Judy Rieger, Nancy L Weigel, Lubov Nathanson, Irina U. Agoulnik. Loss of INPP4B Modulates Cell Signaling and AR Signaling in Prostate Cancer Cells and in Mouse Prostate. 19th European Congress of Endocrinology (ECE 2017), Lisbon, May 20th – May 23th, 2017

Zhang, M, Rieger, JL, Agoulnik, IU. Loss of INPP4B exacerbate high-fat diet induced prostatic intraepithelial neoplasia, 20th Annual Biomedical and Comparative Immunology (BCI) Symposium, Miami, FL, Mar 8th – Mar 9th, 2018

Zhang M, Vasquez JL, Agoulnik IU, Genetic protection from obesity related diseases, Florida Statewide Graduate Student Research Symposium, April 18st, Miami, FL, 2019

Zhang, M ., Lei, R ., Hodgson, MC ., Nathanson, L ., Agoulnik, IU ., Loss of Inositol Polyphosphate 4-Phosphatase Type II (INPP4B) Modulates Androgen Receptor Activity by Activating Cell Signaling and Interfering with Epigenetic Modulator EZH2. 98th Annual Meeting of the Endocrine Society (ENDO 2016), Boston, Mar 30th -April 4th , 2016

Lopez SM, Agoulnik AI, Zhang M, Peterson LE, Suarez E, Gandarillas GA, Frolov A, Li R, Rajapakshe K, Coarfa C, Ittmann M, Weigel N, Irina U. Agoulnik. Regulation of Casodex Response by Androgen Receptor Corepressor NCOR. 5th Florida Prostate Cancer Research Symposium, Clearwater, FL, May 19th – May 20th , 2016

Zhang, M, Rieger, JL, Agoulnik, IU. Inositol polyphosphate-4-phosphatase type II mediates prostate cancer latency. AACR obesity and cancer (2018), Austin, TX, Jan 27th – Jan 30th, 2018

Zhang M, Vasquez JL, Kaftanovskaya EM, Agoulnik AI, Vacher J, Ittmann MM, Agoulnik IU, INPP4B suppresses prostate inflammation and protects mice fed with high-fat diet from the development of prostate intraepithelial neoplasia, ENDO 2019, March 23th – Mar26th New Orleans, LA, 2019

Zhang M, Vasquez JL, Agoulnik IU, Loss of INPP4B in obese mice leads to weight gain, inflammation and the development of prostate intraepithelial neoplasia, BSI symposium, Miami, FL, 2019